UNIVERSIDADE Ð
COIMBRA

Carlos André Viegas Barreto

APPLYING COMPUTATIONAL TOOLS TO THE STUDY OF GPCRs STRUCTURE AND DYNAMICS

Dissertação no âmbito do Mestrado em Biologia Celular e Molecular orientada pela Professora Doutora Irina Sousa Moreira e apresentada ao Departamento de Ciências da Vida da Faculdade de Ciências e Tecnologia da Universidade de Coimbra.

Agosto de 2018

Departamento de Ciências da Vida

APPLYING COMPUTATIONAL TOOLS TO THE STUDY OF GPCRs STRUCTURE AND DYNAMICS

Carlos André Viegas Barreto

Tese no âmbito do Mestrado em Biologia Celular e Molecular orientada pela Professora Doutora Irina Sousa Moreira e apresentada ao Departamento de Ciências da Vida da Faculdade de Ciências e Tecnologia da Universidade de Coimbra.

Agosto de 2018

UNIVERSIDADE Đ COIMBRA

FACULDADE DE CIÊNCIAS E TECNOLOGIA
UNIVERSIDADE Đ COIMBRA

AGRADECIMENTOS

RESUMO

A família de GPCRs e a maior família de receptores de superfície. São responsáveis pela regulação de importantes funções celulares e a desregulação leva a doenças graves. Por essa razão GPCR são o maior alvo dos fármacos disponíveis.

Para puder desenvolver fármacos novos e mais eficazes, conhecimento sobre a estrutura e dinâmica de GPCR a nível atómico e crucial. Nos últimos anos, técnicas computacionais tem ajudado a expandir este conhecimento devido aos seus menores custos e ao maior poder computacional disponível. As técnicas mais usadas incluem modelação por homologia, docking molecular e dinâmica molecular. Neste trabalho, estas técnicas foram aplicadas a dois sistemas biológicos: o receptor da dopamina e o receptor da grelina.

O desenvolvimento de ligandos altamente selectivos para todos os subtipos de DR e ainda um problema importante, especialmente para os subtipos D1-like. Estudos de docking foram aplicados a todos os subtipos de DR com quinze ligandos disponíveis no mercado de forma a obter uma visão geral da dinâmica do local de ligação ortoesterico e secundário.

A alta actividade constitutiva do receptor da grelina não é ainda totalmente conhecida a nível estrutural e dinâmico. A mutação A204E é conhecida por diminuir esta actividade basal. Dinâmicas moleculares de WT e mutante A204E revelou diferenças dinâmicas nestes dois modelos, especialmente nos motivos de activação de GPCRs.

Os dados apresentados nesta tese prova que as técnicas computacionais conseguem ser aplicadas com sucesso ao estudo de GPCRs e ajudar a construir conhecimento preciso desta família de receptores.

PALAVRAS-CHAVE: GPCRs, Docking Molecular, Dinâmica Molecular, Receptor da Dopamina, Receptor da Grelina

ABSTRACT

GPCR family is the largest family of cell-surface receptors. They are responsible for the regulation of several cellular functions and their dysfunction leads to serious diseases. Thus, GPCR represent the largest family in drug targets.

To be able to develop new and more efficient drugs, understanding of GPCR structure and dynamics at the atomic level is crucial. In the past years, computational techniques have been successfully helping expand this knowledge due to their lower costs and increase in computational power. The most used of these techniques include homology modelling, molecular docking and molecular dynamics simulations. In this work, these techniques were applied on two biological systems: the dopamine receptor and the ghrelin receptor.

Finding new highly selective ligands for all subtypes of DR is still an important issue, especially for the D1-like subtypes. Docking studies were performed in all DR subtypes with fifteen commercially available ligands to obtain a full scope of the orthosteric and secondary binding pocket's dynamics.

Ghrelin receptor high constitutive activity is still a not fully understood characteristic at a structural and dynamical level. Single point mutation A204E is known to decrease this unusual basal activity. Molecular dynamics of WT and A204E mutant revealed dynamics differences between the two models, especially in the common activation motifs of GPCRs.

Data presented in this thesis proves that computational techniques can successfully be applied to the study of GPCRs and help building new accurate understanding of this superfamily.

KEYWORDS: GPCRs, Molecular Docking, Molecular Dynamics, Dopamine Receptor, Ghrelin Receptor

TABLE OF CONTENTS

LIST OF ABBREVIATIONS

5-HT2C	Serotonin 2c receptor
7-OH-DPAT	7-Hydroxy-N,N-DiPropyl-2-AminoTetralin
AMPAR	α-Amino-3-hydroxy-5-Methyl-4-isoxazolePropionic Acid Receptor
BA	Binding Affinity
BP	Binding Pocket
cAMP	cyclic Adenosine MonoPhosphate
D1R	Dopamine Receptor 1
D2R	Dopamine Receptor 2
D3R	Dopamine Receptor 3
D4R	Dopamine Receptor 4
D5R	Dopamine Receptor 5
DOPE	Discrete Optimized Protein Energy
DR	Dopamine Receptor
ECL	ExtraCellular Loop
GHSR	Growth Hormone Secretagogue Receptor
GHSR1a	Growth Hormone Secretagogue Receptor 1a (ghrelin receptor)
GHSR1b	Growth Hormone Secretagogue Receptor 1b
GluR	Glutamate Receptor
GPCR	G-Protein Coupled Receptor
ICL	IntraCellular Loop
LGA	Lamarckian Genetic Algorithm
LINCS	LINear Constraint Solver
LTP	Long Term Potentiation
MC3	MelanoCortin receptor 3
MD	Molecular Dynamics
molpdf	molecules robability density functions
MSA	Multiple Sequence Alignment
OBP	Orthosteric Binding Pocket
PCA	Principal Component Analysis
PI-PLC	PhosphatidylInositol-specific PhosphoLipase C
PKC	Protein Kinase C
PME	Particle Mesh Ewald
POPC	1-Palmitoyl-2-Oleoyl-SN-glycero-3-PhosphoCholine
ProQ	Protein Quality
ProSA	Protein Structure Analysis

RMSD	Root Mean Square Deviation
SBP	Secondary Binding Pocket
TM	TransMembrane domain
WT	Wild Type

LIST OF FIGURES

LIST OF TABLES

1 INTRODUCTION

1.1 GPCR Structure and Dynamics

The human G Protein-coupled receptors (GPCR) is the largest family of cell-surface receptors. This family translates external signals into internal stimuli that regulates several cellular functions such as cell growth and differentiation, immune responses and neurotransmission. For representing such an important role in cell life, they have a compelling role in regulating pathophysiology in a diverse set of diseases. Drugs can modulate the effects of these receptors, they represent the largest family in drug targets of the existing drugs [1].

The transmission of the signal is only possible because of the ability of GPCRs to change shape upon binding of extracellular signal, such as hormones, neurotransmitters or chemokines. This event causes conformational changes on the receptor to allow the coupling of intracellular signalling proteins like G-Proteins or Arrestins [2]. This mechanism is highly complex and understanding the structural basis behind it has been a challenge in both scientific research and drug design.

GPCR are composed of seven transmembrane α-helices (TM1-TM7) connected by three extracellular (ECL) and three intracellular loops (ICL) clustered in a bundle [3]. The largest class of this super-family, class A, contains only the transmembrane bundle, while other classes, such as B, C and F also include an extracellular domain that can be used as binding site of native ligands [2].

GPCRs are in constant movement at the atomic level. The motions can be highly localized and very fast (femtoseconds to nanoseconds) or occur in larger parts, which are typically more slowly (nanoseconds to milliseconds). These constant motion opens the possibility for an infinite number of conformations. Conformation generally refers to a three-dimensional arrangement of atoms. Conformations tend to cluster in conformational states [2]. Generally, there are three broad conformational states of these receptors: an inactive state, an agonist-bound state and an active state [1].

The mechanism of activation of GPCR is highly complex and is still a scientific challenge because of the low number of crystallographic structures of both inactive and active forms [1]–[3]. In absence of activating ligands GPCRs exhibit a basal activity which can be as high as 50% of the total activity in receptor such as the ghrelin receptor [1], [4]. The common mechanism of activation has not yet been described, however there are movements and events common to various sub-families of GPCRs that are essential for the activation of the receptor. TM3 and TM6 interact directly with every other helix apart from TM1, which makes them the crucial players in the activation mechanism. The trigger

of the activation must indeed influence helices 3 and 6 in order to the common movements of activation take place. These movements include the inward movement of TM5, the slight rotation and upward movement of TM3, the rotation of TM6 and the inward movement of TM1 and TM7.

The movements of TM3 and TM6 are facilitated by the disruption of the ionic interaction between residue R3.50 and an acidic residue in TM6 [1], [2]. R3.50 is part of D/ERY motif in TM3 of GPCR, which is part of the GPCR activation motifs. The ionic lock is a network of contacts between this motif and residues of TM6 that hold their cytoplasmatic ends in place and maintain an inactive state. Studies with β_2AR demonstrated that R3.50 forms an ionic bond with residue E6.30, that is thought to prevent the receptor to activate in absence of an agonist [5].

Another important rearrangement affects the hydrophobic residues between TM3 and TM6 located in the core of the receptor. In inactive states, this hydrophobic cage hampers the channel of water observed in active states crystal structures. It consists in L3.43, F6.44, X6.40 (where X is a bulky hydrophobic residue such as I, L, V or M). In the inactive state L3.43 is arranged to be held in place by F6.44 on top and by X6.40 on the side. The disruption of stability in these two regions allows the movement of TMs which allows the formation of a water channel through the hydrophobic cage [1].

The outward movement of TM6 is supported by a conformational change in the conserved residue W6.48 located on the CWxP motif. This residue acts as a rotamer toggle switch that rearranges upon activation and modulates the proline-induced kink present in TM6. The rearrangement decreases the bend-angle of the kink and straightens TM6 allowing it to move away from TM3 [6].

Although the largest changes tend to be in the intracellular side of GPCRs, the extracellular side also undergoes important changes, specially the binding pocket. The extracellular loops can also affect binding kinetics and act as binding site to allosteric modulators [2].
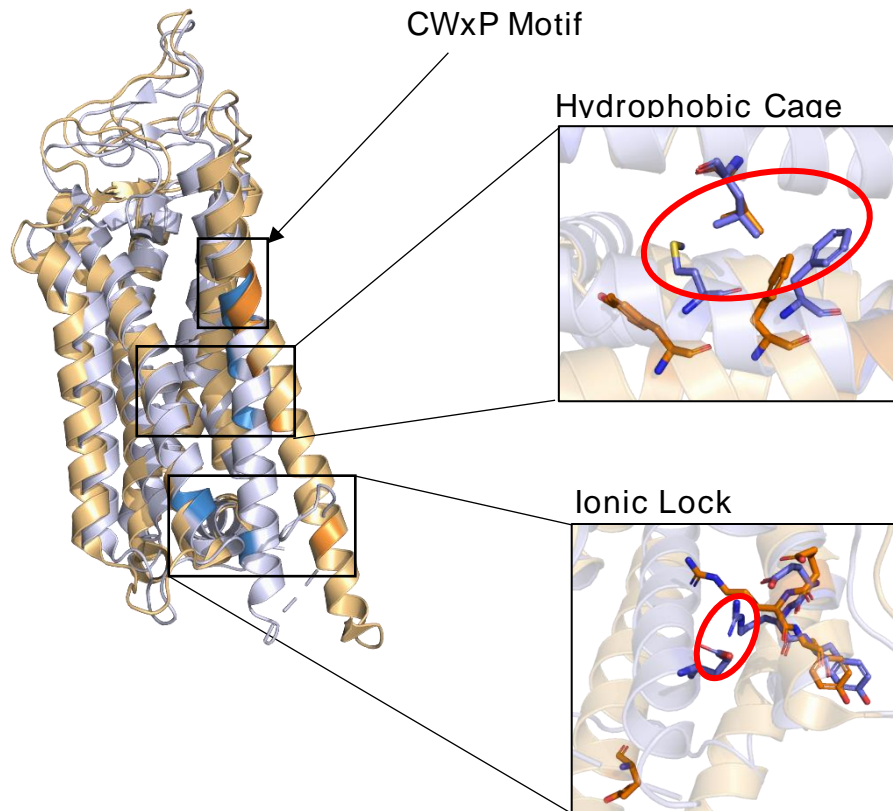
Figure 1 - GPCRs activation motifs. Representation of a GPCR in an inactive state (blue) and active state (orange). The most important activation motifs are highlighted in the structure. The "ionic lock" close up shows the proximity of R3.50 and D/E6.30 stabilizing the inactive state (red circle), in contrast with the active state in which the "lock" is broken and the two residues are far apart. The "hydrophobic cage" close up evidences how the hydrophobic residues are clustered in the inactive state, preventing the formation of the water channel.

1.2 Case Studies

1.2.1 Dopamine Receptor

Since its discovery, dopamine has attracted an incredible amount of attention due to its critical role in cell-signalling and regulation of dopaminergic pathways [7]. Dopaminergic circuits are the most abundant in the human brain and are divided in four major pathways: the mesolimbic; the nigrostriatal, the mesocortical and the mesocorticolimbic [7]. Dopamine activity is critical for central nervous system functions like voluntary movement, feeding, reward, sleep regulation, attention, working memory and learning. Peripherally, dopamine influences the immune, cardiovascular, renal and gastrointestinal systems [8]. Being a part of such vital functions, dysregulation of dopamine signalling is linked to several human disorders like Parkinson's disease, Attention Deficit Hyperactivity Disorder, Tourette's Syndrome, Huntington's disease and schizophrenia [7].

Dopamine is released into the synaptic cleft and activates the Dopamine Receptor (DR), a member of the super-family GPCRs [7]. This receptor shares most of the common features of GPCRs. There are five known type of DRs, numbered 1 to 5, that are divided into two major groups: D1-like and D2-like [9]. This division is given according to their ability to modulate cyclic adenosine monophosphate (cAMP) production and their pharmacological properties [9]. The members of the subfamilies share a high level of homology concerning their TM [9]. Members of D1-like family (D1R and D5R) couple with $G\alpha_s$ and stimulate the production of cAMP [10]. Besides, D1-like members are found exclusively in the postsynaptic terminal [7]. D2-like members (D2R, D3R and D4R) activate $G\alpha_i$ and inhibit the production of cAMP [10]. D2R and D3R can be found pre- and postsynaptically [7].

Since the functions of D4R and D5R are not well described/researched, D1R-D3R seem to play a more important role in locomotor activity [7], [11]. Furthermore, D2R and D3R are considered to be part of more complex tasks as they are also located in the membranes of presynaptic nerve cells [9]. Since these receptors, called autoreceptors, regulate the neuron firing rate through negative feedback-loop mechanism, they are excellent candidates for drug targeting [9], [12].

As mentioned above the dysregulation of the dopaminergic system can lead to severe diseases, in particular to neurodegenerative diseases. For this reason, the dopamine receptors have been highly targeted throughout the years, with special focus in the D2-like family. GPCRdb [6] has registered 244 drugs for the all dopamine receptor family in July 2018. Of this total almost ~60% have been approved and are still commercially available. D2-like family as more hits for either approved or on trials drugs. The numbers for each receptor are summarised on Table 1. Although the majority of these drugs only have been functionally studied, there is no broad structural study that includes binding poses these ligands within all five dopamine receptors.

Table 1 - Number of drugs targetting DRs registered in the GPCRdb. Approved percentage represents the drugs that were approved and are still used. On trial represents the number of drugs that are on currently active clinical trials, discarding finished or interrupted trials.

Receptor	No Entries	Approved	On trial	No Agonists	No Antagonists	No Partial Agonists
D1	38	28 (73.6%)	7 (18.4%)	12	24	1
D2	103	61 (59.2%)	30 (29.1%)	26	66	8
D3	48	25 (52.1%)	13 (27,1%)	25	20	2
D4	38	22 (57.9%)	10 (26.3%)	22	15	-
D5	17	9 (52,9%)	5 (29.4%)	11	5	-
Total	244	145 (59.4%)	65 (26.6%)			

D2R drugs were already discovered in the 1950s, such as Haloperidol and Chlorpromazine [13] and since then many prominent substances have been developed such as Risperidone, Clozapine, Ziprasidone or Quetiapine [14]. However, most of the commonly utilized drugs show significant side effects and nonselective profiles [14], [15]. The issue to find DR subtype selective therapeutics is an ongoing field of research. For targeting the D3R, it has been proposed that substituted 4-phenylpiperazine compounds dissect between D2R and D3R selectivity [16], [17]. In addition, the aminotetraline derivative 7-OH-DPAT was identified as a selective D3R agonist [18], [19], while for D4R available therapeutics are not selective [17], except for Haloperidol which highly targets the D4R but also the other DRs [20]. A study by Sampson et al. synthetizied selective D4R ligands with Ki values in the lower nanomolar range, based on the piperazine analog of Haloperidol as a pharmacophore to target erectile dysfunction [20]. This piperazine moeity of Haloperidol was further explored in other studies, leading to the development of Aripiprazole, a next-generation atypical antipsychotic, which is highly selective for targeting D2R and D2R/D3R heterodimers and displays properties of D2R agonist and antagonist [21]. Regarding the D1-like receptors, D1R and D5R, finding subtype selective ligands has been very difficult [22], [23]. SKF83959 is the only selective agonist for the D1R so far, however its selectivity is controversially discussed [23], while D5R lacks a selective ligand [24], [25]. SCH23390 has been proposed to be the only D1R

selective antagonist [26]. In summary, finding new highly selective ligands for all DR subtypes is still an important issue, especially for the D1-like subtypes, which are poorly described but are proposed to have several pathophysiological roles [27].

1.2.2 Ghrelin Receptor

Ghrelin and physiologic functions

Ghrelin is a 28-amino acid peptide secreted directly into gastric circulation by X/A-like cells of the oxyntic glands, located in the gastric fundus, and then transported to the brain. Ghrelin circulates in two forms: acylated (-5%) and desacylated (95%) [28]. It acts directly in the hypophysis stimulating the release of growth hormone. Also it can have a homeostatic role in other parts of the brain and the rest of the body. The most prominent of these roles is the appetite stimulatory action of ghrelin, that's why is often called "the hunger hormone" [28]. Ghrelin stimulates feeding by activating orexigenic neurons and suppressing neurons containing anorexigenic peptides [28]. This stimulating role seems to be a direct effect of circulating ghrelin on the hypothalamus since orexigenesis is present without vagal afferent signalling. Nevertheless, there are some studies that show vagotomy does result in the loss of ghrelin's appetite stimulating effect [29]. Peripheral effects of ghrelin in metabolism include enhancing of adipogenesis and lipid retention and inhibition of insulin secretion by pancreas' β cells. Deregulation of these functions can lead to clinical problems like obesity or diabetes [28].

In addition to these metabolic changes, ghrelin has been implicated in other physiologic processes in the central nervous system like neuroprotection, neurogenesis, anti-anxiety effects and some higher functions like memory and cognition regulation [30]. Effects of ghrelin on learning and memory have been recently studied and it seems that ghrelin enhances these higher functions by stimulating neurogenesis and synapse formation and activity. Ghrelin specifically promotes dendritic spine synapse formation and induction of long-term potentiation (LTP) in the hippocampus [30]. Furthermore, treatment with an agonist significantly increased cell surface levels of $GluA_1$, an α-amino-3-hydroxy-5-methyl-4-isoxazolepropionic acid receptor (AMPAR) subunit of glutamente receptor-1 ($GluR_1$) [31].

Ghrelin receptor (GHSR1a)

Ghrelin is an endogenous ligand of the growth hormone secretagogue receptor (GHSR), that is transcribed from growth hormone receptor 1 gene. This gene encodes a full functional receptor (GHSR1a) and a truncated, non-functional, isoform (GHSR1b).

GHSR1a is predominantly expressed in the anterior pituitary gland [28]. GHSR1a is a GPCR, being characterized by seven transmembrane-spanning helix domains, connected to three ICL and three ECL. GHSR1a can dimerize with itself producing a homodimer [32] or can dimerize with other GPCRs forming heterodimers. The most common heterodimers are formed with melanocortin receptor 3 (MC3), dopamine receptor 1 (D1R), dopamine receptor 2 (D2R) and serotonin receptor 2c (5-HT2C) [33]. Heterodimers interactions can result in altered trafficking and signalling [32].

The activation of GHSR1a upon ligand coupling leads to conformational changes providing a surface to the coupling of G proteins and β-Arrestin [32], [34]. Binding of different ligands to GHS-R1a can lead to the activation of different downstream signals like phosphatidylinositol-specific phospholipase C (PI-PLC), Ca^{2+} intracellular release and protein kinase C (PKC) [30]. This ligand-dependent signalling in which different ligands stabilize different subsets of receptor conformations, favouring some signalling pathways over others is referred to as functional selectivity [34].

In addition, GHSR1a has high constitutive activity [32]. This high constitutive activity means that GHSR1a is able to adopt an active conformation in the absence of agonists, increasing basal G-protein and effector system activity [35]. It has been suggested that this activity is designed to balance the inhibitory effects of other hormones [36]. Holst et al identified an aromatic cluster within TM6 and TM7 that is structurally important for the constitutive activity. The cluster facilitates the approach of TM6 and TM7 to TM3 to shift the receptor into the active conformation [36]. Also, a point mutation (A204E) in GHSR decreases the constitutive activity while retaining sensitivity to ghrelin [37]. This mutation can be responsible for short stature [37] and obesity [38].

2 METHODOLOGY

GPCRs are one of the most important drug targets and structural understanding of these is the key for application of structure-based drug design techniques. Experimental determination of GPCR structures still constitutes a great challenge in structural biology. One way to surpass some of these difficulties lies on computational methods that gather the pre-existent experimental structural information and predict the 3D structure of GPCR, their interaction with ligands and with other receptors.

2.1 Prediction of the structure

The several approaches that have been applied to modeling GPCRs structure fall into three categories: homology modeling methods, de novo methods and hybrid methods [39]. Of these approaches, homology modeling remains the most accurate [40]. The main objective of this technique is to build a 3D replica for the protein with an unknown structure by sequence similarities to that of a known structure (template) [41]. Homology modeling lies on the fact that three-dimensional structure of proteins has been conserved to a very high degree through evolution [42].

Good template selection is pivotal to an accurate homology model of a GPCR [40]. In that regard, quality of models is intrinsically related to the similarity between the GPCR of study and the template [40]. For a good model, there must be at least 35% of sequence identity between template and target sequence [43].

The complexity of this method rises from the different conformations of GPCR, which include inactive and active states [40]. Although there are many inactive GPCR structures, the number of active structures is still very low. Once again correct template selection becomes essential for accurate models as well as for orthosteric ligand binding [44]. The main differences between the inactive and active structures of GPCR appear to be in TM3, TM5 and ECL2. It is possible to build models of the active conformation through an inactive state structure by modelling ECL2 in the presence of the ligand. Moreover, is key to know that the binding pocket in inactive state is bigger and wider in comparison to active receptor.

Homology modelling consists in four basics steps: template selection, sequence alignment, model building and model evaluation and refinement [41]. The importance of template selection was addressed above. Sequence alignment is important to align the sequences from template and target. The resulting alignment may need to be manually refined to maintain alignment of the highly conserved residues [40]. There are many alignment methods that can be used, the most powerful are the ones that allow multiple

sequence alignment (MSA) like ClustalOmega [45]. After alignment, model construction is achieved through application of rigid-body assembly, segment matching, artificial evolution and spatial restraint [40]. There are many several options for model building like MODELLER [46], [47] and SwissModel. [48]

Model refinement and evaluation is the last step of homology modelling. Refinement is a very important step to review and model more flexible areas like the side chains and loops and usually involves energy minimization. [49] For model evaluation, the scoring function is the most important factor and usually software like MODELLER has built in scoring methods to simplify the process to the user. [40]

2.2 Molecular Docking

Models of GPCRs facilitated the analysis of ligand binding mode to a receptor and advanced knowledge in the design of GPCRs ligands through computational methods. A widely-used approach for predicting protein-ligand interaction is molecular modeling. The principle of this method is to predict the "correct" bound association between two molecules given the atomic coordinates of the two [40]. Docking is achieved through two steps: sampling conformations of the ligand in the active site of the protein and then ranking these conformations [50].

One webserver that utilizes this approach is HADDOCK (High Ambiquity Driven DOCKing) 2.2. [51]. The algorithm used in this server performs three steps: i) proteins are represented as rigid bodies and generate a great number of solutions; ii) flexibility is introduced only in side chains and then to side-chains and backbone flexible segments; and iii) solutions are refined in explicit solvent. The resulting structures are clustered and scored using a combination of van der Waals, electrostatic and restraint energies [52].

2.3 Molecular Dynamics Simulation

Molecular dynamics (MD) simulation bridge between microscopic length and time scale and macroscopic laboratory work. Technology development and increase in computer power allowed the application of MD to large systems like GPCRs with larger simulation times. MD simulation can now be applied to understand motion and activation mechanism of receptors [40]. This approach has been a key method to identify metastable states that occur during the transition from inactive to active state [53].

To perform any MD there are three essentials: an initial structure of the system, the force field and the MD simulation software. An all-atom MD simulation of a GPCR usually contains the receptor, a ligand, a surrounding lipid bilayer and a water bath. Force fields

are used to describe the type of interaction existing between the atoms of the initial structure.

The simulation itself usually consists of numerical, step-by-step, solution of Newton's equations of motion [40]. In each timestep of the simulation, non-bonded interactions such as Leonard Jones potential and Coulomb electrostatics are calculated for each atom, along side bonding potentials which include bonds, bond angles and torsion angles. Simulation package force-fields include their own algorithms and experimental values for atoms characteristics and interactions. MD packages such as AMBER [54], CHARMM [55] and GROMACS [56] were built to work with larger molecules such as proteins.

MD is presently the best method to achieve a complete set of protein conformers. This method can be applied as a refinement step after homology modelling or docking with additional data incorporated or used to assess the stability of a complex [57]. Also, MD simulations open the door to study dynamics of dimerization and oligomerization of GPCRs [58].

In an attempt to understand signalling mode of GPCRs, simulations are currently carried out at longer timescales, and presently the timescales vary between the nanoseconds to the milliseconds [40].

Ligand binding induces conformational changes that are essential to receptors function, thus the ability to measure and simulate dynamic changes upon ligand binding becomes a pivotal issue in designing bioactive compounds [40].

3 METHODS AND MATERIALS

3.1 Case Study 1: Dopamine Receptor

3.1.1 <u>Homology Modeling</u>

The dopamine receptor models were built on MODELLER 9.19 [59], with the D3R complexed with D2R-Antagonist Eticlopride, (Protein DataBank ID: 3PBL [60]) and D4R complexed with D2R/D3R-Antagonist Nemonapride (Protein DataBank ID: 5WIU [61]) as templates. Depending on the sequence similarity obtained with Basic Local Alignment Search Tool (BLAST) [62] and ClustalOmega [45], either D3R or D4R was chosen as template to model the DR. For D2R the 3PBL was used (68% with BLAST and 72% with ClustalOmega) as well as for D3R (93% with BLAST and 99% with ClustalOmega), while for D4R the 5WIU template was chosen (93% with BLAST and 100% with ClustalOmega). For modelling D1R and D5R both templates slightly showed the same percentage of sequence similarity (D1R: 3PBL 35% compared to 5WIU 33%; D5R: 3PBL 34% compared to 5WIU 35%), however a second alignment with BLAST calculated that D1R should be modelled by using 3PBL as template, while D5R was modelled using the 5WIU template. Due to the length of the loop, ECL2 was cut and substituted for four alanine residues in D1R and D5R models.

In the modelling protocol the lengths of the TMs were specified as well as the perimembrane intracellular helix (HX8). In addition, disulphide bonds were specified in pairs cysteines, in particular between C3.25 and an unconserved cysteine in ECL2 and between two unconserved cysteines in the ECL3. Furthermore, loop refinement was performed for extracellular and intracellular loops for all DR.

The number of models which were calculated with MODELLER was set to 100.

3.1.2 <u>Model evaluation</u>

Due to general biological and structural features of GPCRs, visual inspection immediately ruled out some trial models. For a first inspection MODELLER's standard metrics for model assessment, Discrete Optimized Protein Energy (DOPE) [63] and molecules probability density functions (molpdf) were evaluated. Nevertheless, these scores are not reliable enough for membrane proteins, as they are based on the model's free energy and special occupation directed to water soluble proteins.

Therefore additional metrics were taken into account, such as Protein Structure Analysis (ProSA) web service [64] and online Protein Quality (ProQ) [65]. The z-score, provided by ProSA was only used for error recognition, as it indicates overall model quality with respect to an energy distribution derived from random conformations for globular proteins

[64]. Finally, the scores achieved with ProQ, the LGscore [66] and MaxSub [67] were set as base for the evaluation of the models. Furthermore ProQ allows to include secondary structure information calculated with PSIPRED [68] to improve model quality up to 15%, which was also done the set of models, which passed the ProSA analysis. Finally, the Ballesteros and Weinstein numbering system for class A GPCRs was applied [69].

3.1.3 Definition of the binding pocket (methods to characterize)

For the characterization of the binding pocket of the DR, several experimental and computational studies have been published. In this study a comphrehensive review of Floresca and Schetz [70] was used as a base for exploration of the DR binding pocket, since it contains detailed experimental data. In addition, computational data was also reviewed. A summary of the procedure can be reviewed in Bueschbell et al. [71].

3.1.4 Molecular Dynamics

System Setup

Before setting up the system, the DR selected models were subjected to PPM server [72] to calculate spatial orientations respecting to the Membrane Normal defined by the Z-axis. In addition, the state of titratable residues was calculated with PROPKA 3.1 at a pH of 7.0 [73].

The prepared receptor structures were inserted into a rectangular box simulation with dimensions of 114Å x 114Å x 107Å. The box was previously constructed with a lipid bilayer of POPC:Cholesterol (9:1) and explicitly represented water and subjected to a 10ns simulation. Insertion of the receptors in the membrane was performed with g_membed package [74] of GROMACS 4.6.7. [75], [76]. Finally sodium and chloride ions were added to neutralize the system until it reached a total concentration of 0.15M. the final system included approximately 370 1-Palmitoyl-2-oleoyl-SN-glycero-3-phosphocholine (POPC), 40 cholesterol, 125 sodium ions, 139 chloride ions and 28500 water molecules, with small variations from receptor to receptor.

MD simulation forcefield parameters

CHARMM36 parameter set for protein molecules and salt ions was used, as well as the CHARMM TIP3P model for water [77]. POPC and Cholesterol parameters were generated using CHARMM-GUI Membrane Builder [4], [78], [79].

MD simulation protocol

MD simulations of all DR models were performed with the periodic boundary condition to produce isothermical-isobaric ensembles using GROMACS 5.1.1 [80]. The Particle Mesh Ewald (PME) method was used to calculate the full electrostatic energy of a unit cell in a macroscopic lattice of repeating images. Temperature was regulated using the Nosé-Hoover thermostat at 310.15K. Pressure was regulated using the Tarrinello-Rahman algorithm. The equations of motion were integrated using leapfrog algorithm with a time step of 2fs. All bonds involving hydrogens atoms within protein and lipid molecules were constrained using the LINear Constraint Solver (LINCS) algorithm.
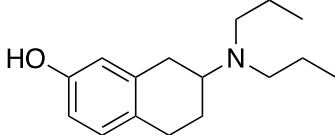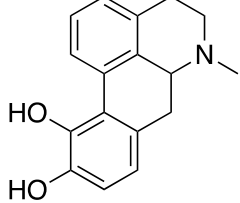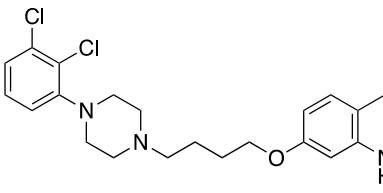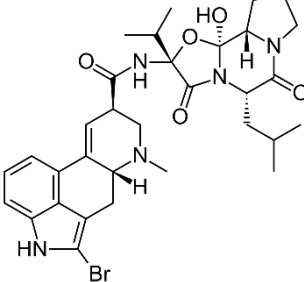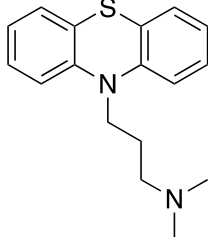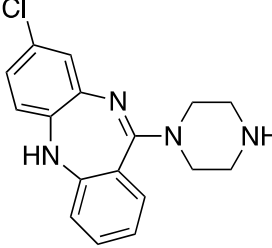
Prior to MD simulation, systems were relaxed to remove any possible steric clashes by a set of 50000 step of Steepest Descent energy minimization. Equilibration was performed after as follows: the system was heated using Nosé-Hoover thermostat from 0 to 310.15K in the NVT ensemble over 100 ps with harmonic restraints of 10.0 kcal/mol. Then systems were subjected through a first step of NPT ensemble of 200 ps with semiisotropic pressure coupling and a pressure of one bar. Further equilibration was performed with sequential release of membrane lipids and protein's atoms with a final step of NPT ensemble with harmonic restraints on the protein of 1.0kcal/mol, for a total of 1.4 ns of restrained equilibration.
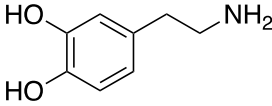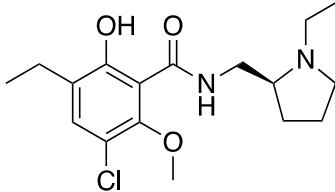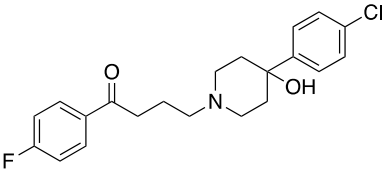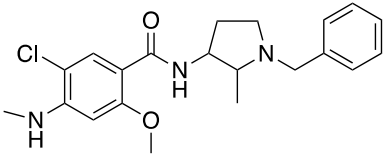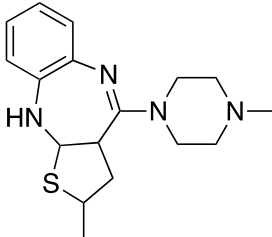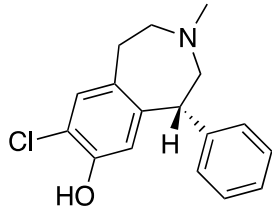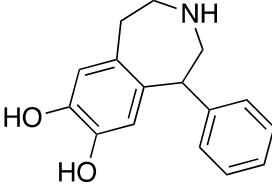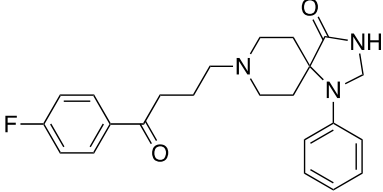
Then an independent simulation was initialized from the final snapshot of the restrained equilibration from each DR, for a total of 5 simulations. Simulations were 100 ns in length for every DR.
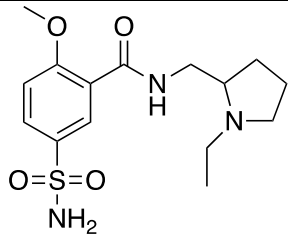
3.1.5 Ligand dataset

The following ligands were docked to the DR models after MD: Dopamine, 7-hydroxy-N,N-dipropyl-2-aminotetralin (7-OH-DPAT), Apomorphine, Bromocriptine, Clozapine, Nemonapride, Sulpiride, SCH23390, SKF38393, Eticlopride, Risperidone, Aripiprazole, Haloperidol, Spiperdone and Chlorpromazine. All structures were obtained from the DrugBank database (https://www.drugbank.ca) or from ChemSpider (http://www.chemspider.com) and if necessary, the file format was changed with OpenBabel (version 3.6) [81].

Table 2 - Ligands used for molecular docking and information on their function. Abbreviations: BP - binding pocket, OBP - orthosteric binding pocket, SBP - secondary binding pocket.

Ligand		Function	BP	References
7-OHDPAT		Synthetic D3R selective agonist	OBP	[70], [82], [83]
Apomorphine		D2R selective agonist	OBP	[70], [83], [84]
Aripiprazole		Partial D2R agonist, D2R/D3R heterodimer antagonist	OBP+SBP	[21], [82]
Bromocriptine		D2R selective agonist	OBP	[70], [83]
Chlorpromazine		Antagonist on all DR	OBP	[70], [83], [85]
Clozapine		"dirty drug", multiple receptor binding	OBP	[70], [83], [86], [87]

Dopamine		Endogenous agonist of all DR	OBP	[70], [83], [84]
Eticlopride		D2R/D3R selective antagonist	OBP+SBP	[82], [88]
Haloperidol		D2R selective antagonist, D4R antagonist	OBP+SBP	[13], [70], [83], [86], [89]
Nemonapride		D2R/D3R selective antagonist	OBP+SBP	[61], [70], [83], [90]
Risperidone		"dirty drug", multiple receptor binding	OBP+SBP	[70], [91]
SCH23390		D1R antagonist	OBP	[26], [70], [83], [92]
SKF38393		D1R selective agonist	OBP	[26], [70], [83], [93]
Spiperdone		Affinity for all DR	OBP+SBP	[70], [82], [83]

| Sulpiride | | "dirty drug", multiple receptor binding | OBP+SBP | [70], [82], [83] |

3.1.6 Molecular Docking

AutoDockTools, a package of MGLTools was used to perform ligand docking. Docking itself was performed using Autodock4.2 (version autodock 4.2.6, released in 2009) [79]. DR hydrogens were added and Kollman united atom charges were assigned. Hydrogens were also added to ligand and Gasteiger-Marsili was used to calculate charges. Before docking an energy grid was created using Autogrid (version autogrid 4.2.6, released 2009) with a box-size varying with the times step and ligand. For each docking simulation 100 independent Lamarckian genetic algorithm (LGA) runs were performed with the number of energy evaluations set to 10.000.000, the population size set to 200 and the maximum number of generations set to 27.000. Default settings were maintained for the rest of the parameters. Docked conformations within a root mean square deviation (RMSD) of 2 Å were clustered. The most populated and lowest energy cluster was used for conformational binding analysis. To find the local energy minimum of the binding site with a limited search space to that region, a low-frequency local search method was used. The 100 conformations obtained from docking were clustered by low-energy and RMSD. The top-ranked conformations within the best 3 clusters were visually inspected. The docking parameters were not changed for any ligand, only the residues treated as flexible in the docking protocol differed between the ligands. To choose the same ligands in each DR model, the Ballesteros and Weinstein numbering (B&W numbering) was applied in advance [94]. The flexible residues for each DR model are summarized in Table 3.

Table 3 - Flexible residues used in the molecular docking different ligands.

Ligand	Flexible residues in B&W numbering
7-OH-DPAT	D3.32, S5.42, S5.43, S5.46, W6.48, F6.51, F6.52, H/N6.55
Apomorphine	D3.32, C3.36/3.35, S5.42, S5.43, S5.46, W6.48, F6.51, F6.52, H/N6.55
Aripiprazole	D3.32, W6.48, V3.33, S5.42, S5.43, S5.46, Y7.43, H/N6.55
Bromocriptine	D3.32, C3.36/3.35, S5.42, S5.43, S5.46, W6.48, F6.51, F6.52, H/N6.55
Chlorpromazine	D3.32, W6.48, S5.42, S5.43, S5.46, H/N6.55, C3.36, F6.51
Clozapine	D3.32, V3.33, C3.36, S5.42, S5.43, S5.46, W6.48, H/N6.55
Dopamine	D3.32, S5.42, S5.43, S5.46, W6.48, F6.51, F6.52, H/N6.55
Eticlopride	D3.32, W6.48, S5.42, S5.43, S5.46, H/N6.55, Y7.43, F6.51, F6.52
Haloperidole	D3.32, W6.48, F6.51, F6.52, C3.36, V2.57, S5.42, S5.43, S5.46
Nemonapride	V2.57, D3.32, S5.42, S5.43, S5.46, W6.48, F6.51, F6.52, Y7.43
Risperidone	D3.32, W6.48, C3.36, H/N6.55, V2.57, S5.42, S5.43, S5.46
SCH23390	D3.32, W6.48, S5.42, S5.43, S5.46, H/N6.55, F6.51, F6.52
SKF38393	D3.32, W6.48, S5.42, S5.43, S5.46, H/N6.55, F6.51, F6.52
Spiperdone	D3.32, W6.48, S5.42, S5.43, S5.46, C3.36, H/N6.55, V2.57
Sulpiride	D3.32, W6.48, S5.42, S5.43, S5.46, H/N6.55, Y7.43, F6.51

3.1.7 Analysis of Molecular Docking

In this study, 15 DR ligands were docked to the snapshots at 55-100 ns of each DR simulation (825 dockings in total). All distances between the center of mass of the ligand and the alpha-C-atom (Cα) of the residues, treated as flexible in the docking protocol, were calculated using PyMOL (version 1.7.4.5 Edu). In addition, for each ligand a different set of flexible residues in the binding pockets of the DR were selected according to experimental and computational data [14], [70], [84], [95]–[97] as well as previously published work [71].

3.2 Case Study 2: Ghrelin Receptor

3.2.1 Homology Modelling

Homology modelling was performed to obtain 3D structure model of ghrelin receptor. Four templates were used, each one to represent a functional state: inactive (4BUO)

[98], pre-activated (4XEE) [99], G-Protein activated (3SN6) [100] and β-Arrestin activated (4ZWJ) [101]. Model of A204E mutant, which results in absence of constitutive activity [37], was also constructed for pre-activated model.

Before starting homology modelling protocol, the original sequence was shortened at N- and C- terminal following Hou et al [102]. MODELLER 9.19 [59] was used to do the alignment and model construction. Structural constraints such as transmembrane domains (TMs) and disulphide (SS) bonds were defined. TM definition from the work of Hou et al was used. One SS bond was defined between residues 81-163 and represents the highly conserved disulphide bond involving extracellular loop 2 (ECL2). One hundred models were built for each template.

Table 4 - Set of TMs used for construction of GHSR1a models.

Segment	Hou et al.
TM1	6-33
TM2	41-67
TM3	79-110
TM4	125-144
TM5	171-210
TM6	218-252
TM7	262-290
Hx8	-

The overall homology and TMs homology values between the target sequence and the templates used are listed below. These values were obtained with a multiple sequence alignment tool, Clustal Omega [45].

Table 5 - Homology values between each template and GHSR1a whole sequence and only TM sequence. The values were obtained using Clustal Omega.

PDB ID	Description	Homology (%)	Hou et al. TM(%)
4BUO_A	Thermostable Agonist-bound Neurotensin Receptor 1	35.6%	42.3%
4XEE_A	Active-like Neurotensin Receptor	34.8%	40.7%
3SN6_R	The Beta2 Adrenergic Receptor-Gs Protein Complex	24.1%	24.7%
4ZWJ_A	Rhodopsin Bound To Arrestin	21.4%	24.6%

The homology levels are much higher in the templates used for inactive and pre-activated state. The homology values when using 3SN6 and 4ZWJ as templates are slightly lower when compared to standard values used in homology modelling and as expected these values were higher comparing only the TM regions part of the sequences. Nevertheless, these two structures constitute the only available templates for active form of GPCRs with the best homology values for GHSR1a.

Model evaluation and selection was performed first according to DOPE score [63] and molpdf. The z-score, provided by ProSA was used for error recognition, as it indicates overall model quality with respect to an energy distribution derived from random conformations for globular proteins [64]. The scores achieved with ProQ, the LGscore [66] and MaxSub [103] were set as base for the evaluation of the models. Furthermore ProQ allows to include secondary structure information calculated with PSIPRED to improve model quality up to 15%. The best structures according to these scores were then visually analysed using PyMOL. A set of structural features reported in literature were considered during model visualization and selection. This special care was taken because of the uniqueness of this receptor: its high constitutive activity. Regarding this characteristic there's an aromatic cluster in the inner face of the receptor (TMVI and TMVII) that is essential for this constitutive activity. Also models with α-helix in the ECL2 were discarded since there's evidence in the literature that interferes with the constitutive activity of the receptor [104].

3.2.2 Mutant Model

Pre-active mutant was built with PyMOL wizard mutagenesis tool [105] using selected models shown in the previous step. Residue 204, an Alanine, was substituted for a Glutamate, to produce the A204E mutant that is known to decrease constitutive activity of GHSR1a.

3.2.3 System Setup

Pre-active and the respective mutant were subjected to molecular dynamics inside a bilayer lipid membrane. Before setting up the system, the two models were subjected to PPM server to calculate spatial orientations respecting to the Membrane Normal defined by the Z-axis [72]. In addition, the state of titratable residues was calculated with Propka 3.1 at a pH of 7.0 [73].

The prepared receptor structures were inserted into a simulation box with dimensions of 11 x 11 x 9 nm. The box was previously constructed with a lipid bilayer of POPC:Cholesterol (9:1) and explicitly represented water and subjected to a 10ns simulation. Insertion of the receptors in the membrane was performed with g_membed [74] package of GROMACS 4.6.7 [75], [76] . Finally, sodium and chloride ions were added to neutralize the system until it reached a total concentration of 0.15M. Final system included approximately 370 POPC, 40 Cholesterol, 110 sodium ions, 13 chloride ions and 230000 water molecules.

.

3.2.4 MD simulation forcefield parameters

CHARMM36 parameter set for protein molecules and salt ions was used, as well as, the CHARMM TIP3P model for water [77]. POPC and Cholesterol parameters were generated using CHARMM-GUI Membrane Builder [4], [78], [79].

3.2.5 MD simulation protocol

MD simulations were performed with the periodic boundary condition to produce isothermical-isobaric ensembles using GROMACS 5.1.1. [80]. The PME method was used to calculate the full electrostatic energy of a unit cell in a macroscopic lattice of repeating images. Temperature was regulated using the Nosé-Hoover thermostat at 310.15K. Pressure was regulated using the Tarrinello-Rahman algorithm. The equations of motion were integrated using leapfrog algorithm with a time step of 2 fs. All bonds involving hydrogens atoms within protein and lipid molecules were constrained using the LINCS algorithm.

Prior to MD simulation, systems were relaxed to remove any possible steric clashes by a set of 50000 step of Steepest Descent energy minimization. Equilibration was performed after as follows: the system was heated using Nosé-Hoover thermostat from 0 to 310.15K in the NVT ensemble over 100 ps with harmonic restraints of 1000 kJ/mol nm^2. Then systems were subjected through a first step of NPT ensemble of 200ps with semiisotropic pressure coupling and a pressure of one bar. Further equilibration was performed with sequential release of membrane lipids and proteins' atoms with a final step of NPT ensemble with harmonic restraints on the protein of 1.0 $kJ/mol.nm^2$, for a total of 1.25 ns of restrained equilibration.

Then an independent simulation was initialized from the final snapshot of the restrained equilibration from each system. Two replicates were produced of 1 μs each. For a total of 4 μs of MD simulation.

4 RESULTS and DISCUSSION

4.1 Case Study 1: Dopamine Receptor

4.1.1 <u>Homology modeling</u>

For evaluation of the model quality, different metrics and scores were used to choose the most accurate models provided by MODELLER in order to perform MD and molecular docking. Molpdf and DOPE [63] scores are MODELLERS standard metrics and were utilized in combination with visual inspection to rule out models which were not calculated correctly. It should be noted, that molpdf and DOPE are not absolute measures, but help to rank the calculated models. While molpdf is simply the sum of a given set of restraints [106], DOPE is spefic for a given target sequence, e.g. it accounts for the finite and spherical shape of native protein states with the lowest free energy [63]. Then out of a small set of potential candidates (selection of 5-10), Pro-SA and ProQ analysis determined the final models with the best combination of scores, for the reason that the achievement of a single acceptable score in one metric did not automatically lead to a good score in the other metrics. While for the z-score provided by ProSA-web analysis values arround - 4 are suggested as acceptable, the ProQ analysis (LGscore and MaxSub) provides absolute measures. Regarding the LGscore, values > 3, for MaxSub values > 0.5 are considered as "good". If secondary structural data was included using the PSIPRED webserver [68] the scores improved. All final DR models (Table 6) achieved LGscores > 4 and MaxSub scores > 0.5. The highest z-score was obtained for the D4R model, whereas the lowest were counted for the D_1-like DR models. In summary, scores seemed appropriate to continue with the models in molecular dynamics.

Table 6 - Metrics and scores of the DR homology models.

DR	LGscore	LGscore +PSIPRED	MaxSub	MaxSub +PSIPRED	z-score
D_1R	2.533	4.257	0.175	0.529	-2.14
D_2R	2.520	4.215	0.205	0.517	-2.22
D_3R	3.144	4.191	0.270	0.553	-3.12
D_4R	3.326	4.247	0.249	0.594	-3.90
D_5R	2.595	4.142	0.150	0.570	-1.49

4.1.2 Molecular docking

After applying the models to MD, docking studies were performed with 15 different ligands targeting the DR. The results of the molecular docking were evaluated by AutoDock4.2., which ranks the possible binding positions by energy level and clusters these positions by RMSD of 2 Å. In addition the total number of conformations in these clusters were counted. Overall docking performance showed, that ligands have different receptor specific affinities which seems also to be related to the time points, dependent on the receptor state (all results of the docking can be reviewed in Appendix 1-5)

Dopamine was selected as reference ligand, since it is the endogenous agonist on all DR and it also showed the best docking performance with low binding energies and a high number of conformations (Error! Reference source not found.). For a general o verview, binding poses with more than 5 conformations per cluster were considered as a valid ligand position, despite the binding energy of this pose. Regarding the docking of dopamine it can be stated that the binding energy on the D2R was the most stable at time points, while for the other subtypes oscillated over the time. For example the binding energy on the D4R decreased at time points 85 and 90 ns and increased at 95 and 100 ns, although all D2-like subtypes have similar affinities for dopamine [107]. The highest number of conformations during all time points were obtained for the D4R and D2R, however for D3R no top cluster had less than 5 conformations. Regarding the D1-like subtypes, the D1R binding energy was more diverse, with the lowest binding energies at time points 75 and 90 ns of all DR. Moreover more conformations per cluster were counted for the D1R compared to the D5R in total, but the D5R only had 2 clusters with less than 5 conformations. For all DR and dopamine the first or the second cluster with the lowest binding energy contained the highest number of conformations over all time points, indicating that the docking of dopamine is stable and reliable.
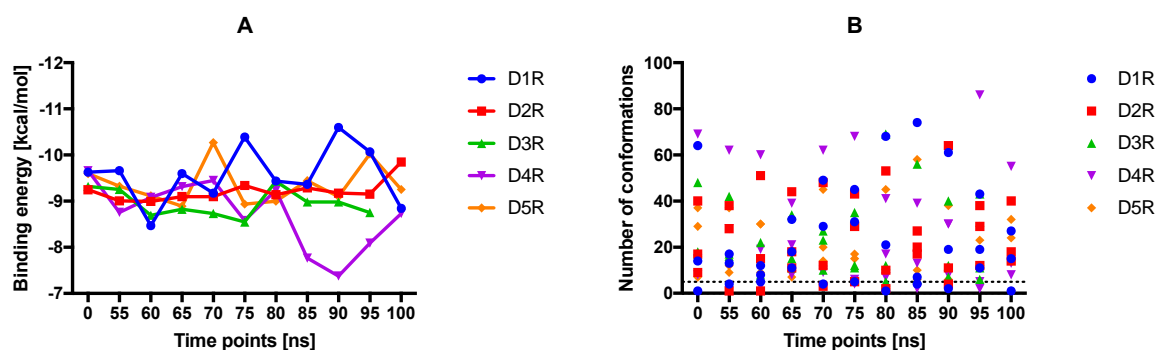
Figure 2 - Results of the molecular docking of dopamine for all DR subtypes at all time steps. For the binding energy (A) the mean of the 3 lowest energies of dopamine was calculated. In B the number of conformations of the three clusters with the lowest binding energies are shown for each time point and receptor.

The binding position of dopamine at all DR seemed stable over time, which is also in line with the average binding energy and number of conformations for each DR. Moreover, it was visible that interacting residues of the OBP are an aspartic acid on TM3 (D3.32) and the three serines on TM5 (S5.42, S5.43 and S5.46). As known from literature dopamine's interaction with the serine microdomain only requires two of the serines binding to the hydroxy groups [70], this was also observed in the docking at all DR over all timepoints. For the D1R a full time scale of the binding positions of dopamine is summarized in Figure 3. It was visible, that the position of dopamine was stable over the time, with a switch in interaction with the serine microdomain, however S5.43 was always one of the binding partners. Furthermore, the only movement observed, was a slight rotation of the benzene ring.

Similar results were obtained for the D2R (Figure 4). In comparison to the D1R, the hydroxyl binding with the serine microdomain was more directed to the S5.42 for time points 0 – 60 ns, after that continued interaction with S5.46 was observed, while S5.43 was always interacting. Similarly, this tendency was observed at the D3R (Figure 5). Lastly, for the D3R at 100 ns, dopamine was no longer located in the binding pocket but more outside the receptor, leading to high positive binding energy values.

The docking of dopamine to the D4R, also showed overall interaction with D3.23 and the serine microdomain, although no time dependent tendency for a certain serine was observed (Figure 6). Interestingly, at time point 100 ns the benzene ring of dopamine was located already almost outside the binding pocket. Lastly, the docking of dopamine to the D5R revealed to be the most rigid binding over the time, as only slight torsions of the benzene ring of dopamine were observed over time, while the ethylamine moiety showed more movement (Figure 7).

In sum, dopamine docking to the all DR subtypes, interaction with D3.32 and the serine microdomain was observed and the binding position was stable over the time which is expressed in a low binding energy and a high number of conformations. Lastly, the eminent decrease in binding energy for the D4R at time point 90 ns, seemed not to affect the binding position of dopamine. Only the docking of dopamine at 100 ns for the D3R had to be excluded from analysis, since the ligand was located outside the receptor and lead to highly positive binding energies. Moreover, these results correspond to what is observed in literature for dopaminergic binding, such as the strong interaction of the D3.32 with the protonable amine of dopamine and the binding switch of dopaminergic hydroxyl groups between the three serines (S5.42, S5.43 and S5.46) [70], [108]. According to Floresca and Schetz, these features are crucial for Dopamine's binding affinity and DR activation [70]. Therefore it seemed appropriate to consider the molecular docking results of dopamine as control data for the results of the other ligands.

D₁R - Dopamine
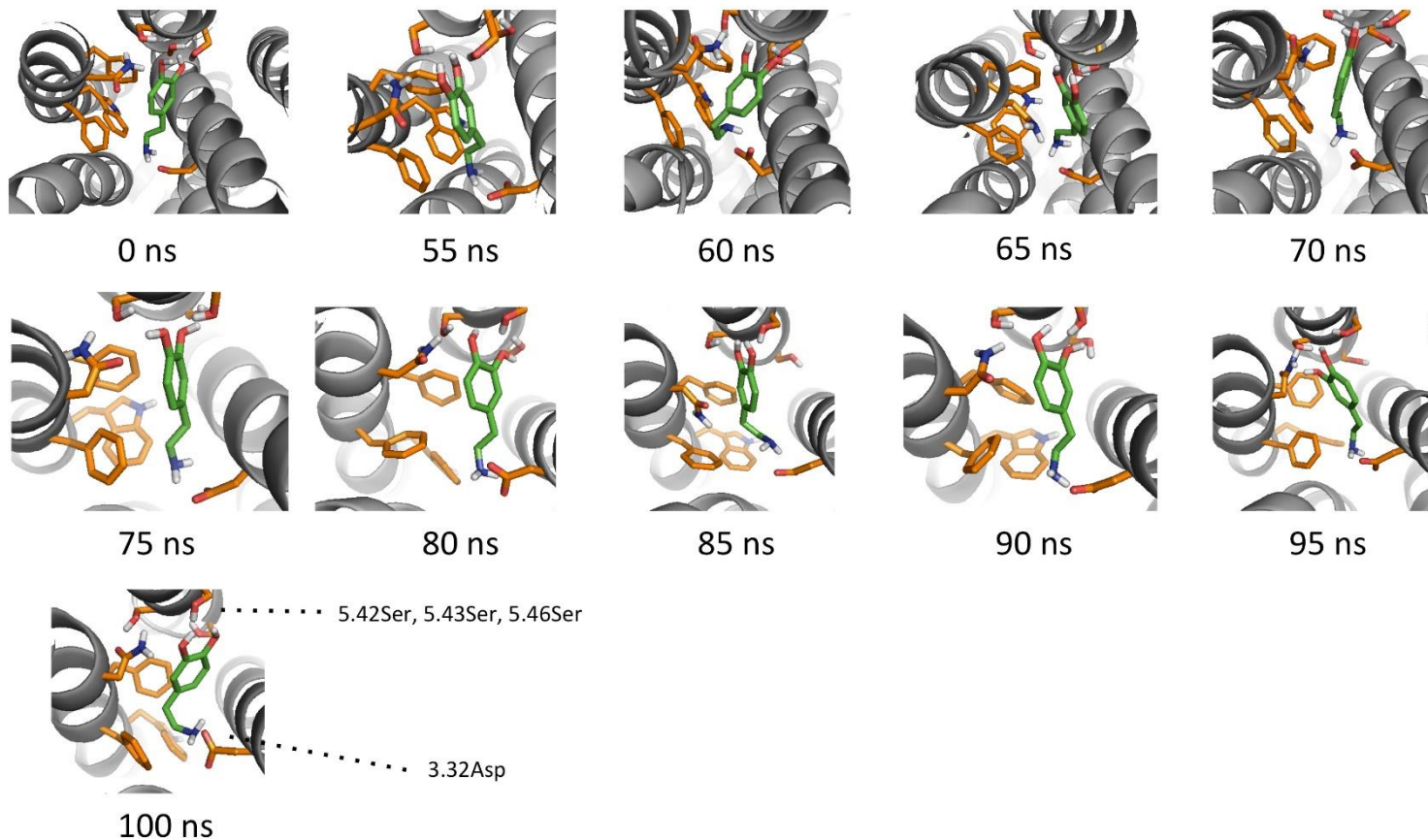
Figure 3 - Molecular docking of Dopamine at the D1R. The images correspond to the cluster with the lowest binding energy [kcal/mol] and highest number of conformations. Dopamine is color-coded green, while the interacting residues of the orthosteric binding pocket are orange. Oxygens are red, nitrogens are blue and hydrogens white. Over time, the binding position of dopamine seems stable. Interacting residues of the binding pocket are the three serines (S5.42, S5.43 and S5.46) on TM5 binding to the hydroxyl groups and an aspartate on TM3 binding to the amine of dopamine (D3.32).

D₂R - Dopamine

0 ns   55 ns   60 ns   65 ns   70 ns

75 ns   80 ns   85 ns   90 ns   95 ns

5.42Ser, 5.43Ser, 5.46Ser

3.32Asp

100 ns

Figure 4 - Molecular docking of Dopamine at the D2R. The images correspond to the cluster with the lowest binding energy [kcal/mol] and highest number of conformations. Dopamine is color-coded green, while the interacting residues of the orthosteric binding pocket are orange. Oxygens are red, nitrogens are blue and hydrogens white. Over time, the binding position of dopamine seems stable. Interacting residues of the binding pocket are the three serines (S5.42, S5.43 and S5.46) on TM5 binding to the hydroxyl groups and an aspartate on TM3 binding to the amine of dopamine (D3.32)

D₃R - Dopamine
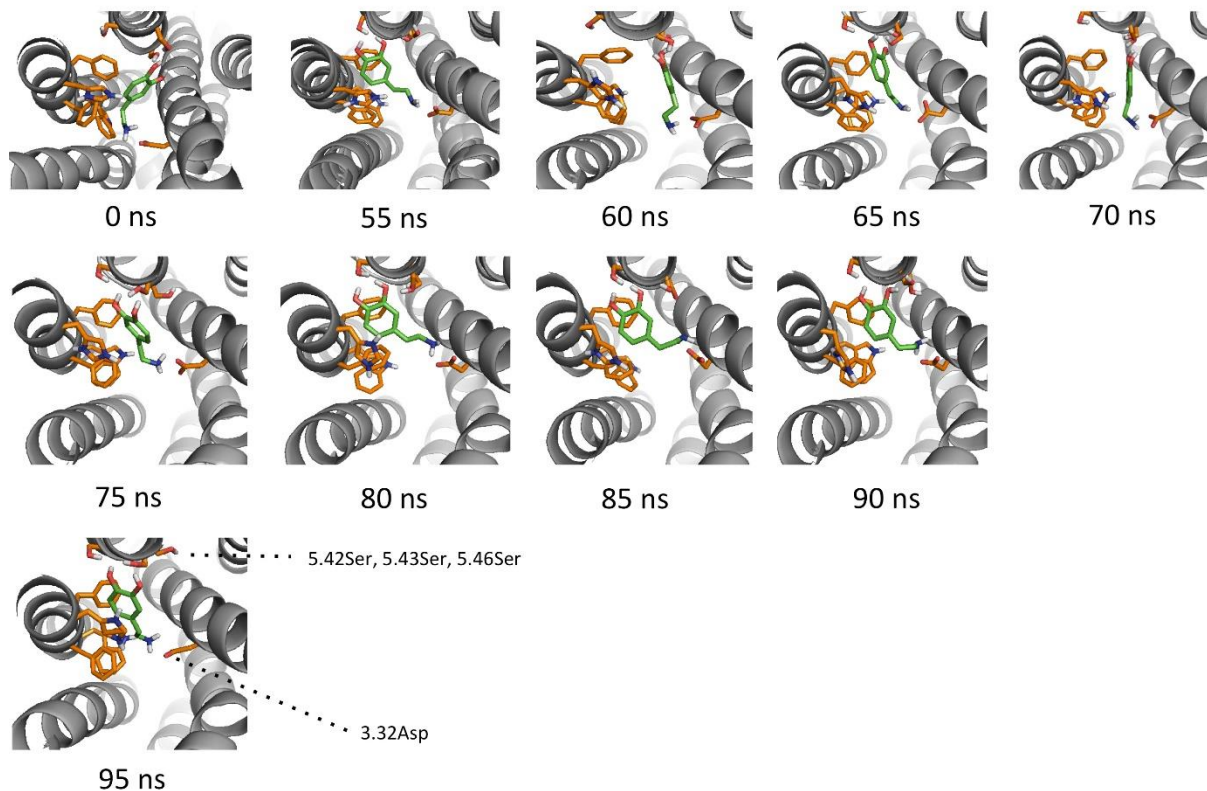
Figure 5 - Molecular docking of Dopamine at the D3R. The images correspond to the cluster with the lowest binding energy [kcal/mol] and highest number of conformations. Dopamine is color-coded green, while the interacting residues of the orthosteric binding pocket are orange. Oxygens are red, nitrogens are blue and hydrogens white. Over time, the binding position of dopamine seems stable. Interacting residues of the binding pocket are the three serines (S5.42, S5.43 and S5.46) on TM5 binding to the hydroxyl groups and an aspartate on TM3 binding to the amine of dopamine (D3.32). Noteworthy, the docking with the D3R at 100 ns resulted in positive binding energy values and dopamine was located outside the previous defined grid box in the AutoDock4.2. docking set up. Therefore these values were excluded from analysis.

D₄R - Dopamine
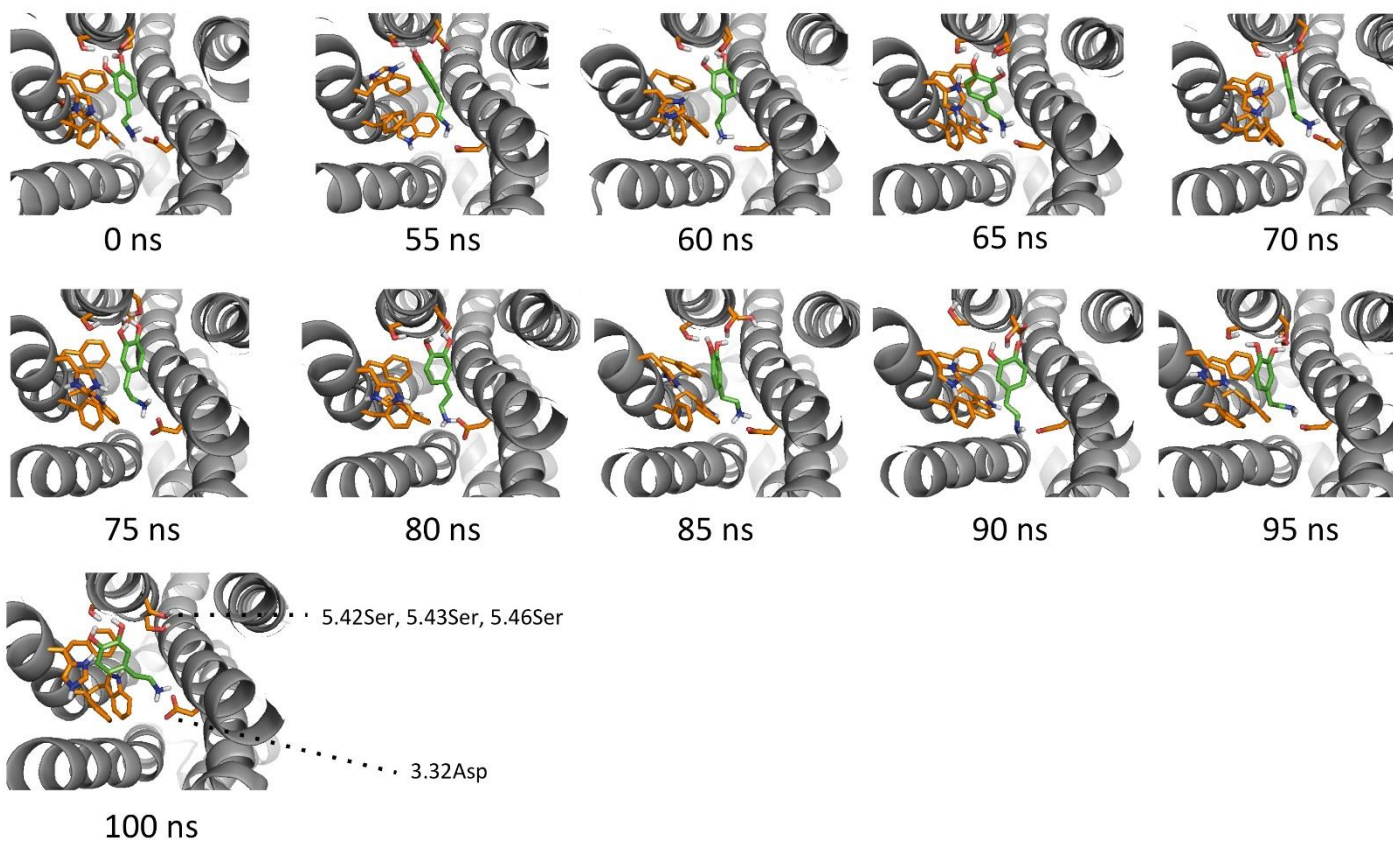
Figure 6 - Molecular docking of Dopamine at the D4R. The images correspond to the cluster with the lowest binding energy [kcal/mol] and highest number of conformations. Dopamine is color-coded green, while the interacting residues of the orthosteric binding pocket are orange. Oxygens are red, nitrogens are blue and hydrogens white. Over time, the binding position of dopamine seems stable. Interacting residues of the binding pocket are the three serines (S5.42, S5.43 and S5.46) on TM5 binding to the hydroxyl groups and an aspartate on TM3 binding to the amine of dopamine (D3.32).

D$_5$R - Dopamine
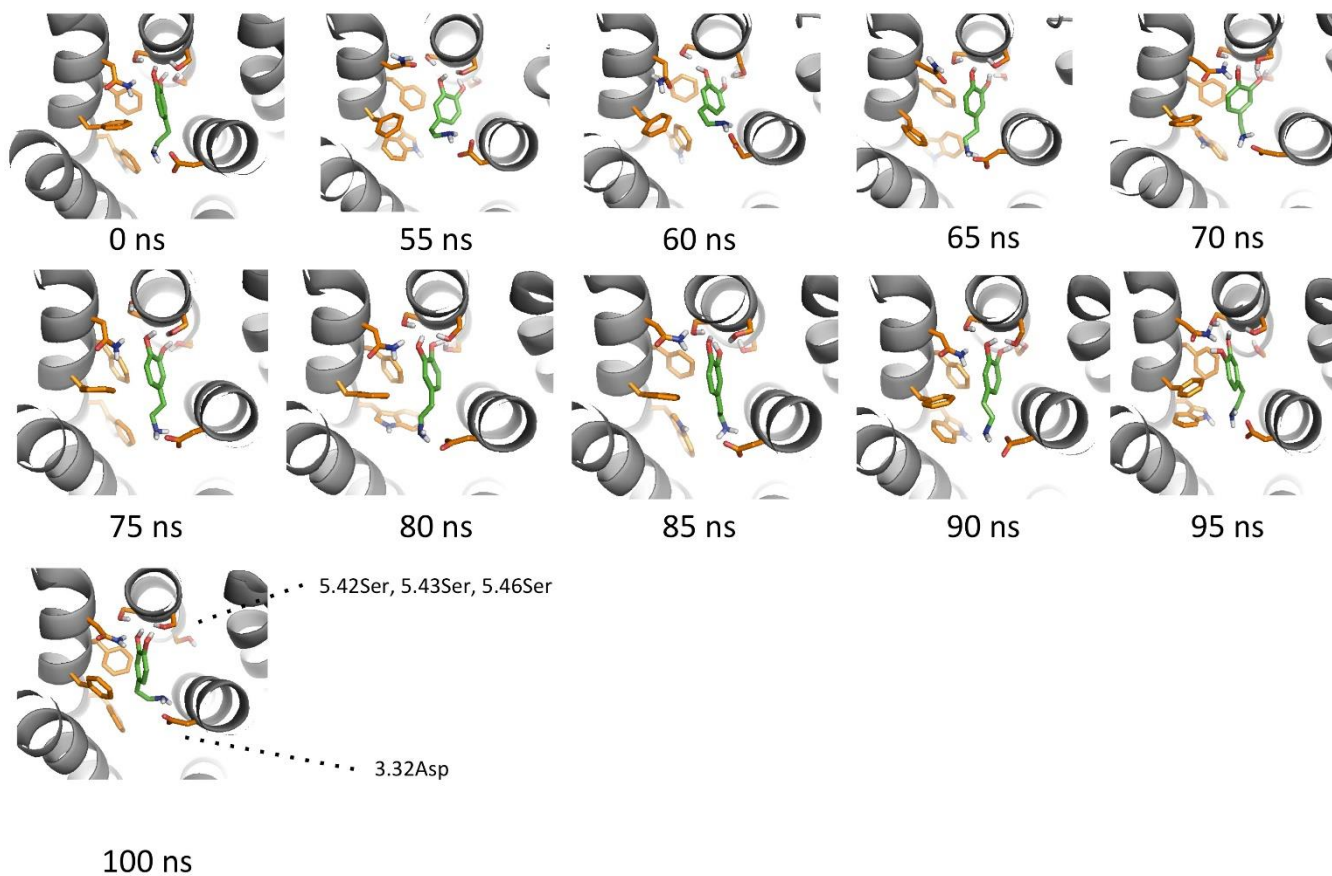
Figure 7 - Molecular docking of Dopamine at the D5R. The images correspond to the cluster with the lowest binding energy [kcal/mol] and highest number of conformations. Dopamine is color-coded green, while the interacting residues of the orthosteric binding pocket are orange. Oxygens are red, nitrogens are blue and hydrogens white. Over time, the binding position of dopamine seems stable. Interacting residues of the binding pocket are the three serines (S5.42, S5.43 and S5.46) on TM5 binding to the hydroxyl groups and an aspartate on TM3 binding to the amine of dopamine (D3.32).

The set, which was chosen for binding consisted out of an array of selective and non-selective ligands. Since non-selective agonistic activity at the DR was already covered by dopamine docking, Chlorpromazine was chosen to consider antagonistic activity at all DR [109], [110]. For reviewing subtype selective binding actions following ligands were selected: SKF38393 as selective D1R agonist [23], [25] and SCH23390 as D1R antagonist [26], [111], Apomorphine as selective D2R agonist [108], 7-OH-DPAT as selective D3R agonist [18] and Nemonapride as D2R and D3R selective antagonist [112] and lastly Haloperidol, due to its affinity for D4R [20]. The obtained binding energies and number of conformations in these clusters are summarized in Figure 8 (graphical output of the other ligands can be found in the Appendix 6).

For 7-OH-DPAT the lowest binding energy was counted at the D1R for all time steps. In addition the binding energy was stable over time. This was also observed for D4R and D5R. On the contrary for the D2R a distinct increase in the binding energy was observed at 60 ns and for the D3R at 100 ns. By visual inspection of these time points it was observed for the D3R that only the dipropylamino moiety was located inside the binding pocket pointing towards the serine microdomain. This was also observed for one cluster of the 7-OH-DPAT binding to D2R at 60 ns, but the others were located more outside the binding pocket possibly leading to these decreased binding energies. Regarding number of conformations, most were counted over the time for D3R (except at 100 ns which was excluded from analysis) and some for D2R.
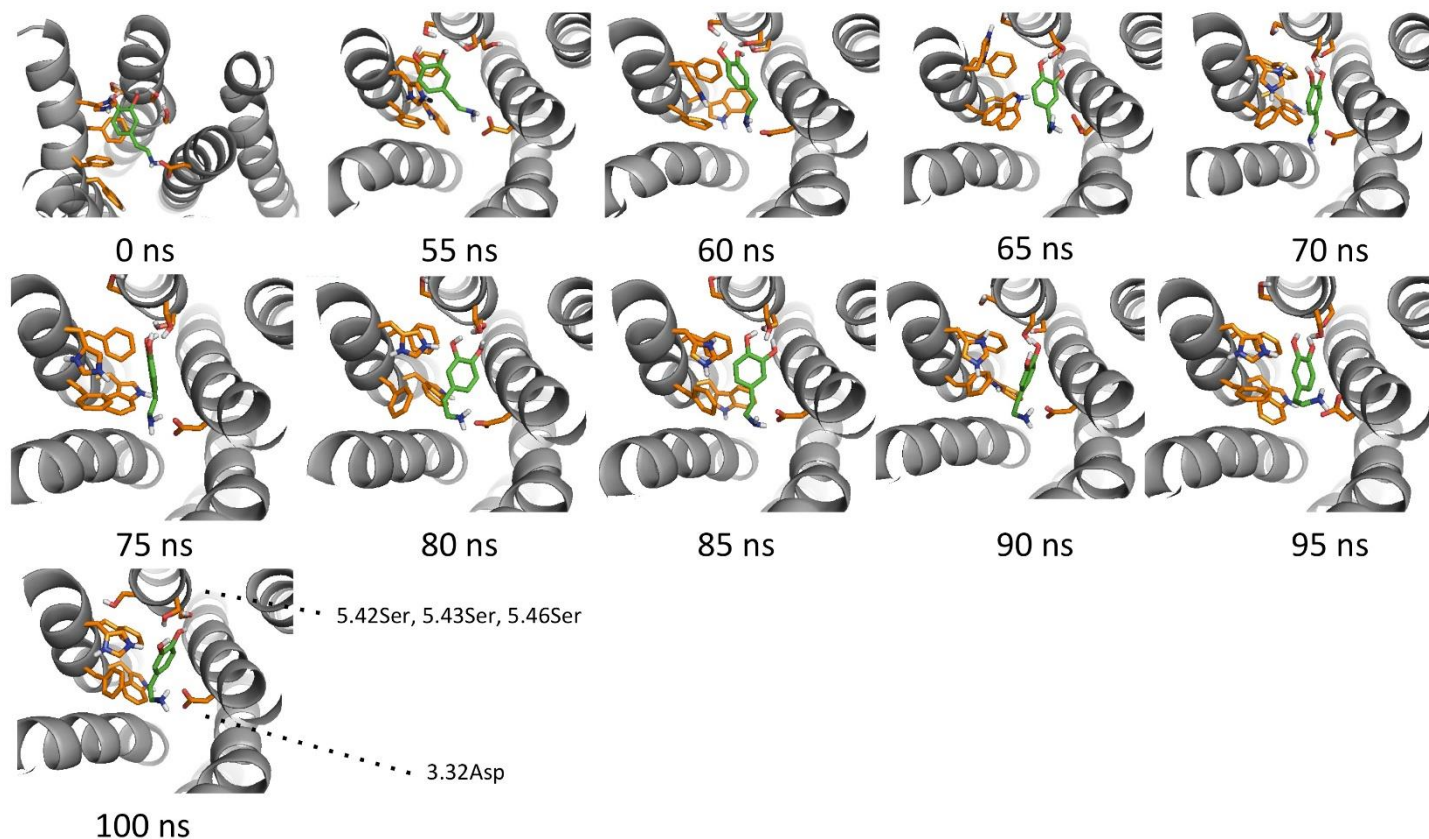
For Apomorphine lowest binding energies were obtained for the D1R and D2R, and a decrease in the binding energy was determined for the D4R at 85 ns. The most conformations were obtained for D5R (with over 60 at 70 ns).

For Nemonapride in total the binding energies between the DR subtypes were similar, except for D5R at 100 ns, where a broad decrease was observed. Compared to the other ligands a relatively low number of conformations were counted in the clusters of all DR for Nemonapride. The highest number was obtained for D2R at 80 ns with over 40.

SCH23390, the D1R antagonist displayed a constant binding energy around 10 kcal/mol at all DR subtypes over time and interestingly highest number of conformations was counted for the D4R at 0, 70 and 90 ns compared to the other DR. At the D1R the highest number of conformations was obtained at 75 ns with around 40.

For SKF38393 binding energies were found to be more diverse: While for the D1R a decrease at 60 ns was observed, in total the lowest binding energy was counted for D5R, especially at 65, 70 and 80 ns. Regarding the number of conformations, most were counted for D1R at 70, 75 and 90 ns, and for D3R at 80 and 85 ns.

The docking performance of the D4R-selective Haloperidol was significantly different for D4R compared to the other DR subtypes: While the binding energy dramatically

decreased at 55 and between 75 and 95 ns, the most number of conformations was counted for D4R. For the other DR subtypes the binding energy was stable over the time around 10 kcal/mol.

Lastly, Chlorpromazine also displayed constantly similar binding energies at all DR subtypes. Only a decrease of the binding energy was counted for D1R at 70 ns. In addition also the number of conformations was similar for all DR over the time with slightly more conformations for the D1R.
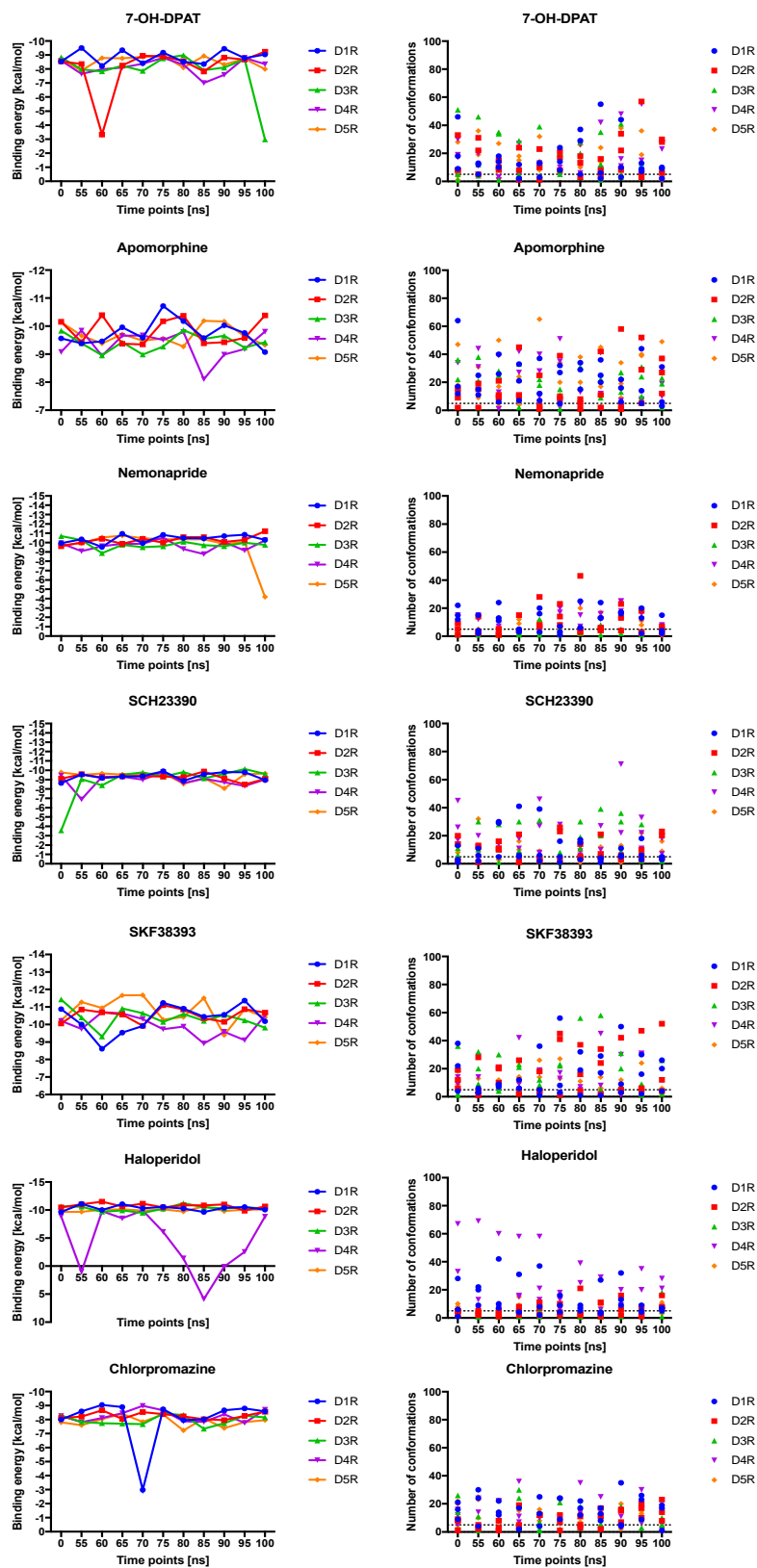
Figure 8 - Results of the molecular docking of 7-OH-DPAT, apomorphine, nemonapride, SCH23390, SKF38393, haloperidol and chlorpromazine for all DR subtypes at time points [ns]. For the binding energy (left graph) the mean of the 3 lowest energies of dopamine was calculated. For the number of conformations (right graph) of the three clusters with the lowest binding energies are shown for each time point and receptor.

4.1.3 Distances between ligands and interacting residues

For additional evaluation of the docking performance and determination of ligand interactions within the residues of the binding pocket, the distance between the center of mass of the ligand and the alpha carbons of these residues was measured. Overall results of all ligand-residues measurement show, that the average distance between certain residues and ligands was similar in all DR subtypes. For example the distance between D3.32 and ligands was arround 6 Å at all DR. However, subtype specific tendencies were observed, for example the distance between the ligands and S5.43 had tendency to decrease compared to the other serines in D1R and D4R, while this was not the case for the rest of the DR.
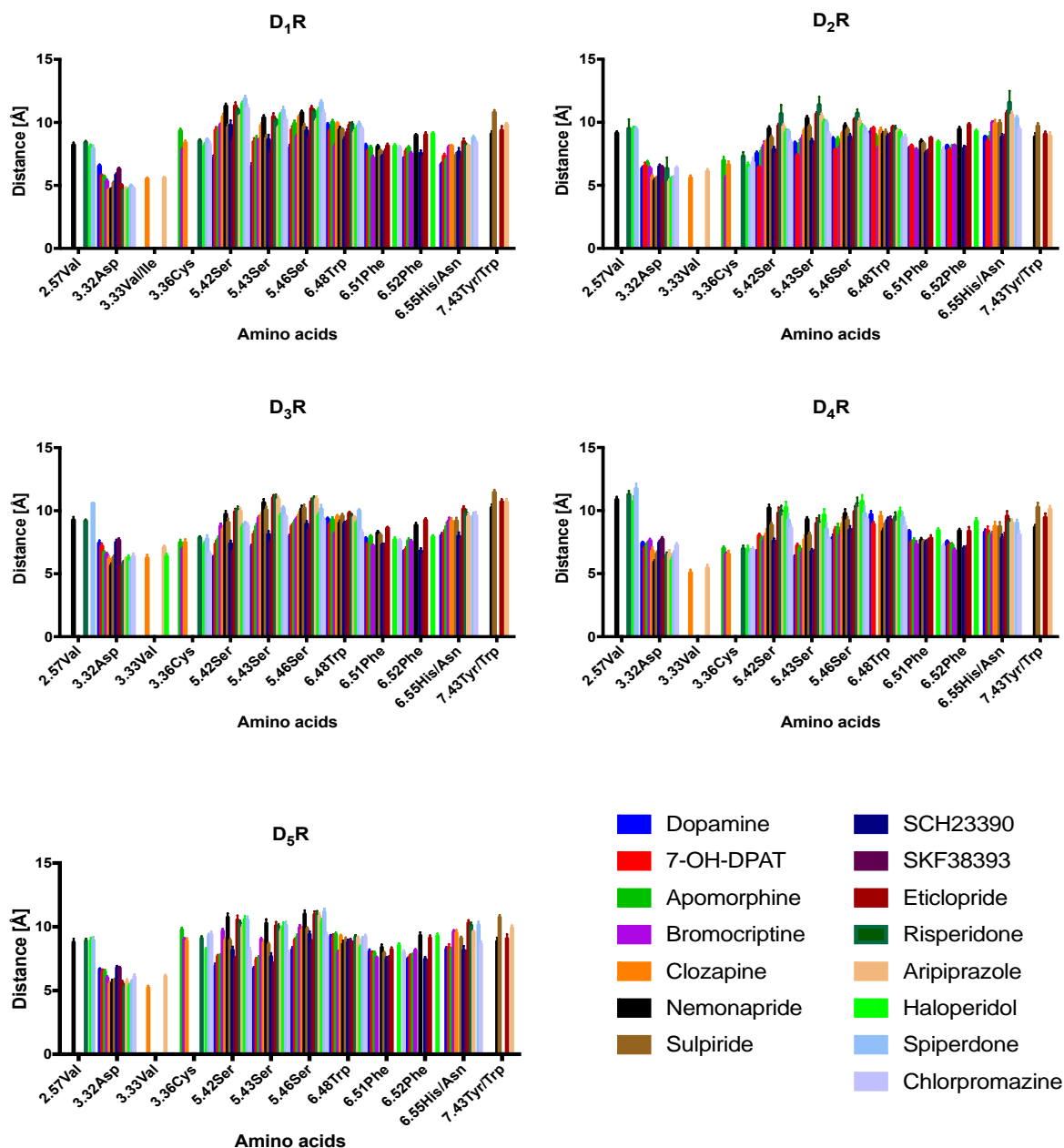
Figure 9 - Summary of the distances between ligands and residues used in molecular docking for all DR subtypes. For each ligand-residue-distance [Å], the mean and SEM of all time points (11) of the three best docked clusters ranked by binding energy [kcal/mol] was calculated. Noteworthy is that not all ligands were set to interact with all residues shown in the x-axis in the molecular docking. For example only Clozapine and Aripiprazole were set to interact with V3.33.

When comparing those residues to the all ligands that were docked (Figure 10), D3.32 showed to have the closest ligand interaction, but not for all ligands at all subtypes, while the other residues were more distant but all in the same range. The distance between D3.32 and SKF38393 was particularly increased at D3R, D4R and D5R. Also the distance between SCH23390 and D3.32 was tendentially increased, but not at the D1R. This effect might occur due to the fact, that SCH23390 and SKF38393 are reported to be D1R-selective [25], [111]. Moreover, at the D4R an increase in the distance between D3.32 and several ligands was noted.
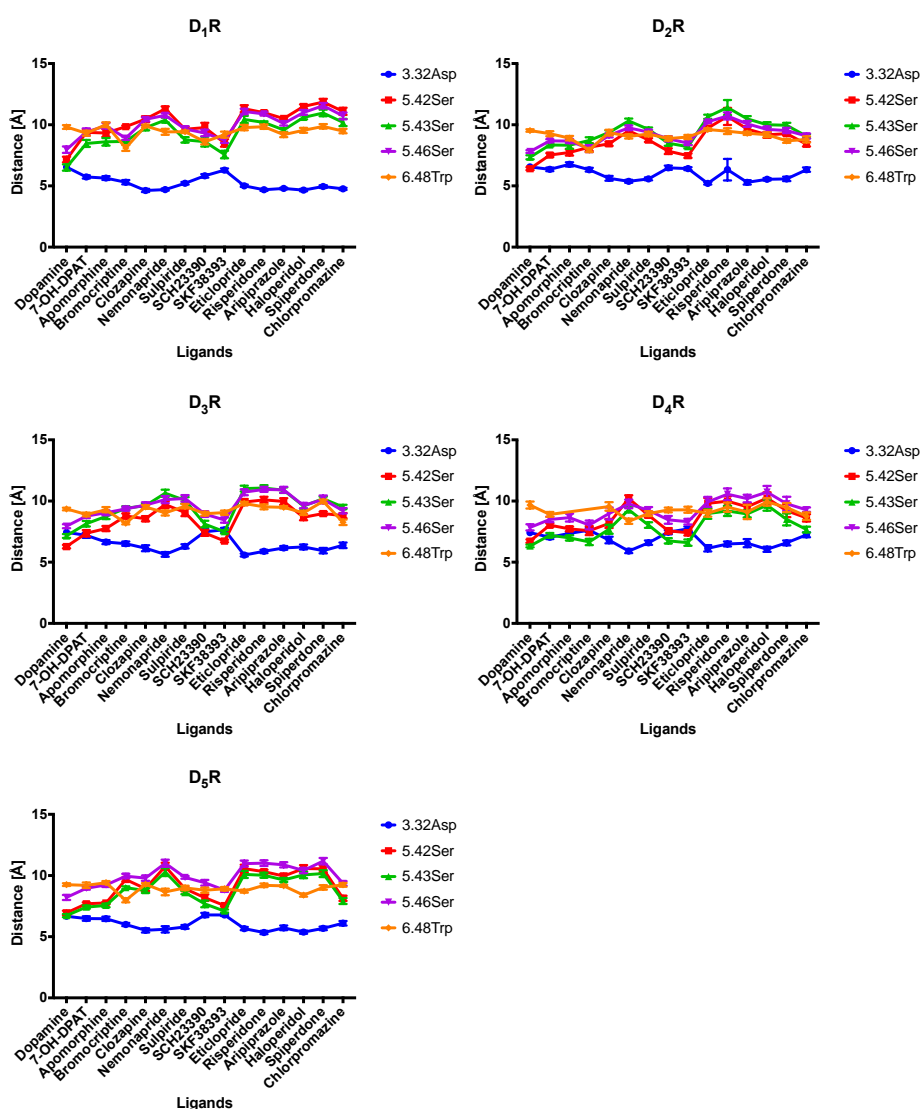
Figure 10 - Comparison of the distances between ligands and common residues. In all docking approaches residues D3.32, S5.42, S5.43, S5.46 and W6.48 were chosen to interact with the ligands, since they are known to be crucial for DR activation. For each ligand-residue-distance [Å], the mean and SEM of all time points (11) of the three best docked clusters ranked by binding energy [kcal/mol] was calculated.

Other effects such as the closest distance for all residues were observed in Dopamine and SKF38393 dockings, while Spiperdone was most distant at the D1R, D4R and D5R. On the other hande, risperidone was further away at the D2R while this happened for eticlopride, risperidone and aripiprazole at the D3R.

Lastly, the results of the distance measurement of the residues were clustered into the mechanism of action of the ligands (Figure 11). The cluster consisted of ligands which had an affinity for all DR: Dopamine, Spiperdone, Chlorpromazine, Clozapine, Sulpiride and Risperidone. The results underline, that Dopamine is the closest to the conserved residues of the binding pocket (D3.32, S5.42, S5.43, S5.46 and W6.48) at all DR, while Risperidone is the farthest. It is noteworthy that Dopamine is an agonist at the DR while Risperidone an antagonist [84].
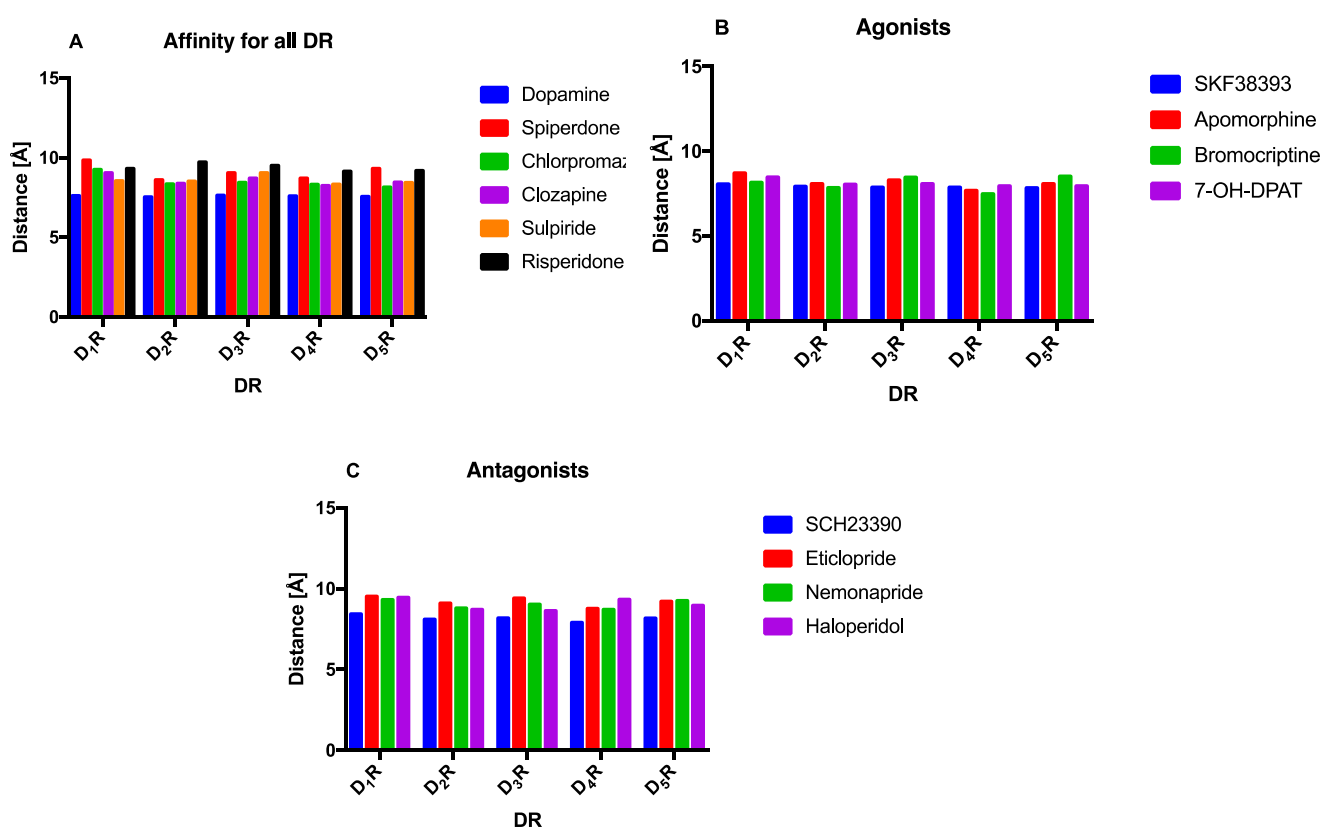
Figure 11 - Comparison of distances between the most conserved residues of the DR binding pocket (D3.32, S5.42, S5.43, S5.46 and W6.48) and ligands, sorted by their function on the DR subtypes. The mean between residues D3.32, S5.42, S5.43, S5.46 and W6.48 for the ligands at all time points for all DR subtypes.

Spiperdone was most distant to the D2-like and closer to the D1-like, while Chlorpromazine, Clozapine and Sulpiride showed no differences in distances between the DR.

SKF38393, Apomorphine, Bromocriptine and 7-OH-DPAT were clustered as selective agonists and compared to each other among the DR (Figure 11). For SKF38393 no difference between the DR subtypes was observed as well as for 7-OH-DPAT, while the distance between Bromocriptine and the conserved ligands was decreased at the D4R as well as Apomorphine. Regarding the antagonists and their distance between the most conserved residues of the DR binding pocket, SCH23390 was found to be the closest of the antagonists. In comparison Eticlopride was found to be the most distant especially at the D3R. Nemonapride binding seemed to be located close the D2R binding pocket compared to the other subtypes, while Haloperidol was the most distant at the D_1-like DR.

Ligand and receptor specific differences in binding (measured in distance between ligand and residues) was observed for the conserved amino acids of the DR binding pocket: D3.32 S5.42, S5.43, S5.46 and W6.48.

4.1.4 Binding affinity with CSM-lig

For prediction of the binding affinites for the ligands towards the DR subtypes CSM-lig webserver was used [113]. In detail, CSM-lig uses the protein-ligand environment of the binding site from the molecular docking to extract physiochemical properties and structural signatures [113]. The predicted affinity, which is the output of this algorithm trained with data sets of the PDBbind [114], is expressed as $-\log_{10}(K_D/K_i)$, e.g. the fraction of the equilibrium dissociation constant of a substrate and inhibitor of the receptors, which is also an epxression for pK_D or pKi [115]. Therefore a high binding affinity corresponds to a high pKi (or pK_D). Overall results of the prediction show, the predicted binding affnity (BA) were higher than the experimentally determinded BA (Figure 12). It was visible that, Dopamine had the lowest binding affinity at all DR (highest BA at D4R and lowest at D2R). In contrary bromocriptine was predicted to have the highest binding affinity at all DR. Ligands affinity towards all DR such as Spiperdone, Chlorpromazine, Clozapine, Risperidone and Sulpiride displayed also a similar BA at all DR. Subtype specific differences were observed between SCH23390 and SKF38393. For D1R, D3R and D5R the affinity towards SCH23390 was higher than for SKF38393, whereas for D2R the affinity was similar. Lastly D4R showed the BA towards SKF38393 was higher than for SCH23390.
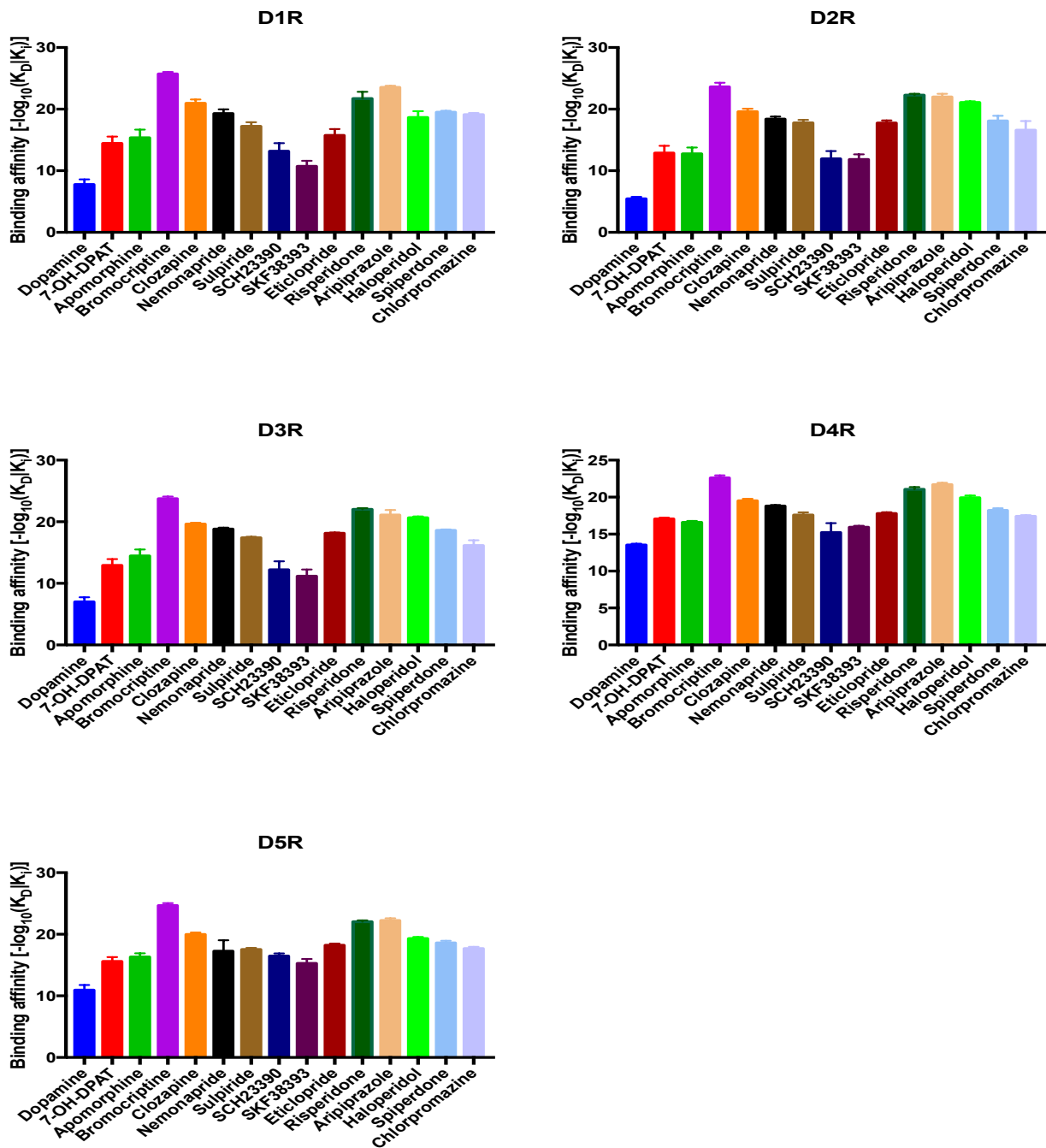
Figure 12 - Binding affinity –log10(KD/Ki) predicted by CSM-lig web server for the ligands at the DR. Mean and SEM over all time points were calculated for each ligand at all DR subtypes.

The predicted values were compared to binding affinity data from literature (Error! R eference source not found.). All in all, it was visible that the predicted values were 2-fold higher than the experimental binding affinities. However, when comparing the value range between the ligands themselves, the predicted values were also found to be in the same range as the experimentally determined binding affinities.

Table 7 - Comparison between predicted binding affinities calculated with CSM-lig and experimental data from literature. The results obtained from CSM-lig are expressed – log10(KD/Ki) which corresponds to pKi/pKD values and therefore directly comparable. Moreover the predicted binding affinites are the mean of all time points at the three best docked positions. The values obtained from literature are marked with references.

Ligand	D₁R			D₂R			D₃R			D₄R			D₅R		
	P	E	Ref	P	E	Ref	P	E	Ref	P	E	Ref	P	E	Ref
Dopamine	7.8	4.3-5.6	[116],[117]	5.4	5.3–6.4	[118],[119]	7.0	6.4–7.3	[119]–[122]	13.5	7.4-7.6	[118],[123]	10.9	6.6	[116]
7-OH-DPAT	14.4	5.3	[83]	12.9	5.6–7.6	[120],[121],[124],[125]	12.9	7.1-9.6	[19],[120]–[122],[124]–[126]	17.1	6.2	[83]	15.6		
Apomorphine	15.3	5.3-6.2	[116],[117]	12.7	5.7–7.6	[119]–[122],[127],[128]	14.5	6.1-7.7	[119]–[122],[127],[128]	16.6	8.4	[127]	16.3	6.4–7.8	[116],[127]
Bromocriptine	25.7	6.2	[116],[127]	23.6	7.3-8.3	[119],[120],[122],[127]	23.8	7.1–8.2	[119],[121],[122],[127]	22.6	6.4	[127]	24.7	6.3	[116],[127]
Clozapine	20.9	6.9	[116]	19.6	5.8–6.9	[119],[120],[124],[128]–[130]	19.6	5.2–6.3	[119],[121],[128]	19.5	7.5	[131]	20.0	6.6	[116]
Nemonapride	19.3			18.4	10.9	72	18.8	9.2–10.3	[124],[130],[132]	18.8	10.0	[133]	17.3		
Sulpiride	17.2	5.5	[83]	17.8	6.3–8.2	[119],[120],[128],[130]	17.4	6.4-8.1	[119]–[121],[128],[130]	17.6	5.7–7.7	[130],[134]	17.6	5.3	[83]
SCH23390	13.2	9.5	[135]	11.9	5.3	[120]	12.2	6.1	[83]	15.2	5.5	[83]	16.5	7.5–9.5	[116],[126]
SKF38393	10.7	6.2-6.8	[116],[117]	11.8	6.8	[83]	11.1	5.3	[83]	15.9	6	[83]	15.5	7.0	[116]
Eticlopride	15.7			17.7	9.2	[124],[130]	18.1	8.8	[124],[130]	17.8	7.0	[136]	18.2		
Risperidone	21.7	8.4	[70]	22.3	9.4	[137]	22.0	7.0	[138]	21.1			22.0		
Aripiprazole	23.6	6.4	[82]	22.0	7.4-9.7	[118],[139],[140]	21.1	8.0	[82]	21.7	7.3	[118]	22.2	5.9	[82]
Haloperidol	18.6	7.6-8.2	[116],[129]	21.1	7.4-9.4	[119],[120],[124],[128],[130],[138],[141],[142]	20.7	7.0-8.6	[119],[121],[128],[129],[142]	19.9	8.7–8.8	[129],[131],[142]	19.3	6.3	[116]
Spiperdone	19.5	6.7	[116]	18.1	8.4-10.2	[119],[124],[130],[138],[143]–[145]	18.6	9.9	[119],[144],[145]	18.2	9.3-9.5	[112],[123],[136]	18.6	5.3	[116]
Chlorpromazine	19.1	7.1	[116]	16.6	7.0–7.6	[119],[120],[128]	16.1	7.2–7.5	[119],[121],[128]	17.4	7.8	[131]	17.7	6.9	[116]

4.2 Case Study 2: Ghrelin Receptor

4.2.1 Homology Modelling

Models for GHSR1a were built for four different activation states. Model selection was performed with a set of scores as described in Methods section. Values of these scores for the ten best models for each activation state are displayed in the Appendix 7-10. Scores for the active models were expectably lower due to small percentage of homology between target and template. Nevertheless it was still possible to produce models for these functional states with good scores.

 After selecting the 10 best models through scoring functions the models were visually inspected to discard models with incompatible structural features for GHSR1a high constitutive activity. Top, front and bottom images of the models are shown in Figure 13. As expected the different models showed varying spacial arrangement of the transmembrane domains. The inactive and pre-activated are much closer to one another than the two active states. Pre-active model shows a slight open off the channel that is accompanied with some rotation of TM3 and TM5 compared to the inactive model. When comparing the first two models with the activated ones the most prominent difference is in the TM5-ICL3-TM6 section, which rotates outward of the middle axis of the receptor and gets much more elongated.
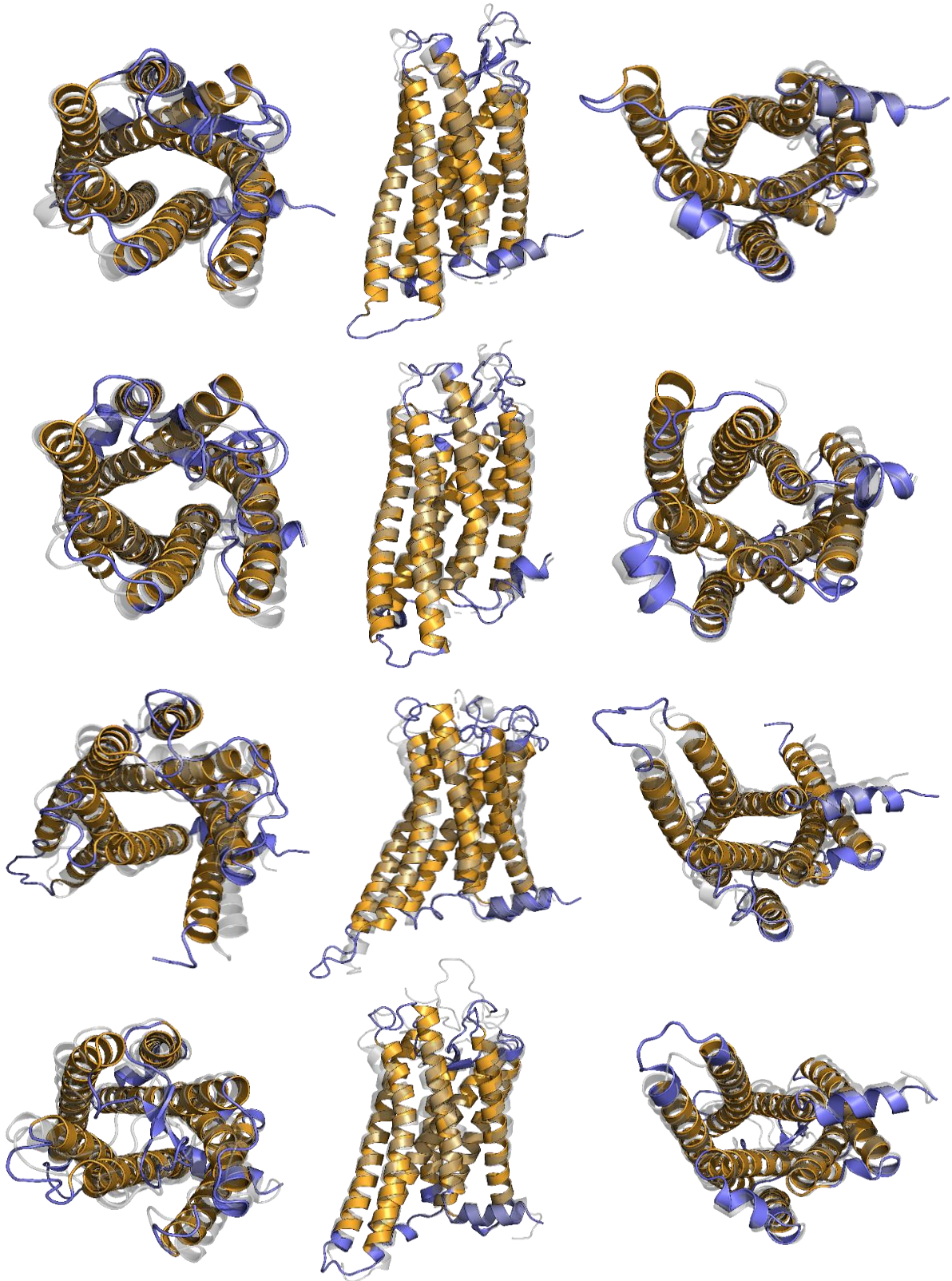
Figure 13 - GHSR1a models produced through homology modeling. First column corresponds to top view, second column to front view and third column to bottom view. Each line represents a different active state in the follow order: inactive, pre-active, G-protein coupled and Arrestin coupled. Transmembrane domains are shown as lightorange and connecting loops as lightblue. Silver shadow represents the template structure.

The differences observed between the inactive and active models produced in this step are in line with the literature in GPCR activation. As described in the Introduction section, the most crucial movements during GPCR activation are the disruption of the ionic lock and the opening of the water pocket in the core of the receptor. The differences in the transmembrane domains arrangement between the models reflect the movements caused by the events referred above. Further measuring the distances between the residues that constitute the ionic lock and the hydrophobic cage in the crystal used for template and in the models produced (Table 8) showed again that the models indeed corresponded to different activation stages. Inactive model distances are identical to the crystal structure with PDB ID 4BUO which corresponds to an inactive structure of neurotensin receptor. The crystal structure used as template for the pre-active state does not have the conserved DRY motif, thus distances measured in the model are characteristic of active state. This suggests that the pre-active model is identical in spacial arrangement to the active states, additionally the ionic lock is not present. This simple structural analysis indicates that produced models indeed represent the desired functional states.

Table 8 **–** Distances between C-α of residues from ionic lock and hydrophobic cage motifs from crystal structures 4BUO, 4XEE, 3SN6 and 4ZWJ and the models produced. The distances were calculated with PyMOL measurement wizard function. Values are in nm.

	Ionic Lock			Hydrophobic Cage	
	D/E3.49 **–** D/E6.30	R3.50 **–** D/E6.30	Y3.51 **–** D/E6.30	R3.50 **–** L3.46	R3.50 **–** L6.37
CRYSTALLOGRAPHIC STRUCTURES					
4BUO	1.46	1.21	1.38	0.85	0.88
4XEE	-	-	-	0.63	1.03
3SN6	2.27	1.90	1.99	0.63	1.19
4ZWJ	1.83	1.46	1.445	0.60	1.15
MODELS					
Inactive	1.52	1.20	1.30	0.62	0.88
Pre-Active	2.12	1.76	1.79	0.62	0.98
Active with G-Protein	2.59	2.22	2.18	0.63	1.09
Active with Arrestin	2.32	1.95	1.89	0.61	1.13

4.2.2 Molecular Dynamics Results

Based on a crystal structure of Neurotensin Receptor, a pre-active model of GHSR1a was constructed and used to set simulation systems. Additionally, based on the aforementioned model, a mutant (A204E) was constructed and also used for simulation. Each system was simulated for 1 µs with two replicates in a total simulation time of 4 µs. All replicates took at least 100ns to equilibrate which were discarded for analysis. The trajectories of the replicates were then concatenated. Analysis was performed on 1.8 µs of each system.

The average RMSD computed for the protein atoms shows that the two systems were very stable, with steady RMSD values of 0.481 ± 0.031 for wild-type model and 0.467 ± 0.029 for mutant model. The RMSD plots for both systems are presented in Figure 14.
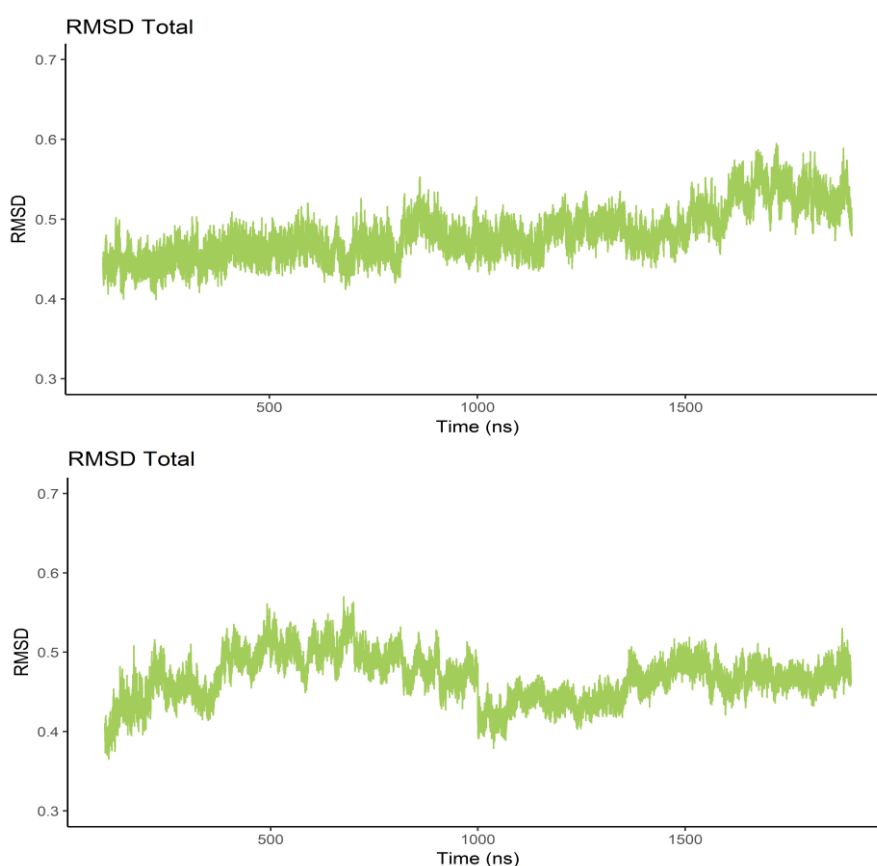
Figure 14 - Total RMSD of pre-active (top graph) and the respective mutant (bottom graph) throughout the simulation time.

As described earlier the GHSR1a has a high constitutive activity and the A204E mutant is known to impair this unique characteristic. To understand this effect at a structural and dynamical level typical GPCR activation movements were searched in the trajectories produced.

First, RMSD for each TM was computed in order to understand if there were differences in the amount of movement of TMs. Figure 15 show RMSD of each TM through time. In both models, TM5 and TM6 seem to move more than the other TMs, although the difference is much more accentuated in the WT model.

In Figure 16, RMSD value of each frame was plotted in a density graph to better perceive the differences in the graph aforementioned. This confirms the initial observation that TM5 and TM6 move more than the other domains. Also, in both models, TM3 and TM4 are the TMs with least movement. For the WT type TM5 and TM6 have a RMSD of 0.388 ± 0.043 and 0.317 ± 0.025 respectively, where TM3 and TM4 have RMSD values of 0.187 ± 0.013 and 0.222 ± 0.013. For the mutant model, RMSD are much closer: 0.198 ± 0.015 for TM3 and 0.322 ± 0.024.
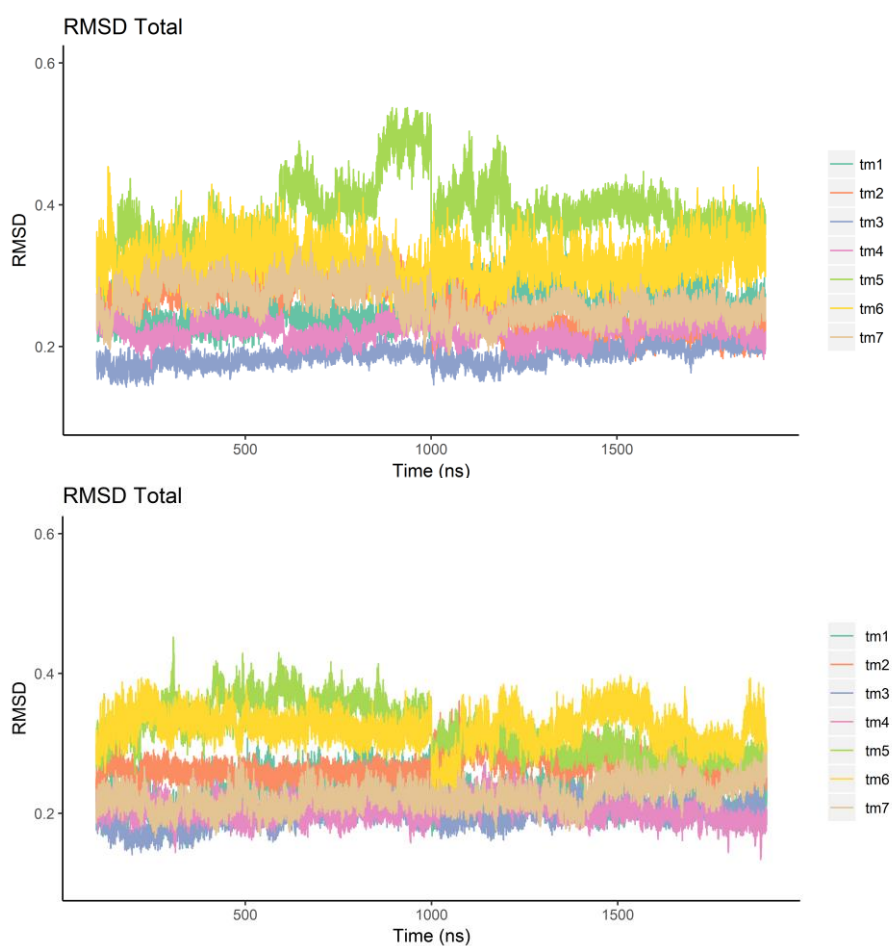
Figure 15 - Total RMSD of all seven individual TMs for the pre-active model and respective mutant throughout the simulation time.
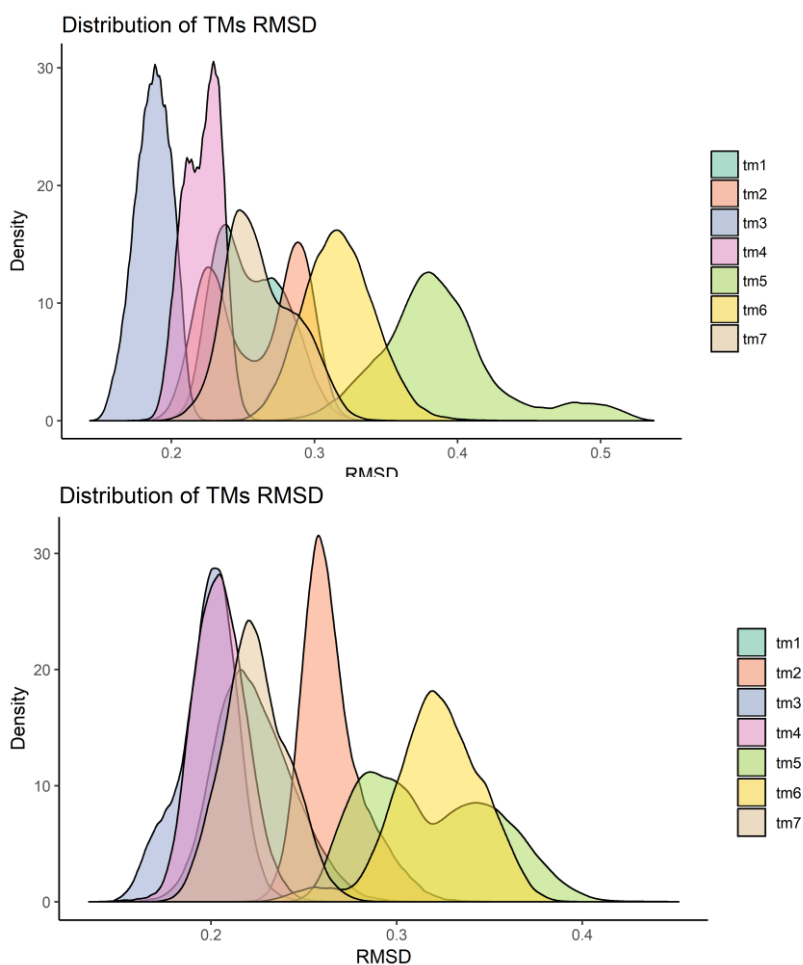
Figure 16 – Distribuition of TMs RMSD values throughout simulation time on WT model (top) and A204E (bottom).

To further understand these movements between TMs, distances between C_α of residues from activation motifs of GPCR were computed throughout the trajectory time. Below Table 9 shows the distances between residues of the activation motifs in the templates used and the average in the GHSR1a dynamics.

Table 9 **– Distances within the activation motifs' residues in crystallographic structures** and during the GHSR1a molecular dynamics simulations. Distances are in nm. Angles are in degrees.

	D/E3.49– D/E6.30	R3.50 – D/E6.30	Y3.51 – D/E6.30	R3.50 – L3.46	R3.50 – L6.37	CWxP
CRYSTALLOGRAPHIC STRUCTURES						
4BUO	1.46	1.21	1.38	0.85	0.88	40.00
4XEE	-	-	-	0.63	1.03	30.46
3SN6	2.27	1.90	1.99	0.63	1.19	70.44
4ZWJ	1.83	1.46	1.445	0.60	1.15	76.28
MOLECULAR DYNAMICS SIMULATIONS						
Pre-Active-WT	2.30 ± 0.14	1.86 ± 0.13	1.79 ± 0.12	0.64 ± 0.03	1.22 ± 0.10	62.45 ±12.64
Pre-Active-A204E	1.54 ± 0.46	1.37 ± 0.43	1.42 ± 0.46	0.66 ± 0.05	0.71 ± 0.23	53.32 ± 28.50

Ionic Lock

The first three columns present distances between the DRY motif and D/E 6.30 residue, which constitute the ionic lock. Distances in the WT are closer to the active crystal structures, indicating that the ionic lock was mainly disrupted throughout the whole simulation. In contrast the data from mutant simulation showed distances identical to the inactive crystal structure used in comparison. Nevertheless, throughout the simulation of the mutant no bond was formed between R3.50 and D/E6.30.

The distribution of the distances between these residues showed one clear state for WT (Figure 17). For the mutant the graphs show two peaks of distribution which indicates two different conformational states. The shorter distances are the most populated, however there's a smaller peak at the values of the WT. The second peak can represent the time that the receptor took from a pre-active state, that seemed very stable in the WT simulation, to the low activity/inactive structure. The mutant structure also visits distances higher than those of the WT.
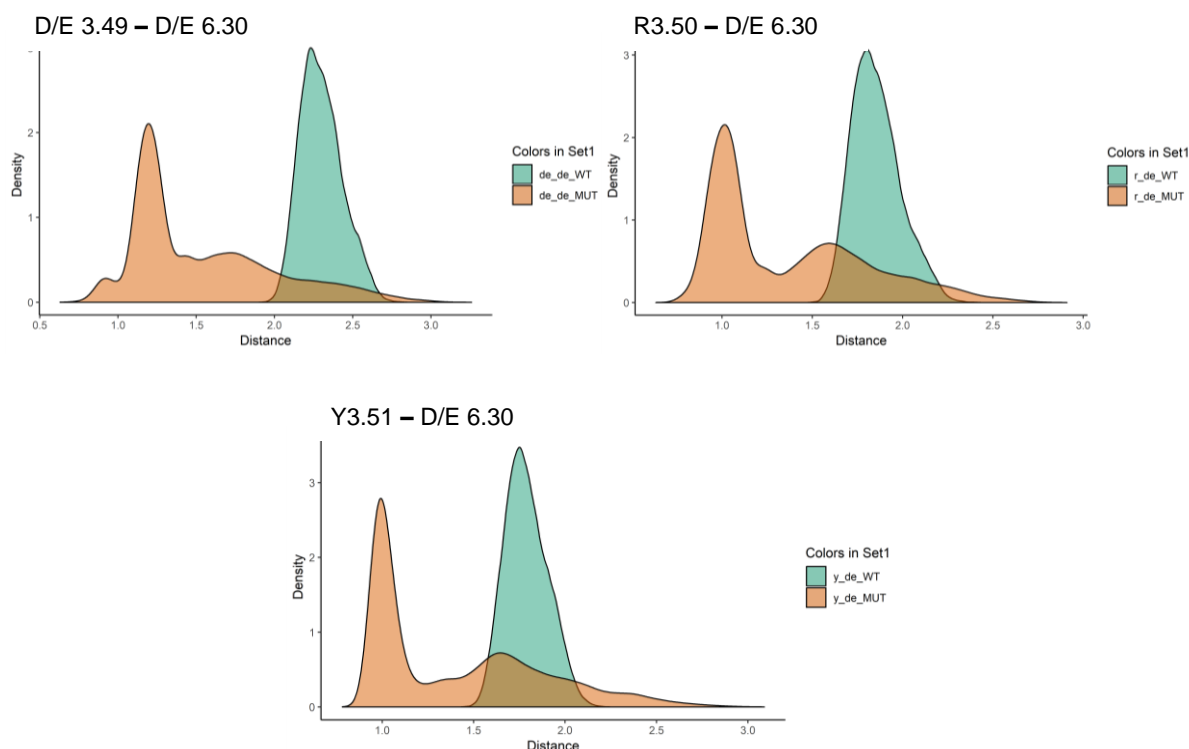
Figure 17 – Distribution of the distances between the residues of D/ERY motif and residue D/E 6.30 during the MD of WT and Mutant of GHSR1a. Distances are in nm.

Hydrophobic Cage

The next two columns represent the hydrophobic cage that is present in the core of many GPCRs. The distance from R3.50 – L3.46 shows that elongation of the TM3 is similar to the activated crystal in both WT and A204E mutant. R.350 – L6.37 distance average values from the WT simulation shows similar values to the activated crystals, where the values from the mutant simulation show similar values to the inactive crystal, following the same pattern as the ionic lock.

Analyzing the distribution of distances, the R3.50-L3.46 seems very stable in both models and the values around 0.65nm are similar to the activated structures. The distance between R3.50 and L6.37 shows completely different behaviour from the two models. WT is very stable around 1.22nm, which is similar to the active crystal structures used for comparison. A204E mutant showed smaller distances, resgistering two peaks, one at 0.5nm and the other at 0.9nm (Figure 18).

R3.50 - L3.46

R3.50 – L6.37
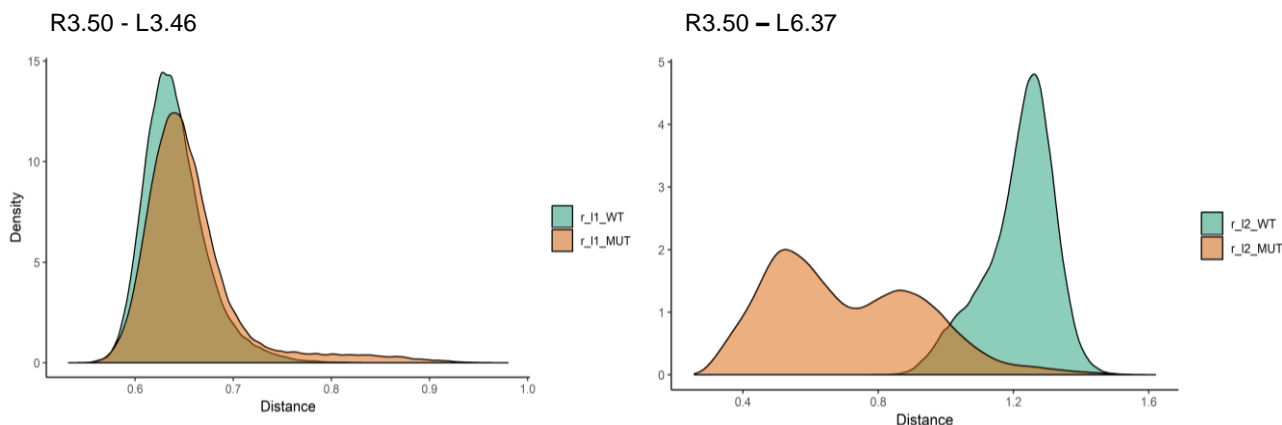
Figure 18 - Distribution of the distances within the hydrophobic cage. Distances are in nm.

GPCR activation is a complex process, that as not been describe in its entirety. However common pathways have been described analysing the experimental and computational data available. The disruption of the ionic lock and the opening of the water channel in the hydrophobic cage have been described as the two major events in the transition of the a receptor's inactive state to an active state. These two events drive the major structural rearrangements: the slight rotation and upward movement of TM3 and the outward rotation of TM6 away from the z axis of the receptor. MD of GHSR1a showed that the WT model maintained for the most part of the simulation distances values within the ionic lock and the hydrophobic cage similar to the active state values, whereas A204E mutant structure showed distances values similar to closed ionic lock and hydrophobic cage.

CWxP motif

The movement of CWxP angle facilitates the movement of TM6 away fro TM3 during activation. During activation , the kink present in TM6 decreases, elongating TM6 and allowing its movement. The crystal from active structure showed that the dihedral is more open,, i.e. the dihedral has higher values of angle degrees. Data from MD simulation s of GHSR1a showed a difference between the WT and A204E, where the first had an average of 62.45° and the second 53.32°. However the difference its as big as the one showed between inactive and active crystal structures.

To further understand the role of this motif distances between two pairs of residues.It has been shown that in inactive structures there is an interaction between C6.47 and 7.44/7.45 that generates a constraint and keeps N7.49 from interacting with D2.50. In active structures this interaction does not exist, leaving N7.49 free to interact with D2.50.

This suggests that C6.47 has an active role in the rearrangement of TM6/TM7 interface [146]. In light of this, distances between D2.50 and N7.49, and C6.47 and 7.45, were calculated to understand the relationship of this interactions in GHSR1a (Figure 19). The WT did not show differences between these two distances, as there was almost a complete overlap throughout the simulation. However A204E mutant showed some interesting differences. From 500ns to 1000ns distance between D2.50 and N7.49 increases and is kept higher than the C6.47-7.45 distance. This suggests that the interaction between these pair of residues has been interrupted. Snapshots from MD prove that theres no interaction between D2.50 and N7.49 during that period (Figure 20).
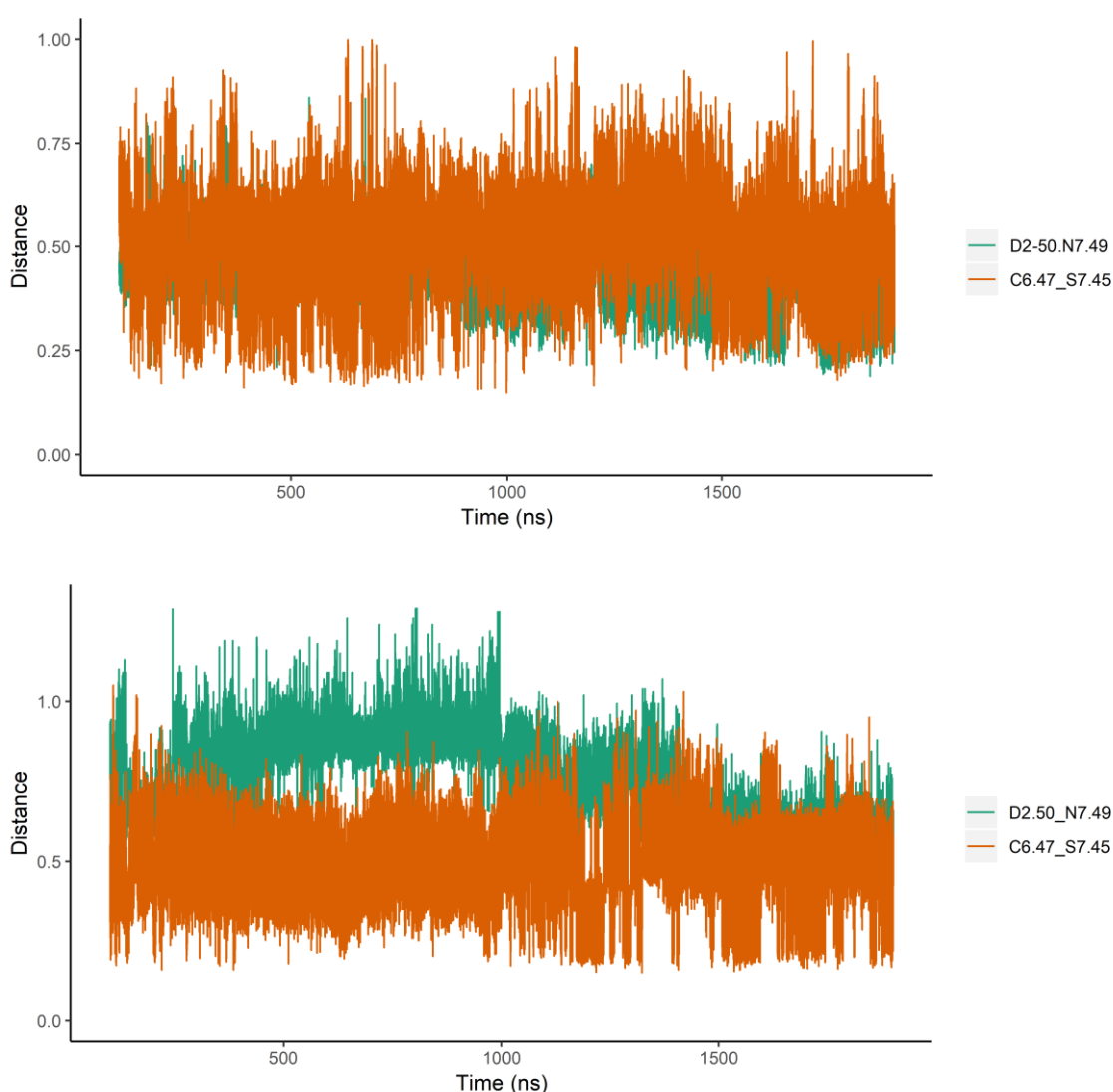
Figure 19 – Distances between D2.50 - N7.49 (green line) and C6.47 – 7.45 (orange line) during WT (top graph) and A204E (bottom graph) MD simulation.

t=100 ns   t=500 ns   t=1000 ns   t=1800 ns
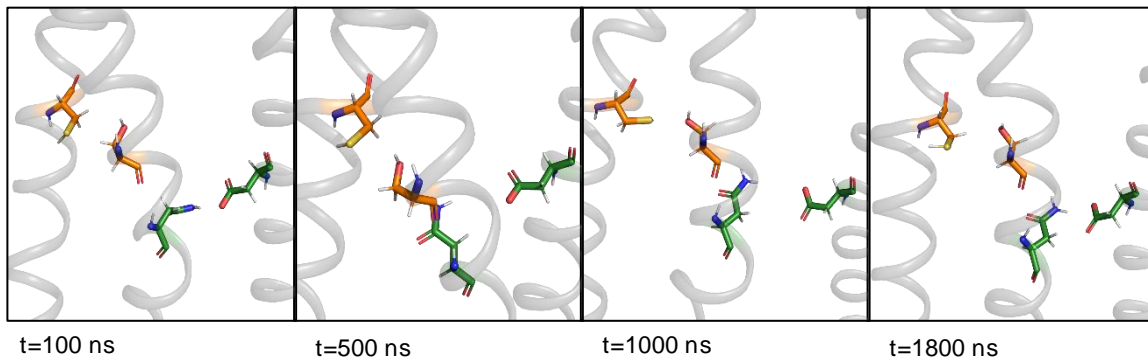
Figure 20 – Snapshots of C6.47 interactions in A204E model. Residues from left to righ in each snapshot: C6.47, 7.45, N7.49, D2.50. In the snapshots from 500 and 1000 ns the green pair are too far away to have any interaction.

Principal component analysis

To under the major movements from the two simulations, a principal component analysis (PCA) was performed for three components (Figure 21). For WT model, three first components described 54.4% of the whole trajectory. PC1 clearly separates all conformations in to two distinctive groups. PC2 and PC3 were not able to distinguish different conformations from PC1 results. A204E model had similar results: the first three components described 66.6% of the trajectory. PC1 was also able to identify two distinctive groups. PC2 and PC3 were again not successful in distinguish more conformations. In the next step, the two conformations obtained from PC1 were analyzed.
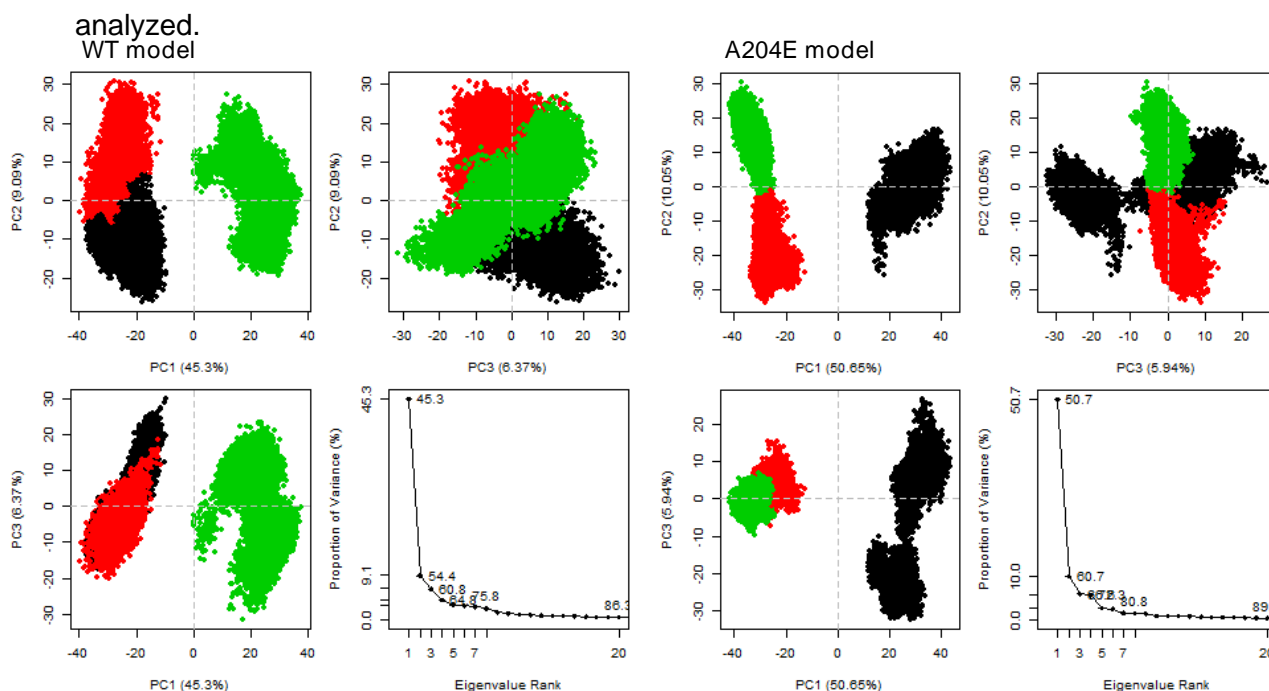
Figure 21 – Principal Component Analysis of the WT and A204E trajectories.

Conformations obtained from PC1 of WT model represent typical GPCR activation movements (Figure 22). The more noticeable are the outward movement of TM6 and the inward movement of TM7. Mutant conformations obtained from PC1 suggest the transition from a pre-active state to an inactive state with the outward movement of TM1, TM5 and TM7. TM6 had a slight inward rotation, closing the gap between TM3 and TM6 and closing the intracellular pocket.
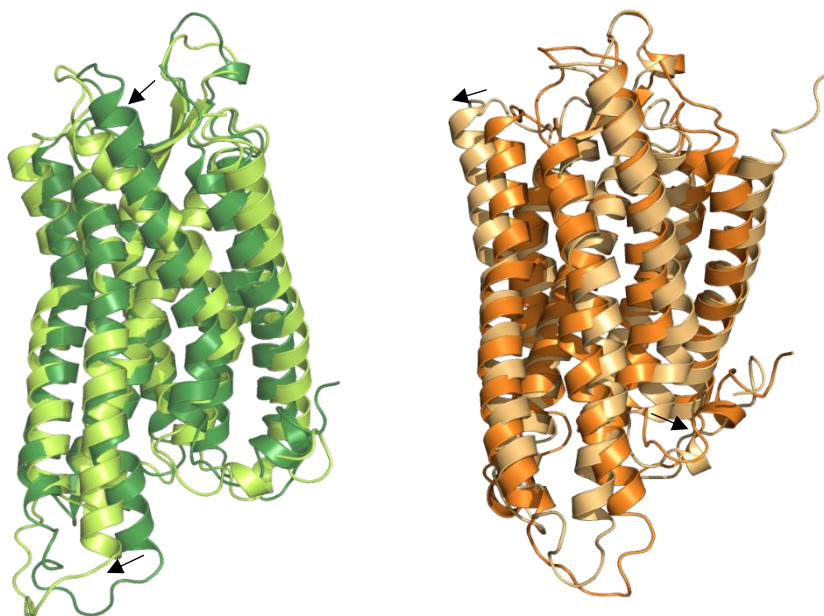
Figure 22 – Conformations of GHSR1a-WT (green) and GHSR1a-A204E (orange) that represent the two groups from PC1. Movements of WT model are typical of GPCR activation, with an outward movement of TM6 and slight inward movement of TM7. In opposition, the mutant model movements indicating transition from active to inactive state: outward movement of TM1,TM5 and TM7.

The data from GHSR1a monomer MD simulation is agreement with the literature available. The WT model was very stable with only slight refinement towards a more active-like conformations. Stability of the receptor is the final proof for the success of homology modelling protocol followed. A204E mutant was also very stable but with slightly more movement than WT. Data collected from A204E simulations showed the receptor transitioning to a inactive-like conformations. Ionic lock and hydrophobic cage reached an arrangement very similar to the inactive crystal used for comparison. Also, CWxP motif showed the disruption of the interaction between D2.50 and N7.49, typical of inactive state. This indicates that GHSR1a reaches an active-like state without the ligand through the common activation pathway of GPCRs.

5 CONCLUSIONS

Understanding GPCR structure and dynamics is crucial for development of new and better drugs for serious diseases like Parkinson's and Alzheimer's. Computational biology and biochemistry presents a great variety of techniques and tools that help get faster and less expensive results that can have a great impact in drug development.

In this work some of these techniques were applied to two different systems with great scientific relevance: dopamine receptor and ghrelin receptor. Homology modeling protocols were applied with great success to these two systems.

The work on the dopaminergic system was centered in molecular docking protocols. Dopamine docking was performed with success and served as comparative measure to the rest of the docking. Using selective ligands with different functions (agonists and antagonists) helped to set a pattern of residues that vary from receptor to receptor. The data obtained can help understand binding pocket dynamics of dopamine receptor and guide development of more selective and potent drugs.

Molecular dynamics study with GHSR1a monomer gave new light on dynamics of the receptor in the absence of a ligand. Simulation with A204E mutant showed transition from an intermediate active state to an inactive conformation. This is only the first step on the atomic-level understanding of ghrelin receptor. Simulations with fully active states coupled with intracellular partner could give more reliable information on the activation pathway of ghrelin receptor.

In sum, the computational techniques applied to these biological systems helped solve real scientific challenges that lead to new knowledge on the big scientific field that is GPCRs structure and dynamics.

6 APPENDIX

Appendix 1: Docking results for the D1R. AutoDock4.2. measured the lowest binding energy ΔGbind [kcal/mol] of every run and clustered the calculated conformations ranked by energy level. A populated cluster indicates, that the position docked into the receptor is more likely to depict the conformational binding position of the ligand. Henceworth, the three best clusteres were chosen and analyzed.

Receptor state of the MD simluation [ns]	0	55	60	65	70	75	80	85	90	95	100
Ligand	Lowest binding energy [kcal/mol] Number of conformations in cluster										
7-OH-DPAT	-9.33 / -8.19 / -8.09 46 / 9 / 18	-10.16 / -9.68 / -8.66 13 / 12 / 5	-8.39 / -8.33 / -7.97 10 / 14 / 18	-10.09 / -9.18 / -8.77 2 / 12 / 2	-9.08 / -8.38 / -7.79 13 / 13 / 3	-9.85 / -9.23 / -8.45 24 / 14 / 8	-9.27 / -9.00 / -7.59 37 / 29 / 5	-9.62 / -7.82 / -7.65 55 / 2 / 6	-9.98 / -9.46 / -8.91 44 / 10 / 3	-9.04 / -8.73 / -8.57 13 / 7 / 9	-9.78 / -9.07 / -8.25 10 / 9 / 2
Apomorphine	-10.39 / -9.33 / -8.96 64 / 12 / 17	-10.47 / -8.87 / -8.82 25 / 11 / 15	-9.93 / -9.58 / -8.86 40 / 26 / 6	-10.79 / -10.08 / -9.00 33 / 21 / 7	-10.11 / -9.41 / -9.24 12 / 37 / 7	-11.39 / -11.17 / -9.60 27 / 32 / 5	-10.79 / -10.53 / -9.21 29 / 34 / 15	-10.09 / -9.99 / -8.64 36 / 20 / 25	-10.77 / -9.97 / -9.34 22 / 16 / 6	-10.44 / -9.88 / -8.95 44 / 14 / 5	-9.93 / -8.80 / -8.49 31 / 6 / 3
Aripiprazole	-10.26 / -9.74 / -9.64 8 / 1 / 8	-11.59 / -11.24 / -10.28 7 / 3 / 11	-10.11 / -8.93 / -8.17 10 / 5 / 11	-11.79 / -10.64 / -9.43 5 / 18 / 1	-10.73 / -10.02 / -9.37 14 / 1 / 2	-9.99 / -9.31 / -9.20 12 / 6 / 2	-10.51 / -9.86 / -9.63 6 / 8 / 1	-10.29 / -10.06 / -9.67 19 / 1 / 7	-11.12 / -10.08 / -9.96 16 / 9 / 3	-9.85 / -8.72 / -8.43 29 / 14 / 4	-10.68 / -9.95 / -9.94 5 / 9 / 16

Bromocriptine	+7.85 / +47.13 / +59.56 7 / 21 / 34	+2.32 / +10.47 / +22.09 51 / 28 / 2	+35.03 / +72.18 / +74.60 37 / 22 / 16	+15.82 / +16.34 / +40.56 49 / 22 / 5	+2.66 / +5.87 / +9.03 33 / 35 / 19	-5.33 / -4.82 / +1.52 25 / 28 / 44	-	+26.43 / +49.89 / +54.28 10 / 5 / 3	+15.05 / +29.78 / +35.11 5 / 46 / 3	+35.22 / +40.32 / +52.86 58 / 37 /3	+31.70 / +53.05 / +73.04 25 / 35 / 28
Chlorpromazine	-8.10 / -7.98 / -7.92 16 / 9 / 21	-8.70 / -8.55 / -8.52 24 / 30 / 4	-9.19 / -9.00 / -8.95 14 / 22 / 12	-9.04 / -8.87 / -8.79 17 / 2 / 2	-8.92 / -8.39 / -8.35 25 / 13 / 4	-8.93 / -8.70 / -8.59 24 / 24 / 9	-8.02 / -7.94 / -7.92 12 / 22 / 17	-8.06 / -8.01 / -8.00 13 / 17 / 8	-8.68 / -8.67 / -8.63 5 / 4 / 35	-8.91 / -8.75 / -8.72 23 / 26 / 9	-8.82 / -8.51 / -8.43 1 / 17 / 19
Clozapine	-8.09 / -7.23 / -7.12 43 / 54 / 2	-9.32 / -9.14 / -8.94 36 / 1 / 4	-9.47 / -8.87 / -8.63 31 / 50 / 12	-9.43 / -8.84 / -8.24 39 / 52 / 9	-8.49 / -8.33 / -7.22 80 / 18 / 1	-9.52 / -9.00 / -8.28 45 / 2 / 9	-8.89 / -8.41 / -7.99 74 / 9 / 13	-9.14 / -8.91 / -8.09 14 / 38 / 4	-9.05 / -8.39 / ? 88 / 12 / ?	-8.76 / -8.56 / -8.48 38 / 17 / 40	-8.33 / -7.18 / -6.28 84 / 18 / 1
Dopamine	-10.71 / -9.56 / -8.61 64 / 14 / 1	-10.19 / -9.63 / -9.16 13 / 17 / 4	-9.29 / -8.64 / -7.48 12 / 8 / 5	-10.65 / -9.45 / -8.70 18 / 32 / 11	-9.92 / -9.42 / -8.18 49 / 29 / 4	-11.50 / -10.67 / -9.00 45 / 31 / 5	-10.67 / -9.81 / -7.82 68 / 21 / 1	-10.31 / -8.93 / -8.85 74 / 7 / 4	-10.96 / -10.80 / -10.04 61 / 19 / 2	-10.73 / -9.91 / -9.56 19 / 11 / 43	-9.35 / -9.21 / -7.97 15 / 27 / 1
Eticlopride	-9.65 / -9.57 / -8.43 12 / 2 / 7	-10.53 / -9.56 / -9.37 13 / 7 / 8	-9.39 / -8.69 / -8.44 10 / 14 / 19	-10.99 / -10.52 / -9.73 7 / 29 / 7	-9.85 / -9.26 / -9.19 12 / 9 / 1	-10.47 / -10.34 / -10.04 2 / 6 / 14	-10.06 / -8.88 / -8.82 6 / 3 / 25	-10.61 / -9.61 / -9.51 16 / 14 / 3	-9.67 / -9.61 / -9.14 16 / 3 / 2	-10.15 / -9.82 / -9.18 25 / 23 / 12	-9.75 / -9.66 / -9.29 4 / 4 / 14

Haloperidol	-9.84 / -9.81 / -9.33 28 / 6 / 1	-11.35 / -10.99 / -10.91 20 / 22 / 9	-10.73 / -9.68 / -9.64 42 / 7 / 10	-11.68 / -10.87 / -10.61 4 / 31 / 4	-10.58 / -10.21 / -10.10 37 / 2 / 8	-10.65 / -10.50 / -10.50 4 / 9 / 16	-10.55 / -10.49 / -9.73 9 / 5 / 7	-9.87 / -9.52 / -9.51 27 / 4 / 3	-11.19 / -10.08 / -9.90 32 / 13 / 9	-10.93 / -10.58 / -10.51 4 / 5 / 9	-10.47 / -10.15 / -9.60 7 / 5 / 7
Nemonapride	-10.01 / -9.91 / -9.90 15 / 22 / 12	-10.84 / -10.24 / -10.00 2 / 15 / 4	-9.81 / -9.54 / -9.23 24 / 11 / 13	-11.15 / -10.90 / -10.79 5 / 4 / 3	-10.76 / -9.83 / -9.25 20 / 16 / 3	-11.02 / -10.77 / -10.70 7 / 1 / 3	-10.80 / -10.39 / -10.24 6 / 6 / 25	-10.73 / -10.26 / -10.00 24 / 13 / 13	-11.82 / -11.37 / -11.30 16 / 17 / 17	-11.08 / -10.79 / -10.66 13 / 20 / 2	-11.52 / -9.81 / -9.51 4 / 2 / 15
Risperidone	-9.17 / -8.29 / -7.62 9 / 27 / 6	-10.19 / -9.42 / -8.90 31 / 20 / 5	-7.51 / -6.36 / -5.11 6 / 25 / 15	-9.12 / -8.82 / -7.91 30 / 19 / 3	-8.50 / -8.16 / -7.95 32 / 4 / 7	-9.96 / -8.98 / -8.02 32 / 18 / 8	-9.60 / -8.62 / -8.40 40 / 3 / 4	-10.35 / -9.11 / -7.08 42 / 29 / 3	-9.72 / -9.40 / -8.78 31 / 8 / 4	-11.60 / -10.48 / -9.31 10 / 28 / 7	-9.66 / -8.71 / -8.70 8 / 24 / 6
SCH23390	-9.31 / -8.44 / -8.16 13 / 3 / 1	-9.86 / -9.62 / -9.15 2 / 6 / 11	-9.33 / -9.21 / -9.02 30 / 29 / 5	-9.49 / -9.27 / -9.23 41 / 5 / 6	-9.78 / -9.51 / -8.71 39 / 6 / 2	-10.01 / -9.86 / -9.84 16 / 5 / 1	-9.05 / -9.03 / -8.54 15 / 17 / 3	-9.94 / -9.72 / -9.09 4 / 4 / 1	-10.01 / -9.71 / -9.69 11 / 5 / 6	-10.59 / -9.62 / -9.17 18 / 6 / 3	-9.45 / -8.73 / -8.68 5 / 3 / 4
SKF38393	-12.23 / -11.00 / -9.40 38 / 22 / 4	-11.73 / -9.15 / -9.13 3 / 6 / 3	-8.91 / -8.58 / -8.36 8 / 7 / 9	-10.11 / -9.45 / -9.05 6 / 6 / 12	-11.44 / -9.25 / -9.05 36 / 1 / 5	-13.06 / -11.90 / -8.74 56 / 8 / 3	-11.87 / -11.32 / -9.55 32 / 19 / 1	-12.18 / -10.37 / -8.79 29 / 17 / 1	-12.50 / -11.35 / -9.45 50 / 3 / 9	-12.00 / -11.09 / -10.99 16 / 30 / 2	-11.88 / -9.41 / -9.26 26 / 4 / 20

Spiperdone	-9.70 / -9.31 / -9.02 29 / 14 / 5	-11.12 / -10.95 / -10.56 9 / 11 / 4	-9.30 / -9.23 / -8.99 8 / 10 / 17	-10.93 / -10.46 / -10.05 13 / 7 / 13	-11.09 / -9.99 / -9.81 2 / 4 / 9	-10.37 / -10.03 / -9.75 1 / 3 / 12	-10.76 / -9.97 / -9.81 4 / 8 / 3	-10.56 / -10.33 / -9.50 2 / 35 / 10	-10.76 / -10.71 / -10.48 11 / 8 / 16	-10.81 / -10.10 / -9.77 26 / 4 / 6	-10.35 / -9.93 / -9.63 7 / 7 / 10
Sulpiride	-11.43 / -11.24 / -10.73 4 / 3 / 3	-11.73 / -11.25 / -10.67 14 / 3 / 2	-8.76 / -7.61 / -7.37 5 / 16 / 5	-10.55 / -10.22 / -9.98 8 / 14 / 2	-12.51 / -11.16 / -8.85 11 / 2 / 3	-11.38 / -11.07 / -9.06 8 / 1 / 5	-10.88 / -10.68 / -10.13 12 / 4 / 1	-10.87 / -10.70 / -10.15 10 / 3 / 2	-11.64 / -11.30 / -11.01 6 / 2 / 5	-10.43 / -10.43 / -9.29 3 / 3 / 2	-10.95 / -10.76 / -10.35 7 / 2 / 4

Appendix 2: Docking results for the D2R. AutoDock4.2. measured the lowest binding energy ΔGbind [kcal/mol] of every run and clustered the calculated conformations ranked by energy level. A populated cluster indicates, that the position docked into the receptor is more likely to depict the conformational binding position of the ligand. Henceworth, the three best clusteres were chosen and analyzed.

Receptor state of the MD simluation [ns]	0	55	60	65	70	75	80	85	90	95	100
Ligand	Lowest binding energy [kcal/mol] Number of conformation in cluster										
7-OH-DPAT	-8.96 / -8.77 / -7.92 8 / 33 / 8	-8.52 / -8.38 / -8.20 22 / 31 / 5	-3.74 / -3.42 / -2.82 15 / 10 / 8	-8.50 / -8.30 / -7.95 8 / 24 / 1	-9.17 / -9.16 / -8.52 23 / 10 / 1	-9.20 / -8.88 / -8.60 17 / 21 / 8	-9.09 / -8.63 / -7.99 3 / 16 / 18	-8.55 / -8.00 / -6.94 16 / 4 / 8	-9.06 / -9.04 / -8.37 8 / 22 / 34	-9.20 / -8.99 / -7.85 57 / 7 / 3	-9.41 / -9.32 / -8.99 30 / 6 / 28
Apomorphine	-10.99 / -10.06 / -9.41 9 / 2 / 15	-9.70 / -9.32 / -9.28 15 / 2 / 19	-11.11 / -10.04 / -10.02 21 / 9 / 11	-9.83 / -9.37 / -8.91 45 / 10 / 11	-9.58 / -9.26 / -9.20 3 / 25 / 1	-10.34 / -10.18 / -10.00 10 / 39 / 8	-10.99 / -10.11 / -10.01 1 / 5 / 8	-9.95 / -9.15 / -9.05 42 / 2 / 11	-9.78 / -9.42 / -9.08 58 / 3 / 1	-10.26 / -9.28 / -9.19 29 / 5 / 52	-10.94 / -10.42 / -9.79 12 / 27 / 37
Aripiprazole	-10.35 / -10.29 / -10.08 6 / 2 / 7	-10.59 / -10.13 / -9.94 5 / 6 / 1	-10.79 / -10.67 / -9.92 1 / 2 / 1	-10.84 / -9.92 / -9.60 9 / 2 / 11	-9.47 / -9.14 / -8.26 8 / 8 / 5	-9.38 / -9.24 / -9.12 4 / 4 / 1	-11.73 / -8.96 / -8.91 10 / 7 / 5	-11.22 / -9.71 / -9.70 21 / 4 / 2	-10.43 / -10.24 / -10.21 8 / 20 / 13	-12.23 / -9.82 / -9.80 15 / 5 / 3	-10.49 / -10.19 / -9.64 3 / 1 / 6
Bromocriptine	-16.81 / -11.62 / -9.84	-11.84 / -11.56 / -6.70 38 / 9 / 2	+6.08 / +16.11 / +22.50	+4.87 / +16.74 / +22.39	+73.41 / +94.05 / +111.72 1 / 43 / 12	+39.07 / +49.92 / +64.65 7 / 25 / 5	-3.29 / +32.56 / +51.90 10 / 4 / 1	+28.94 / +52.89 / +78.83 4 / 28 / 13	+69.02 / +90.82 / +121.16 62 / 3 / 5	+63.67 / +115.18 / +157.32 11 / 4 / 24	+154.34 / +158.94 / +168.37 43 / 3 / 5

	36 / 4 / 10		11 / 34 / 1	17 / 10 / 7							
Chlorpromazine	-8.38 / -8.01 / -7.96 1 / 9 / 8	-8.48 / -8.15 / -8.00 3 / 5 / 2	-8.81 / -8.60 / -8.58 3 / 8 / 1	-8.31 / -7.98 / -7.87 5 / 3 / 19	-8.66 / -8.53 / -8.41 12 / 12 / 12	-8.64 / -8.31 / -8.20 7 / 1 / 12	-8.32 / -8.22 / -8.14 5 / 11 / 3	-8.23 / -7.95 / -7.90 2 / 17 / 11	-8.09 / -7.91 / -7.88 7 / 16 / 15	-8.38 / -8.32 / -8.12 10 / 20 / 17	-8.69 / -8.62 / -8.38 8 / 23 / 14
Clozapine	-8.61 / -7.81 / -7.58 41 / 19 / 1	-9.00 / -7.82 / -7.48 36 / 2 / 11	-7.98 / -7.35 / -7.07 47 / 9 / 7	-8.51 / -8.40 / -8.15 14 / 18 / 2	-8.47 / -7.61 / -5.41 68 / 14 / 7	-7.97 / -7.75 / -7.56 55 / 21 / 3	-7.72 / -7.50 / -6.71 25 / 6 / 7	-7.79 / -7.78 / -7.72 43 / 3 / 16	-7.65 / -7.36 / -6.12 27 / 3 / 5	-8.30 / -8.26 / -7.90 7 / 9 / 41	-8.03 / -8.01 / -7.20 12 / 38 / 43
Dopamine	-9.72 / -9.27 / -8.75 40 / 17 / 9	-9.57 / -9.29 / -8.16 38 / 28 / 1	-10.29 / -8.36 / -8.33 51 / 1 / 15	-9.58 / -9.16 / -8.55 44 / 18 / 11	-9.71 / -8.81 / -8.77 48 / 3 / 12	-9.62 / -9.27 / -9.13 29 / 5 / 43	-10.15 / -9.71 / -7.56 53 / 10 / 2	-10.08 / -9.37 / -8.40 27 / 20 / 17	-10.64 / -8.84 / -8.42 64 / 11 / 4	-9.76 / -9.63 / -8.06 38 / 29 / 12	-10.01 / -9.77 / -9.77 40 / 18 / 14
Eticlopride	-9.56 / -9.03 / -8.81 53 / 7 / 1	-9.70 / -9.29 / -8.96 25 / 9 / 4	-9.55 / -9.51 / -9.00 5 / 6 / 7	-9.40 / -9.40 / -9.32 3 / 12 / 1	-11.31 / -10.62 / -9.42 11 / 41 / 7	-9.75 / -9.31 / -9.15 26 / 13 / 4	-9.75 / -9.68 / -9.66 17 / 15 / 9	-10.45 / -9.89 / -9.29 15 / 16 / 3	-10.39 / -9.93 / -9.30 34 / 18 / 5	-10.13 / -9.97 / -9.90 7 / 3 / 26	-11.47 / -10.51 / -10.48 39 / 11 / 19
Haloperidol	-10.64 / -10.44 / -10.34 5 / 5 / 2	-11.21 / -10.93 / -10.86 2 / 3 / 5	-12.24 / -11.36 / -10.89 5 / 2 / 1	-11.03 / -10.54 / -10.31 2 / 8 / 5	-11.42 / -11.11 / -10.89 11 / 7 / 2	-11.11 / -10.16 / -10.12 4 / 10 / 2	-11.15 / -10.85 / -10.44 2 / 2 / 21	-11.08 / -10.78 / -10.59 1 / 3 / 11	-11.29 / -11.07 / -10.80 16 / 2 / 6	-10.01 / -9.87 / -9.79 8 / 2 / 1	-10.68 / -10.67 / -10.54 16 / 8 / 7

Nemonapride	-10.10 / -9.43 / -9.34 9 / 5 / 1	-10.56 / -9.92 / -9.60 14 / 3 / 2	-11.39 / -10.04 / -9.79 1 / 5 / 1	-10.08 / -9.79 / -9.73 4 / 4 / 15	10.58 / -10.30 / -10.30 28 / 7 / 8	-10.32 / -9.88 / -9.80 14 / 23 / 8	-11.11 / -10.64 / -9.98 43 / 3 / 3	-10.72 / -10.60 / -10.43 6 / 5 / 4	-10.23 / -10.00 / -9.97 13 / 4 / 23	-10.45 / -10.35 / -10.08 2 / 18 / 3	-11.86 / -11.17 / -10.62 7 / 2 / 5
Risperidone	-12.16 / -12.00 / -10.94 2 / 5 / 4	-8.83 / -8.73 / -8.70 7 / 7 / 7	-9.17 / -9.16 / -9.13 22 / 6 / 1	-9.79 / -9.36 / -9.20 8 / 34 / 7	-9.07 / -9.01 / -8.33 57 / 18 / 3	+83.50 / +125.50 / +132.50 3 / 3 / 12	-9.20 / -8.88 / -8.52 51 / 26 / 5	-10.33 / -9.65 / -9.28 11 / 14 / 11	-9.30 / -8.06 / -7.67 34 / 40 / 6	-8.99 / -8.99 / -8.82 12 / 25 / 2	-9.39 / -8.77 / -8.54 11 / 53 / 10
SCH23390	-9.50 / -9.12 / -8.71 14 / 3 / 20	-10.25 / -9.36 / -9.13 12 / 13 / 1	-9.58 / -9.08 / -9.03 10 / 16 / 11	-9.81 / -9.13 / -9.11 21 / 2 / 1	-9.49 / -9.39 / -9.26 2 / 3 / 4	-9.56 / -9.35 / -9.07 26 / 23 / 2	-9.57 / -9.26 / -8.95 5 / 4 / 14	-10.02 / -9.99 / -9.60 7 / 24 / 4	-9.51 / -8.98 / -8.87 3 / 4 / 6	-8.69 / -8.53 / -8.27 10 / 3 / 6	-9.40 / -9.12 / -8.71 20 / 4 / 23
SKF38393	-10.81 / -10.13 / -9.23 6 / 12 / 19	-12.10 / -10.62 / -9.85 28 / 4 / 1	-11.82 / -10.32 / -9.93 21 / 10 / 20	-10.65 / -10.55 / -10.50 26 / 2 / 2	-10.17 / -9.86 / -9.73 18 / 4 / 4	-12.35 / -10.79 / -10.16 45 / 41 / 1	-12.08 / -10.94 / -9.55 16 / 37 / 4	-11.14 / -10.16 / -9.77 24 / 34 / 2	-10.94 / -9.81 / -9.70 5 / 42 / 4	-11.56 / -11.08 / -9.96 5 / 47 / 6	-11.12 / -11.10 / -9.81 52 / 12 / 4
Spiperdone	-10.96 / -10.37 / -9.84 1 / 3 / 2	-10.77 / -10.59 / -10.36 2 / 3 / 4	-10.99 / -10.91 / -9.87 7 / 3 / 2	-11.79 / -10.54 / -10.53 5 / 4 / 1	-11.04 / -10.54 / -10.54 3 / 17 / 3	-10.92 / -9.91 / -9.59 10 / 3 / 2	-10.25 / -10.09 / -10.06 3 / 12 / 3	-11.67 / -10.95 / -10.27 1 / 3 / 5	-10.52 / -10.16 / -9.61	-10.83 / -10.06 / -9.82 4 / 1 / 1	-10.65 / -10.58 / -10.05 5 / 4 / 3

Sulpiride	-11.25 / -10.44 / -10.03 5 / 1 / 7	-10.39 / -10.14 / -10.05 1 / 6 / 7	-11.38 / -10.55 / -10.38 8 / 2 / 2	-12.18 / -10.72 / -10.50 10 / 3 / 1	-11.71 / -11.36 / -10.55 3 / 15 / 3	-10.81 / -10.67 / -10.34 3 / 3 / 1	-11.19 / -10.79 / -9.51 6 / 8 / 1	-10.99 / -10.94 / -10.65 14 / 7 / 3	-11.24 / -11.03 / -10.83	-12.39 / -10.90 / -10.70 2 / 1 / 7	-12.46 / -11.36 / -11.05 15 / 6 / 11

Appendix 3: Docking results for the D3R. AutoDock4.2. measured the lowest binding energy ΔGbind [kcal/mol] of every run and clustered the calculated conformations ranked by energy level. A populated cluster indicates, that the position docked into the receptor is more likely to depict the conformational binding position of the ligand. Henceworth, the three best clusteres were chosen and analyzed.

Receptor state of the MD simluation [ns]	0	55	60	65	70	75	80	85	90	95	100
Ligand	Lowest binding energy [kcal/mol] Number of conformation in cluster										
7-OH-DPAT	-9.11 / -8.89 / -8.52 5 / 51 / 1	-8.35 / -7.99 / -7.60 46 / 4 / 12	-8.43 / -7.56 / -7.53 35 / 34 / 1	-9.43 / -7.67 / -7.61 29 / 3 / 5	-8.37 / -7.70 / -7.54 39 / 12 / 4	-9.47 / -8.53 / -8.29 20 / 7 / 5	-9.75 / -8.93 / -7.92 28 / 20 / 3	-8.20 / -8.02 / -7.55 35 / 12 / 1	-8.36 / -8.07 / -7.87 41 / 5 / 3	-9.38 / -8.91 / -7.83 13 / 3 / 4	-8.57 / -8.21 / -7.85 8 / 9 / 8
Apomorphine	-9.89 / -9.81 / -9.81 36 / 22 / 14	-10.19 / -9.46 / -8.51 2 / 38 / 21	-9.40 / -9.02 / -8.45 28 / 25 / 10	-10.18 / -9.34 / -8.75 22 / 33 / 2	-9.28 / -8.93 / -8.75 18 / 22 / 2	-9.51 / -9.33 / -8.97 1 / 11 / 15	-10.52 / -9.64 / -9.42 3 / 31 / 16	-9.91 / -9.46 / -9.26 9 / 22 / 3	-10.11 / -9.68 / -9.18 27 / 13 / 23	-9.40 / -9.17 / -9.12 10 / 31 / 24	-9.87 / -9.28 / -9.13 23 / 19 / 2
Aripiprazole	-10.40 / -10.27 / -9.99 3 / 4 / 2	-8.59 / -8.24 / -8.23 3 / 3 / 2	-8.89 / -8.66 / -8.45 1 / 1 / 1	-8.97 / -8.96 / -8.86 1 / 1 / 1	-9.79 / -9.25 / -8.97 3 / 1 / 2	-10.13 / -9.33 / -9.10 2 / 1 / 2	-10.37 / -10.30 / -10.19 5 / 3 / 5	-9.24 / -8.95 / -8.94 12 / 3 / 3	-9.74 / -9.45 / -9.27 5 / 1 / 1	-10.34 / -10.22 / -10.16 4 / 12 / 4	-10.44 / -9.61 / -9.59 8 / 2 / 3
Bromocriptine	-2.28 / +13.56 / +16.35 73 / 4 / 1	+29.67 / +81.44 / +100.91 5 / 8 / 1	+33.62 / +34.66 / +36.66 3 / 4 / 2	+10.12 / +11.36 / +22.89 18 / 12 / 7	+23.21 / +24.67 / +28.29 2 / 5 / 11	+10.12 / +10.32 / +15.51 13 / 22 / 3	+19.76 / +34.46 / +52.78 2 / 2 / 27	+1.48 / +10.88 / +26.06 27 / 27 / 1	+11.26 / +20.50 / +23.50 17 / 6 / 7	+42.39 / +61.90 / +80.64 19 / 9 / 20	+4.31 / +23.94 / +43.10 34 / 2 / 3

Chlorpromazine	-8.29 / -8.28 / -8.27 26 / 10 / 14	-7.88 / -7.81 / -7.81 2 / 11 / 1	-8.03 / -7.69 / -7.51 1 / 14 / 1	-7.79 / -7.71 / -7.63 5 / 30 / 24	-7.89 / -7.64 / -7.49 1 / 7 / 2	-8.91 / -8.33 / -8.06 1 / 2 / 21	-8.63 / -8.38 / -7.98 5 / 18 / 4	-7.61 / -7.30 / -7.13 5 / 5 / 3	-8.06 / -7.60 / -7.56 7 / 7 / 18	-8.56 / -8.17 / -8.16 23 / 9 / 3	-8.74 / -7.95 / -7.81 2 / 5 / 10
Clozapine	-8.48 / -8.43 / -8.20 13 / 7 / 8	-7.16 / -7.12 / -6.95 6 / 38 / 42	-8.72 / -7.23 / -7.22 17 / 11 / 8	-8.12 / -7.27 / -7.26 14 / 24 / 32	-8.36 / -7.47 / -7.38 25 / 14 / 12	-8.16 / -7.69 / -7.65 9 / 1 / 7	-9.15 / -7.90 / -7.85 40 / 12 / 7	-8.33 / -7.29 / -7.24 25 / 31 / 4	-8.49 / -8.08 / -7.85 2 / 6 / 36	-8.37 / -8.37 / -8.19 49 / 17 / 17	-8.51 / -8.46 / -7.90 21 / 7 / 3
Dopamine	-9.76 / -9.55 / -8.64 17 / 48 / 18	-9.63 / -9.48 / -8.64 42 / 17 / 16	-8.92 / -8.67 / -8.49 8 / 14 / 22	-9.34 / -8.79 / -8.34 34 / 11 / 15	-8.97 / -8.95 / -8.27 23 / 27 / 10	-8.75 / -8.72 / -8.18 35 / 12 / 11	-9.88 / -9.59 / -8.82 69 / 5 / 12	-9.87 / -8.81 / -8.26 56 / 6 / 6	-9.77 / -9.00 / -8.18 40 / 7 / 12	-9.51 / -8.79 / -7.96 43 / 11 / 6	+8.34e+07 / +8.34e+07 / +8.34e+07 3 / 7 / 3
Eticlopride	-9.98 / -9.34 / -9.07 14 / 2 / 13	-8.71 / -8.69 / -8.64 31 / 5 / 1	-7.99 / -7.95 / -7.88 7 / 2 / 2	-9.04 / -8.90 / -8.80 9 / 12 / 12	-9.45 / -9.02 / -8.76 7 / 8 / 2	-9.36 / -8.81 / -8.79 5 / 5 / 17	-9.58 / -9.10 / -8.83 1 / 10 / 2	-9.19 / -8.99 / -8.92 9 / 12 / 9	-9.41 / -9.37 / -9.20 2 / 15 / 8	-9.85 / -9.47 / -9.43 7 / 27 / 17	-9.23 / -9.17 / -9.03 6 / 5 / 3
Haloperidol	-11.07 / -10.63 / -10.24 3 / 2 / 2	-11.00 / -10.79 / -10.01 1 / 1 / 1	-10.36 / -9.44 / -9.21 1 / 1 / 3	-10.89 / -9.45 / -9.42 1 / 3 / 2	-9.68 / -9.50 / -9.30 1 / 5 / 5	-10.26 / -10.21 / -10.18 2 / 3 / 3	-11.88 / -11.20 / -10.57 1 / 5 / 1	-10.84 / -10.35 / -10.34 1 / 5 / 1	-10.31 / -10.28 / -10.23 3 / 3 / 1	-10.67 / -10.50 / -10.38 2 / 6 / 5	-10.43 / -10.30 / -10.12 18 / 1 / 5
Nemonapride	-10.97 / -10.86 / -10.26 2 / 3 / 1	-10.63 / -10.23 / -9.96 4 / 1 / 2	-9.12 / -8.92 / -8.68 1 / 4 / 2	-10.00 / -9.85 / -9.40 1 / 3 / 2	-9.91 / -9.48 / -9.12 12 / 3 / 1	-9.85 / -9.53 / -9.45 1 / 5 / 2	-10.72 / -9.82 / -9.71 2 / 2 / 2	-9.89 / -9.66 / -9.59 8 / 6 / 1	-9.94 / -9.59 / -9.32 5 / 2 / 4	-10.09 / -10.00 / -9.90 5 / 2 / 4	-10.01 / -9.71 / -9.55 5 / 2 / 6

Risperidone	-8.87 / -8.23 / -8.17 16 / 5 / 2	-8.09 / -7.76 / -7.73 1 / 23 / 2	-7.91 / -7.77 / -7.73 6 / 3 / 3	-8.88 / -8.71 / -8.61 2 / 1 / 4	-8.67 / -7.89 / -7.87 12 / 4 / 1	-9.59 / -9.43 / -9.07 7 / 12 / 4	-9.44 / -9.14 / -9.09 2 / 4 / 9	-9.46 / -9.06 / -8.93 15 / 1 / 15	-9.51 / -9.48 / -9.37 12 / 1 / 7	-9.11 / -9.05 / -9.03 7 / 5 / 10	-9.72 / -9.47 / -8.86 5 / 4 / 11
SCH23390	-10.59 / -9.69 / -9.56 11 / 2 / 6	-9.38 / -9.07 / -8.70 30 / 12 / 10	-8.64 / -8.33 / -8.21 10 / 1 / 28	-9.96 / -9.65 / -8.98 3 / 9 / 30	-10.13 / -9.72 / -9.47 31 / 5 / 2	-9.76 / -9.19 / -9.03 1 / 8 / 5	-10.34 / -9.64 / -9.44 11 / 30 / 19	-9.59 / -9.16 / -8.64 5 / 20 / 39	-10.39 / -9.81 / -8.71 9 / 30 / 36	-10.71 / -10.00 / -9.71 28 / 9 / 2	-9.72 / -9.68 / -9.41 2 / 23 / 2
SKF38393	-11.86 / -11.34 / -11.08 1 / 36 / 2	-10.68 / -10.28 / -10.23 20 / 9 / 32	-9.36 / -9.33 / -9.25 30 / 6 / 4	-11.04 / -10.88 / -10.83 21 / 5 / 23	-11.53 / -10.24 / -10.15 12 / 8 / 8	-10.47 / -10.30 / -9.66 23 / 22 / 1	-11.15 / -10.69 / -9.95 16 / 56 / 2	-10.41 / -10.35 / -9.87 58 / 5 / 2	-10.85 / -10.69 / -10.07 31 / 20 / 8	-10.69 / -10.24 / -9.78 9 / 1 / 7	-10.08 / -9.74 / -9.63 26 / 2 / 2
Spiperdone	-9.29 / -8.67 / -8.58 4 / 3 / 2	-9.25 / -9.00 / -8.75 2 / 3 / 2	-8.75 / -7.88 / -7.88 3 / 1 / 3	-8.88 / -8.75 / -8.50 3 / 1 / 1	-9.38 / -9.00 / -8.88 1 / 1 / 1	-9.50 / -8.75 / -8.62 1 / 2 / 1	-9.50 / -9.38 / -9.38 5 / 1 / 7	-8.75 / -8.62 / -8.62 2 / 2 / 4	-9.12 / -9.00 / -8.75 1 / 3 / 1	-9.38 / -9.38 / -9.12 15 / 1 / 14	-9.50 / -9.25 / -9.12 2 / 9 / 1
Sulpiride	-10.55 / -10.25 / -9.59 12 / 6 / 7	-9.69 / -8.90 / -8.89 1 / 7 / 1	-9.77 / -9.41 / -8.44 1 / 1 / 4	-8.93 / -8.91 / -8.85 2 / 1 / 2	-9.30 / -8.86 / -8.70 3 / 3 / 3	-9.94 / -9.84 / -9.68 2 / 2 / 3	-10.24 / -9.63 / -9.34 4 / 4 / 3	-10.01 / -9.78 / -9.71 2 / 2 / 2	-9.73 / -8.85 / -8.55 4 / 2 / 1	-9.99 / -9.46 / -9.17 1 / 19 / 7	-10.55 / -9.81 / -9.79 3 / 1 / 12

Appendix 4: Docking results for the D4R. AutoDock4.2. measured the lowest binding energy ΔGbind [kcal/mol] of every run and clustered the calculated conformations ranked by energy level. A populated cluster indicates, that the position docked into the receptor is more likely to depict the conformational binding position of the ligand. Henceworth, the three best clusteres were chosen and analyzed.

Receptor state of the MD simluation [ns]	0	55	60	65	70	75	80	85	90	95	100
Ligand	Lowest binding energy [kcal/mol] Number of conformation in cluster										
7-OH-DPAT	-9.52 / -8.44 / -7.84 30 / 19 / 17	-7.75 / -7.68 / -7.52 11 / 20 / 20	-8.28 / -7.97 / -7.71 13 / 3 / 1	-8.32 / -7.82 / -7.71 5 / 1 / 27	-8.74 / -8.25 / -8.17 13 / 10 / 1	-9.25 / -8.70 / -8.46 14 / 10 / 7	-8.98 / -8.45 / -7.54 6 / 13 / 26	-7.46 / -7.05 / -6.53 42 / 9 / 4	-7.56 / -7.60 / -7.50 11 / 48 / 16	-9.62 / -9.41 / -7.38 15 / 3 / 55	-8.83 / -8.17 / -8.04 23 / 1 / 2
Apomorphine	-9.24 / -9.05 / -8.94 34 / 16 / 9	-10.33 / -9.69 / -9.51 44 / 19 / 31	-9.48 / -9.09 / -8.25 13 / 39 / 1	-10.11 / -9.59 / -9.27 27 / 7 / 42	-10.19 / -9.50 / -9.32 28 / 40 / 10	-9.92 / -9.83 / -8.77 2 / 51 / 35	-10.08 / -9.72 / -9.56 3 / 5 / 13	-8.41 / -8.09 / -7.82 12 / 1 / 41	-9.26 / -8.98 / -8.72 7 / 21 / 4	-9.91 / -9.86 / -7.77 8 / 7 / 51	-10.10 / -10.01 / -9.30 10 / 19 / 2
Aripiprazole	-8.92 / -8.86 / -8.10 2 / 11 / 6	-11.08 / -9.85 / -9.44 6 / 1 / 3	-8.05 / -7.53 / -7.28 2 / 9 / 2	-11.43 / -10.35 / -10.34 6 / 33 / 3	-12.23 / -9.26 / -9.08 12 / 2 / 4	-7.46 / -4.85 / -4.65 10 / 2 / 3	-4.70 / -4.05 / -3.83 7 / 2 / 4	-1.97 / -1.45 / -0.97 14 / 4 / 5	-7.60 / -7.05 / -6.73 9 / 3 / 2	-8.30 / -7.83 / -6.55 6 / 5 / 11	-9.26 / -8.92 / -7.75 2 / 20 / 8
Bromocriptine	+103.73 / +142.07 / +198.99	+34.39 / +39.22 / +49.74	+43.40 / +73.40 / +88.72	+138.76 / +139.02 / +169.12	+154.29 / +162.10 / +176.68	+65.12 / +127.27 / +141.46	+35.85 / +79.19 / +95.36	+87.57 / +129.02 / +161.26	+133.51 / +156.83 / +158.24	+238.63 / +240.75 / +250.54	+57.61 / +68.87 / +113.81

	12 / 18 / 3	38 / 32 / 3	45 / 15 / 21	57 / 10 / 8	4 / 51 / 2	36 / 1 / 6	22 / 2 / 9	26 / 1 / 54	23 / 18 / 8	5 / 11 / 8	58 / 10 / 4
Chlorpromazine	-8.55 / -8.42 / -7.80 5 / 12 / 16	-7.88 / -7.82 / -7.75 24 / 14 / 3	-8.24 / -8.09 / -8.02 8 / 22 / 22	-8.60 / -8.40 / -8.36 11 / 36 / 7	-9.09 / -9.00 / -8.84 10 / 12 / 10	-8.91 / -8.66 / -8.42 6 / 8 / 7	-8.08 / -8.00 / -7.53 3 / 35 / 14	-8.20 / -7.78 / -7.56 1 / 25 / 11	-8.44 / -8.35 / -8.35 3 / 11 / 5	-8.24 / -7.80 / -7.26 30 / 6 / 9	-9.16 / -8.64 / -8.30 1 / 5 / 6
Clozapine	-7.73 / -7.44 / -6.75 59 / 2 / 13	-7.05 / -7.05 / -6.96 50 / 6 / 17	-7.12 / -7.06 / -6.47 8 / 13 / 21	-7.95 / -7.17 / -6.76 11 / 22 / 45	-7.64 / -6.25 / -6.04 38 / 2 / 31	-6.04 / -4.27 / -1.84 49 / 27 / 7	-8.96 / -6.58 / -4.58 65 / 13 / 7	-4.70 / -2.40 / -0.68 27 / 40 / 3	-5.20 / -3.52 / -3.46 15 / 14 / 5	-1.03 / -0.72 / +1.59 8 / 44 / 4	-6.09 / -3.17 / -2.93 58 / 1 / 4
Dopamine	-10.04 / -9.54 / -9.40 69 / 15 / 8	-9.84 / -8.68 / -7.75 62 / 28 / 1	-9.60 / -8.96 / -8.68 60 / 19 / 3	-9.99 / -9.60 / -8.36 39 / 21 / 8	-10.09 / -9.45 / -8.80 62 / 10 / 9	-9.78 / -8.16 / -7.71 68 / 6 / 4	-9.41 / -9.23 / -9.06 41 / 17 / 7	-8.53 / -7.81 / -6.95 39 / 13 / 2	-7.52 / -7.45 / -7.16 30 / 30 / 8	-9.87 / -7.41 / -6.99 86 / 5 / 2	-9.29 / -9.11 / -7.79 13 / 55 / 8
Eticlopride	-9.60 / -9.38 / -8.64 20 / 8 / 13	-7.73 / -7.70 / -7.68 9 / 8 / 1	-8.55 / -8.48 / -8.36 11 / 9 / 4	-9.53 / -9.23 / -9.20 2 / 11 / 9	-10.50 / -9.73 / -9.42 3 / 1 / 7	-9.78 / -9.53 / -9.44 32 / 6 / 10	-9.57 / -7.77 / -7.49 46 / 5 / 4	-9.10 / -7.24 / -6.86 24 / 13 / 6	-9.58 / -9.48 / -8.90 6 / 23 / 29	-8.34 / -8.09 / -8.08 10 / 2 / 28	-9.02 / -8.71 / -8.63 7 / 2 / 4

Haloperidol	-9.41 / -8.26 / -33 / 67 / - 6	-0.40 / +0.88 / +2.57 69 / 13 / 6	-10.32 / -9.66 / -9.36 2 / 7 / 60	-9.16 / -8.32 / -8.08 58 / 16 / 15	-10.42 / -9.36 / -9.98 58 / 13 / 21	-6.29 / -6.08 / -5.94 6 / 18 / 13	-1.94 / -1.34 / -0.80 30 / 25 / 2	+5.37 / +5.41 / +6.89 29 / 1 / 6	-0.35 / +0.12 / +0.56 9 / 20 / 6	-4.67 / -1.78 / -1.14 35 / 20 / 2	-9.18 / -8.73 / -8.55 21 / 7 / 28
Nemonapride	-10.46 / -9.85 / -9.50 10 / 3 / 15	-9.12 / -9.07 /-9.07 15 / 14 / 12	-10.45 /-9.31 / -9.08 1 / 7 / 3	-10.09 / -9.98 / -9.55 1 / 1 / 3	-10.68 / -9.50 / -9.45 5 / 1 / 4	-10.89 / -10.41 / -10.29 20 / 17 / 1	-9.92 / -9.12 / -8.93 23 / 15 / 7	-9.84 / -8.77 / -7.71 12 / 16 / 6	-10.48 / -10.15 / -9.53 25 / 25 / 18	-9.59 / -9.53 / -8.34 19 / 16 / 12	-10.62 / -10.26 / -9.86 7 / 8 / 1
Risperidone	-8.30 / -8.27 / -7.08 12 / 18 / 11	-9.60 / -9.45 / -8.23 37 / 1 / 2	-9.16 / -9.04 / -8.93 1 / 6 / 6	-7.80 / -6.79 / -5.45 28 / 14 / 3	-8.25 / -8.04 / -7.86 10 / 14 / 2	-4.64 / -2.42 / -2.31 14 / 3 / 1	-6.17 / -6.13 / -3.76 9 / 17 / 17	-1.21 / +0.50 / +0.51 12 / 5 / 10	-5.83 / -5.57 / -5.42 20 / 12 / 2	-4.65 / -4.63 / -2.60 14 / 6 / 8	-7.74 / -7.20 / -6.97 2 / 6 / 10
SCH23390	-9.69 / -9.38 / -9.22 45 / 17 / 26	-7.15 / -6.89 / -6.74 20 / 4 / 5	-9.50 / -9.37 / -9.04 11 / 4 / 14	-9.45 / -9.43 / -9.02 11 / 6 / 18	-9.71 / -8.85 / -8.42 27 / 46 / 8	-10.84 / -9.47 / -9.20 28 / 2 / 3	-8.93 / -8.50 / -8.50 6 / 9 / 12	-9.93 / -8.98 / -8.41 27 / 10 / 5	-8.92 / -8.75 / -8.50 71 / 2 / 22	-8.52 / -8.25 / -8.23 33 / 22 / 11	-9.60 / -8.81 / -8.64 7 / 2 / 18
SKF38393	-10.94 / 10.19 / -9.48 14 / 9 / 3	-9.93 / -9.70 / -9.60 29 / 14 / 1	-11.02 /-9.87 / -9.76 4 / 21 / 7	-10.82 / -10.72 / -10.36 42 / 3 / 9	-11.87 / -9.90 / -9.17 19 / 17 / 2	-10.18 / -9.63 / -9.38 13 / 17 / 3	-10.17 /-10.10 / -9.35 5 / 3 / 7	-9.16 / -8.99 / -8.60 45 / 16 / 8	-10.16 / -9.66 / -8.94 1 / 30 / 3	-9.62 / -9.01 / -8.68 31 / 30 / 4	-10.67 / -10.58 / -10.28 3 / 12 / 2

Spiperdone	-9.02 / -8..79 / -8.45 1 / 16 / 1	-9.64 / -9.02 / -9.01 9 / 10 / 15	-10.16 / -9.36 / -9.11 24 / 1 / 12	-10.23 / -9.72 / -9.40 17 / 16 / 3	-9.16 / -9.05 / -8.59 5 / 2 / 26	-9.99 / -8.42 / -7.20 4 / 16 / 11	-8.91 / -8.29 / -8.05 6 / 12 / 9	-7.42 / -6.50 / -6.26 5 / 9 / 6	-10.27 / -10.17 / -9.85 19 / 35 / 4	-9.93 / -9.05 / -8.49 14 / 3 / 9	-11.67 / -11.37 / -11.14 10 / 20 / 18
Sulpiride	-10.62 / -10.43 / -9.59 14 / 1 / 2	-10.20 / -9.83 / -9.52 4 / 5/ 7	-11.12 / -10.71 / -10.25 6 / 5 / 1	-10.65 / -10.23 / -10.08 6 / 8 / 1	-12.10 / -11.06 / -11.06 1 / 4 / 2	-11.36 / -11.08 / -10.91 7 / 4 / 4	-9.20 / -8.39 / -8.35 2 / 7 / 10	-8.98 / -8.63 / -8.33 2 / 5 / 1	-10.71 / -10.49 / -10.28 2 / 2 / 6	-10.53 / -10.48 / -9.97 6 / 6 / 5	-12.14 / -11.29 / -10.26 1 / 4 / 3

Appendix 5: Docking results for the D5R. AutoDock4.2. measured the lowest binding energy ΔGbind [kcal/mol] of every run and clustered the calculated conformations ranked by energy level. A populated cluster indicates, that the position docked into the receptor is more likely to depict the conformational binding position of the ligand. Henceworth, the three best clusteres were chosen and analyzed.

Receptor state of the MD simluation [ns]	0	55	60	65	70	75	80	85	90	95	100
Ligand	Lowest binding energy [kcal/mol] Number of conformation in cluster										
7-OH-DPAT	-8.85 / -8.66 / -8.50 28 / 4 / 1	-8.33 / -7.83 / -7.55 36 / 19 / 4	-9.32 / -8.68 / -8.57 27 / 2 / 12	-9.10 / -8.84 / -8.35 25 / 18 / 15	-9.34 / -9.05 / -8.21 14 / 32 / 8	-9.77 / -8.80 / -8.30 18 / 6 / 18	-9.44 / -7.89 / -6.98 26 / 15 / 10	-10.09 / -8.46 / -8.26 24 / 14 / 1	-9.46 / -7.88 / -7.63 38 / 9 / 4	-9.93 / 8-14 / -8.12 36 / 4 / 19	-8.79 / 8-42 / -6.77 2 / 3 / 1
Apomorphine	-10.92 / -10.37 / -9.14 47 / 18 / 14	-10.35 / -10.31 / -8.32 31 / 9 / 2	-10.11 / -9.26 / -8.78 50 / 17 / 3	-10.99 / -10.52 / -10.15 24 / 4 / 7	-10.30 / -9.12 / -9.02 65 / 2 / 12	-10.61 / -9.14 / -10.48 34 / 8 / 20	-10.39 / -8.73 / -8.69 38 / 3 / 24	-11.41 / -10.27 / -8.89 45 / 11 / 17	-10.73 / -10.69 / -9.07 34 / 19 / 9	-10.41 / -9.53 / -8.96 39 / 7 / 40	-10.06 / -9.01 / -8.91 49 / 3 / 37
Aripiprazole	-10.87 / -10.78 / -10.20 9 / 2 / 10	-10.91 / -9.84 / -9.64 2 / 2 / 3	-10.59 / -9.74 / -9.67 2 / 6 / 1	11.52 / -10.08 / -9.71 7 / 11 / 5	-12.00 / -9.97 / -9.68 2 / 3 / 2	-10.81 / -9.14 / -8.93 3 / 2 / 5	-110.4 / -10.08 / -9.97 4 / 1 / 8	-10.15 / -10.07 / -9.45 3 / 3 / 3	-10.95 / -9.73 / -9.44 10 / 3 / 3	-11.08 / -9.84 / -9.64 5 / 6 / 6	-10.55 / -10.39 / -9.90 1 / 3 / 7
Bromocriptine	-5.09 / -4.79 / -3.19 22 / 7 / 3	-19.65 / -7.87 / -7.20 16 / 1 / 8	-7.33 / -7.05 / -5.01 33 / 25 / 6	-9.33 / -1.84 / ? 11 / 1 / 3	-7.25 / 0.25 / ? 9 / 1 / 11	-2.14 / ? / ? 3 / 23 / 6	-8.74 / -7.79 / -6.67 2 / 5 / 20	-9.59 / -4.62 / -3.99 15 / 4 / 5	-9.15 / -5.91 / ? 17 / 6 / 10	-12.23 / -10.85 / -10.62 17 / 12 / 1	-5.89 / -0.24 / ? 24 / 8 / 11

Chlorpromazine	-8.06 / -7.78 / -7.56 20 / 22 / 3	-7.69 / -7.65 / -7.45 25 / 23 / 10	-8.22 / -7.96 / -7.94 7 / 8 / 8	-8.77 / -8.60 / -7.87 15 / 17 / 3	-7.98 / -7.90 / -7.64 8 / 16 / 14	-8.60 / -8.51 / -7.99 12 / 23 / 6	-7.46 / -7.12 / -7.10 7 / 13 / 14	-8.16 / -8.08 / -7.99 13 / 13 / 4	-7.60 / -7.28 / -7.28 6 / 2 / 20	-8.02 / -7.74 / -7.69 13 / 10 / 15	-8.11 / -7.89 / -7.88 17 / 4 / 14
Clozapine	-8.11 / -7.79 / -7.58 30 / 15 / 13	-7.80 / -7.68 / -7.57 2 / 15 / 12	-8.78 / -7.93 / -7.70 45 / 4 / 9	-8.88 / -8.45 / -8.31 8 / 16 / 32	-8.52 / -8.06 / -7.95 53 / 15 / 17	-8.33 / -8.07 / -7.49 62 / 3 / 2	-7.68 / -7.53 / -7.36 51 / 8 / 1	-8.73 / -7.94 / -7.88 58 / 8 / 2	-8.02 / -7.46 / -7.11 45 / 11 / 6	-8.53 / -8.19 / -7.47 15 / 15 / 17	-8.24 / -8.09 / -7.53 25 / 40 / 5
Dopamine	-10.86; -9.67; -8.26 29 / 37 / 7	-10.36 / -9.59 / -8.02 37 / 12 / 9	-9.72 / -9.20 / -8.42 30 / 30 / 9	-9.52 / -9.29 / -7.86 32 / 10 / 7	-10.86 / -10.28 / -9.66 45 / 14 / 20	-10.45 / -9.14 / -7.22 30 / 17 / 15	-10.38 / -8.68 / -7.93 45 / 9 / 2	-10.59 / -9.47 / -8.27 58 / 10 / 6	-10.55 / -8.54 / -8.21 38 / 10 / 8	-10.14 / -10.09 / -9.84 23 / 29 / 12	-10.16 / -9.77 / -7.83 32 / 24 / 1
Eticlopride	-8.86 / -8.80 / -8.77 6 / 2/ 12	-10.12 / -8.55 / -8.10 2 / 10 / 3	-10.49 / -9.99 / -9.71 5 / 7 / 18	-10.00 / -9.78 / -9.64 5 / 4 / 17	-9.34 / -9.17 / -.889 6 / 3 / 10	-9.39 / -9.34 / -9.27 3 / 7 / 2	-8.89 / -8.62 / -8.48 2 / 9 / 14	-9.87 / -8.70 / -8.53 9 / 2 / 4	-10.29 / -9.79 / -9.20 4 / 9 / 10	-9.86 / -9.82 / -8.56 5 / 5 / 12	-8.89 / -8.82 / -8.51 28 / 2 / 6
Haloperidol	-9.88 / -9.54 / -9.54 8 / 4 / 10	-10.35 / -9.40 / -9.31 2 / 4 / 2	-10.36 / -9.94 / -9.91 1 / 3 / 2	-10.26 / -10.23 / -9.83 9 / 7 / 15	-9.98 / -9.96 / -9.80 1 / 5 / 1	-10.38 / -10.04 / -9.90 17 / 1 / 5	-9.94 / -9.67 / -9.62 2 / 8 / 5	-10.92 / -10.71 / -10.32 3 / 9 / 1	-10.28 / -9.57 / -9.53 14 / 15 / 3	-10.36 / -9.92 / -9.87 3 / 9 / 3	-10.13 / -10.12 / -10.05 11 / 16 / 3

Nemonapride	-9.84 / -9.70 / -9.66 15 / 9 / 2	-10.45 / -10.41 / -8.93 5 / 2 / 1	-10.98 / -10.39 / -10.28 13 / 6 / 7	-11.11 / -10.71 / 10.43 12 / 9 / 4	-10.78 / -10.74 / -9.87 11 / 10 / 5	-10.68 / -10.48 / -9.92 5 / 5 / 7	-10.86 / -10.58 / -9.61 5 / 20 / 6	-10.97 / -10.06 / -10.03 17 / 7 / 14	-10.09 / -9.79 / -9.70 15 / 14 / 13	-10.58 / -10.06 / -9.52 11 / 2 / 8	-4.42 / -4.08 / -4.07 1 / 1 / 1
Risperidone	-9.98 / -8.97 / -8.91 2 / 9 / 2	-9.76 / -8.63 / -8.34 5 / 6 / 2	-12.22 / -11.92 / -10.94 7 / 11 / 10	-11.4 / -1055 / -10.29 2 / 13 / 17	-9.02 / -8.94 / -8.79 4 / 14 / 1	-9.77 / -9.49 / -8.52 3 / 1 /13	-8.85 / -8.84 / -8.80 4 / 8 / 3	-10.46 / -9.72 / -8.59 5 / 1 / 9	-8.50 / -8.15 / -7.54 2 / 30 / 15	-10.74 / -10.71 / -10.39 5 / 3 / 6	-10.96 / -10.70 / -10.50 17 / 8 / 10
SCH23390	-10.05 / 10.00 / -9.31 3 / 8 / 2	-9.95 / -9.44 / -9.12 32 / 9 / 4	-9.75 / -9.70 / -9.53 13 / 6 / 7	-10.53 / -9.13 / -8.96 216 / 2/ 10	-10.62 / -9.25 / -8.89 9 / 2 / 2	-9.97 / -9.68 / -9.53 4 / 5 / 2	-9.32 / -8.31 / -8.04 9 / 1 / 3	-9.02 / -8.94 / -8.55 2 / 3 / 12	-8.11 / -8.08 / -8.01 1 / 4 / 13	-9.88 / -9.67 / -9.16 4 / 22 / 5	-10.16 / -10.00 / -8.79 3 / 9 / 16
SKF38393	-11.18 / -9.80 / -9.75 5 / 18 / 9	-12.56 / -10.78 / -10.48 30 / 13 / 3	-11.58 / -10.70 / -10.54 9 / 12 / 9	-12.16 / -11.53 / -11.30 10 / 14 / 14	-12.88 / -11.25 / -10.90 6 / 14 / 26	-11.10 / -10.74 / -9.00 27 / 13 / 1	-11.81 / -9.98 / -9.51 11 / 5 / 2	-13.61 / -11.02 / -9.89 14 / 6 / 6	-10.12 / -9.04 / -9.03 2 / 3 / 12	-12.19 / -10.29 / -10.11 24 / 3 / 1	-11.01 / -10.55 / -9.68 6 / 20 / 2
Spiperdone	-10.57 / -9.80 / -9.38 21 / 9 / 5	-10.14 / -9.87 / -9.25 1 / 4 / 1	-10.45 / -10.20 / -9.88 4 / 2 / 3	-10.17 / -9.55 / -9.53 5 / 4 / 4	-10.29 / -10.21 / -9.94 2 / 2 / 3	-10.45 / -10.12 / -10.11 3 / 20 / 5	-9.39 / -10.53 / -10.47 4 / 9 / 9	-10.60 / -10.38 / -10.14 1 / 7 / 2	-9.53 / -9.42 / -9.42 13 / 2 / 2	-11.51 / -10.73 / -10.58 2 / 1 / 9	-10.54 / -10.51 / -10.20 1 / 2 / 1

Sulpiride	-10.25 / -10.10 / -10.08 5 / 3 / 2	-11.82 / -9.31 / -9.10 3 / 2 / 1	-10.13 / -9.74 / -9.48 1 / 2 / 1	-110.08 / -10.99 / -10.51 2 / 2 / 2	-10.68 / -10.03 / -10.01 2 / 5 / 3	-10.42 / -10.33 / -10.32 6 / 3 / 3	-19.97 / -10.53 / -10.47 4 / 3 / 3	-11.73 / -11.62 / -11.47 5 / 4 / 3	-11.40 / -10.39 / -9.56 7 / 6 / 1	-12.53 / -11.56 / -11.46 2 / 6 / 5	-11.56 / -10.62 / -10.11 6 / 4 / 3

Appendix 6: Results of the molecular docking of bromocriptine, clozapine, sulpiride, eticlopride, risperidone, aripiprazole and spiperdone for all DR subtypes at time points [ns]. For the binding energy (left graph) the mean of the 3 lowest energies of dopamine was calculated. For the number of conformations (right graph) of the three clusters with the lowest binding energies are shown for each time point and receptor.
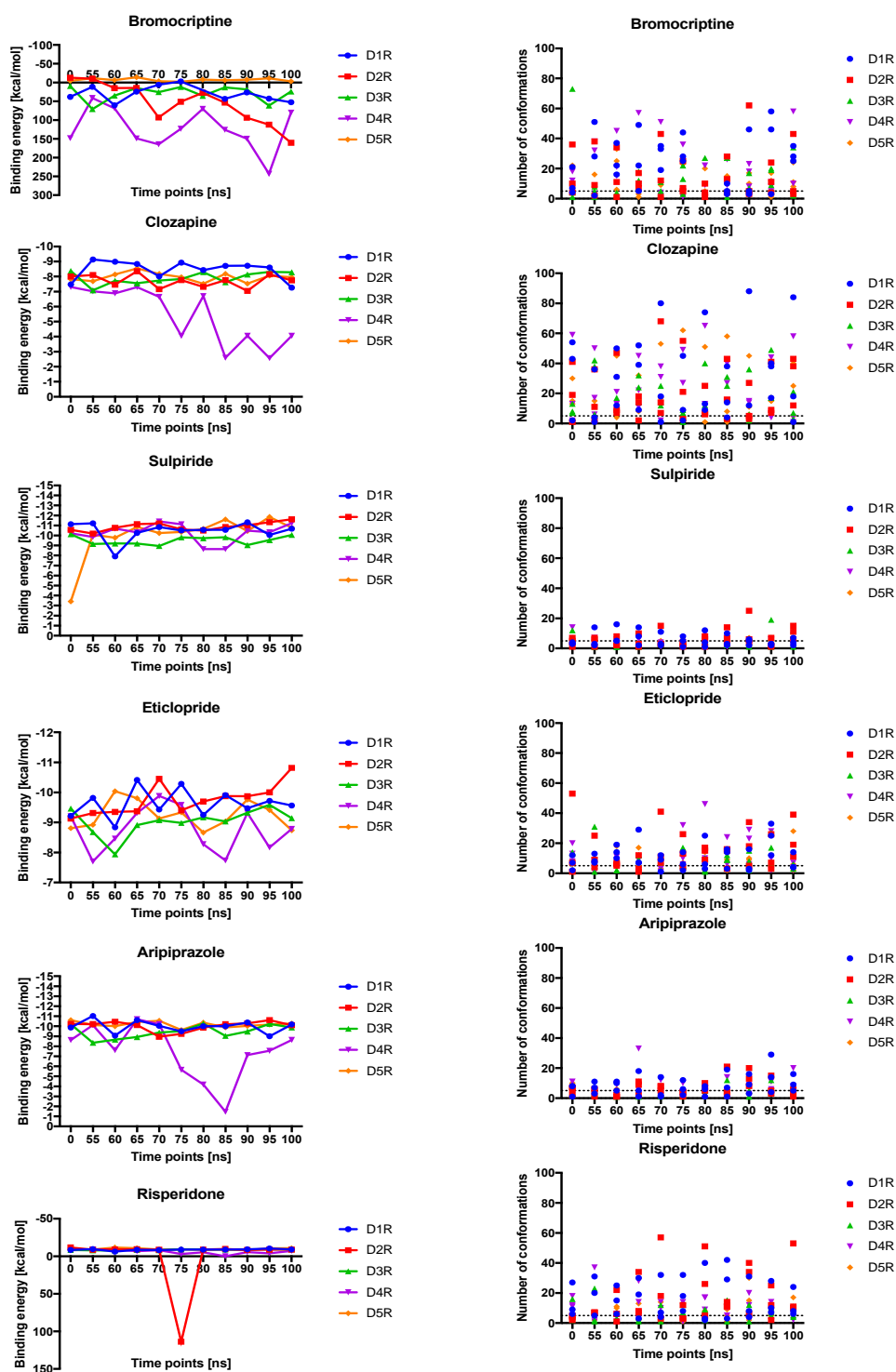
Appendix 7: Scoring functions of top 10 best models for each state. Selected model is highlighted in yellow

Inactive state

model_no	molpdf	DOPE score	z-score	RAMPAGE	ERRAT2
ghsr1a.B99990006.pdb	31697.89	-40692.70	-3.10	95.70%	52.86%
ghsr1a.B99990094.pdb	31537.29	-40643.16	-2.85	95.00%	63.97%
ghsr1a.B99990020.pdb	30940.38	-40579.73	-2.90	95.00%	69.93%
ghsr1a.B99990036.pdb	31579.06	-40556.43	-2.94	95.00%	74.75%
ghsr1a.B99990005.pdb	31411.38	-40526.89	-3.00	95.70%	71.04%
ghsr1a.B99990049.pdb	31847.23	-40503.73	-3.12	96.00%	65.32%
ghsr1a.B99990100.pdb	31470.48	-40478.39	-3.07	95.40%	57.91%
ghsr1a.B99990098.pdb	31401.20	-40464.42	-2.69	94.40%	60.94%
ghsr1a.B99990038.pdb	31464.74	-40436.14	-3.11	96.70%	74.75%
ghsr1a.B99990045.pdb	31484.07	-40409.39	-3.07	95.40%	71.38%

Pre-Active State

model_no	molpdf	DOPE score	z-score	RAMPAGE	ERRAT2
ghsr1a.B99990064.pdb	30563.79	-39878.75	-2.32	95.40%	62.63%
ghsr1a.B99990078.pdb	30705.39	-39866.78	-1.96	95.70%	53.20%
ghsr1a.B99990094.pdb	30547.60	-39648.43	-2.22	95.00%	58.92%
ghsr1a.B99990059.pdb	30828.85	-39600.10	-1.99	94.10%	61.95%
ghsr1a.B99990060.pdb	31063.34	-39529.27	-2.46	94.10%	49.16%
ghsr1a.B99990091.pdb	30617.86	-39493.52	-1.97	94.70%	58.92%
ghsr1a.B99990007.pdb	30582.32	-39486.76	-2.57	95.70%	51.85%
ghsr1a.B99990093.pdb	30599.83	-39483.70	-2.27	94.10%	51.85%
ghsr1a.B99990042.pdb	30647.20	-39473.43	-2.05	95.00%	60.61%
ghsr1a.B99990046.pdb	30986.43	-39460.45	-2.60	95.00%	61.95%

G-Protein Active State

model_no	molpdf	DOPE score	z-score	RAMPAGE	ERRAT2
ghsr1a.B99990064.pdb	26489.30	-39137.45	-1.77	94.70%	54.88%
ghsr1a.B99990081.pdb	26847.68	-39107.45	-2.2	92.70%	52.86%
ghsr1a.B99990055.pdb	26666.70	-39106.76	-2.11	95.70%	57.24%
ghsr1a.B99990022.pdb	26943.90	-39076.61	-2.49	95.40%	59.60%

ghsr1a.B99990027.pdb	27561.24	-39043.73	-2.35	95.70%	53.87%
ghsr1a.B99990008.pdb	27439.12	-38999.84	-2.63	95.00%	55.89%
ghsr1a.B99990049.pdb	27835.13	-38998.51	-2.22	94.10%	50.51%
ghsr1a.B99990077.pdb	26594.29	-38988.64	-2.31	95.00%	55.56%
ghsr1a.B99990019.pdb	26721.29	-38954.52	-2.12	95.00%	52.19%
ghsr1a.B99990026.pdb	26555.56	-38942.73	-2.03	94.70%	53.87%

Arrestin Active State

model_no	molpdf	DOPE score	z-score	RAMPAGE	ERRAT2
ghsr1a.B99990056.pdb	13311.95	-39926.92	-1.85	95.00%	42.42%
ghsr1a.B99990041.pdb	13326.03	-39766.19	-2.22	95.00%	50.51%
ghsr1a.B99990089.pdb	13731.82	-39757.20	-2.02	93.70%	43.43%
ghsr1a.B99990024.pdb	13441.02	-39602.92	-2.07	94.70%	43.10%
ghsr1a.B99990046.pdb	13495.95	-39583.67	-1.86	94.40%	50.17%
ghsr1a.B99990071.pdb	13915.81	-39567.84	-2.10	95.00%	41.41%
ghsr1a.B99990087.pdb	13382.26	-39547.87	-1.70	93.10%	46.47%
ghsr1a.B99990017.pdb	13379.78	-39535.85	-1.70	95.40%	43.43%
ghsr1a.B99990096.pdb	13402.71	-39521.41	-1.89	93.40%	46.80%
ghsr1a.B99990032.pdb	13841.90	-39505.94	-1.73	95.40%	47.48%

7 REFERENCES

[1] B. G. Tehan, A. Bortolato, F. E. Blaney, M. P. Weir, and J. S. Mason, "Unifying Family A GPCR Theories of Activation," Pharmacol. Ther., vol. 143, no. 1, pp. 51–60, 2014.

[2] N. R. Latorraca, A. J. Venkatakrishnan, and R. O. Dror, "GPCR dynamics: Structures in motion," Chem. Rev., vol. 117, no. 1, pp. 139–155, Jan. 2017.

[3] I. S. Moreira, "Structural features of the G-protein/GPCR interactions," Biochim. Biophys. Acta - Gen. Subj., vol. 1840, no. 1, pp. 16–33, 2014.

[4] S. Jo, T. Kim, V. G. Iyer, and W. Im, "CHARMM-GUI: A web-based graphical user interface for CHARMM," J. Comput. Chem., vol. 29, no. 11, pp. 1859–1865, Jun. 2008.

[5] J. A. Ballesteros et al., "Activation of the β2-Adrenergic Receptor Involves Disruption of an Ionic Lock between the Cytoplasmic Ends of Transmembrane Segments 3 and 6 ," J. Biol. Chem. , vol. 276, no. 31, pp. 29171–29177, Aug. 2001.

[6] L. Shi, G. Liapakis, R. Xu, F. Guarnieri, J. A. Ballesteros, and J. A. Javitch, "β2 Adrenergic Receptor Activation: MODULATION OF THE PROLINE KINK IN TRANSMEMBRANE 6 BY A ROTAMER TOGGLE SWITCH ," J. Biol. Chem. , vol. 277, no. 43, pp. 40989–40996, Oct. 2002.

[7] J.-M. Beaulieu and R. R. Gainetdinov, "The Physiology, Signaling, and Pharmacology of Dopamine Receptors," Pharmacol. Rev., vol. 63, no. 1, pp. 182–217, 2011.

[8] S. D. Iversen and L. L. Iversen, "Dopamine: 50 years in perspective.," Trends Neurosci., vol. 30, no. 5, pp. 188–93, May 2007.

[9] J. M. Beaulieu, S. Espinoza, and R. R. Gainetdinov, "Dopamine receptors - IUPHAR review 13," Br. J. Pharmacol., vol. 172, no. 1, pp. 1–23, Jan. 2015.

[10] A. E. Moritz, R. Benjamin Free, and D. R. Sibley, "Advances and challenges in the search for D 2 and D 3 dopamine receptor-selective compounds," Cell. Signal., Jul. 2017.

[11] C. W. Lindsley and C. R. Hopkins, "Return of D 4 Dopamine Receptor Antagonists in Drug Discovery," J. Med. Chem., vol. 60, no. 17, pp. 7233–7243, Sep. 2017.

[12] K. A. Johnson and D. M. Lovinger, "Presynaptic G Protein-Coupled Receptors: Gatekeepers of Addiction?," Front. Cell. Neurosci., vol. 10, p. 264, Nov. 2016.

[13] B. K. Madras, "History of the discovery of the antipsychotic dopamine D2 receptor: A basis for the dopamine hypothesis of schizophrenia," J. Hist. Neurosci., vol. 22, no. 1, pp. 62–78, 2013.

[14] R. Ekhteiari Salmas, Y. Serhat Is, S. Durdagi, M. Stein, and M. Yurtsever, "A QM protein–ligand investigation of antipsychotic drugs with the dopamine D2 Receptor (D2R)," J. Biomol. Struct. Dyn., no. August, pp. 1–10, 2017.

[15] D. A. Sykes et al., "Extrapyramidal side effects of antipsychotics are linked to their association kinetics at dopamine D2 receptors," Nat. Commun., vol. 8, no. 1, p. 763, 2017.

[16] A. K. Banala et al., "N-(3-Fluoro-4-(4-(2-methoxy or 2,3-dichlorophenyl)piperazine-1-yl)arylcarboxamides as selective dopamine D3 receptor ligands: critical role of the carboxamide linker for D3 recetpor selectivity," J. Med. Chem., vol. 54, pp. 3581–3594, 2011.

[17] A. H. Newman et al., "Molecular determinants of selectivity and efficacy at the dopamine D3 receptor," J. Med. Chem., vol. 55, no. 15, pp. 6689–6699, 2012.

[18] G. Damsma et al., "Pharmacological aspects of R-(+)-7-OH-DPAT, a putative dopamine D3 receptor ligand," Eur. J. Pharmacol., vol. 249, pp. 9–10, 1993.

[19] D. Lévesque et al., "Identification, characterization, and localization of the dopamine D3 receptor in rat brain using 7-[3H]hydroxy-N,N-di-n-propyl-2-aminotetralin.," Proc. Natl. Acad. Sci. U. S. A., vol. 89, no. 17, pp. 8155–9, 1992.

[20] D. Sampson et al., "Identification of a new selective dopamine D4receptor ligand," Bioorganic Med. Chem., vol. 22, no. 12, pp. 3105–3114, 2014.

[21] K. D. Burris et al., "Aripiprazole, a novel antipsychotic, is a high-affinity partial agonist at human dopamine D2 receptors.," J. Pharmacol. Exp. Ther., vol. 302, no. 1, pp. 381–389, 2002.

[22] J. Zhang, B. Xiong, X. Zhen, and A. Zhang, "Dopamine D1 receptor ligands: Where are we now and where are we going," Med. Res. Rev., vol. 29, no. 2, pp. 272–294, 2009.

[23] J. L. Conroy, R. B. Free, and D. R. Sibley, "Identification of G Protein-Biased Agonists That Fail to Recruit β-Arrestin or Promote Internalization of the D1 Dopamine Receptor," ACS Chem. Neurosci., vol. 6, no. 4, pp. 681–692, 2015.

[24] S. Butini et al., "Polypharmacology of dopamine receptor ligands," Prog. Neurobiol., vol. 142, pp. 68–103, 2016.

[25] S. M. Lee et al., "SKF-83959 is not a highly-biased functionally selective D1dopamine receptor ligand with activity at phospholipase C," Neuropharmacology, vol. 86, pp. 145–154, 2014.

[26] E. Arimitsu et al., "The ligand binding ability of dopamine D1 receptors synthesized using a wheat germ cell-free protein synthesis system with liposomes," Eur. J. Pharmacol., vol. 745, pp. 117–122, 2014.

[27] G. Giorgioni, a Piergentili, S. Ruggieri, and W. Quaglia, "Dopamine D5 receptors: a challenge to medicinal chemists.," Mini Rev. Med. Chem., vol. 8, no. 10, pp. 976–95, 2008.

[28] R. Churm, J. S. Davies, J. W. Stephens, and S. L. Prior, "Ghrelin function in human obesity and type 2 diabetes: a concise review.," Obes. Rev., vol. 18, no. 2, pp. 140–148, Feb. 2017.

[29] C. W. Le Roux et al., "Ghrelin does not stimulate food intake in patients with surgical procedures involving vagotomy," J. Clin. Endocrinol. Metab., vol. 90, no. 8, pp. 4521–4524, 2005.

[30] Q. Jiao et al., "The neurological effects of ghrelin in brain diseases: Beyond metabolic functions," Neuroscience and Biobehavioral Reviews, vol. 73. pp. 98–111, 2017.

[31] L. F. Ribeiro et al., "Ghrelin triggers the synaptic incorporation of AMPA receptors in the hippocampus.," Proc. Natl. Acad. Sci. U. S. A., vol. 111, no. 1, pp. E149-58, 2014.

[32] A. Laviano, A. Molfino, S. Rianda, and F. R. Fanelli, "The growth hormone secretagogue receptor (Ghs-R)," Curr. Pharm. Des., vol. 18, pp. 4749–4754, 2012.

[33] O. Al Massadi, M. López, M. Tschöp, C. Diéguez, and R. Nogueiras, "Current Understanding of the Hypothalamic Ghrelin Pathways Inducing Appetite and Adiposity," Trends Neurosci., 2017.

[34] R. Schrage and E. Kostenis, "Functional selectivity and dualsteric/bitopic GPCR targeting.," Curr. Opin. Pharmacol., vol. 32, pp. 85–90, 2016.

[35] R. Seifert and K. Wenzel-Seifert, "Constitutive activity of G-protein-coupled receptors: cause of disease and common property of wild-type receptors," Naunyn. Schmiedebergs. Arch. Pharmacol., vol. 366, no. 5, pp. 381–416, Nov. 2002.

[36] B. Holst and T. W. Schwartz, "Constitutive ghrelin receptor activity as a signaling set-point in appetite regulation," Trends Pharmacol. Sci., vol. 25, no. 3, pp. 113–117, Mar. 2004.

[37] J. Pantel et al., "Loss of constitutive activity of the growth hormone secretagogue receptor in familial short stature," J. Clin. Invest., vol. 116, no. 3, pp. 760–768, Mar. 2006.

[38] H.-J. Wang et al., "Ghrelin Receptor Gene: Identification of Several Sequence Variants in Extremely Obese Children and Adolescents, Healthy Normal-Weight and Underweight Students, and Children with Short Normal Stature," J. Clin.

Endocrinol. Metab., vol. 89, no. 1, pp. 157–162, Jan. 2004.

[39]   J. Koehler Leman, M. B. Ulmschneider, and J. J. Gray, "Computational modeling of membrane proteins," Proteins Struct. Funct. Bioinforma., vol. 83, no. 1, pp. 1–24, Jan. 2015.

[40]   A. A. Kaczor, E. Rutkowska, D. Bartuzi, K. M. Targowska-Duda, D. Matosiuk, and J. Selent, Computational methods for studying G proteincoupled receptors (GPCRs), vol. 132, no. December. Elsevier Ltd, 2016.

[41]   F. I. Khan, D. Q. Wei, K. R. Gu, M. I. Hassan, and S. Tabrez, "Current updates on computer aided protein modeling and designing," Int. J. Biol. Macromol., vol. 85, pp. 48–62, 2016.

[42]   S. Costanzi, "Modeling G protein-coupled receptors and their interactions with ligands," Curr. Opin. Struct. Biol., vol. 23, no. 2, pp. 185–190, 2013.

[43]   M. Filizola, G Protein-Coupled Receptors - Modeling and Simulation, vol. 796. 2014.

[44]   M. Marti-Solano, A. A. Kaczor, R. Guixà-González, and J. Selent, Computational Strategies to Incorporate GPCR Complexity in Drug Design, vol. 1. 2015.

[45]   F. Sievers et al., "Fast, scalable generation of high-quality protein multiple sequence alignments using Clustal Omega," Mol. Syst. Biol., vol. 7, no. 1, p. 539, Oct. 2011.

[46]   A. Sali and T. L. Blundell, "Comparative protein modelling by satisfaction of spatial restraints," J. Mol. Biol., no. 234, pp. 779–815, 1993.

[47]   B. Webb and A. Sali, "Comparative Protein Structure Modeling Using MODELLER," in Current Protocols in Bioinformatics, Hoboken, NJ, USA: John Wiley & Sons, Inc., 2014, p. 5.6.1-5.6.32.

[48]   M. Biasini et al., "SWISS-MODEL: Modelling protein tertiary and quaternary structure using evolutionary information," Nucleic Acids Res., vol. 42, no. W1, pp. W252–W258, Jul. 2014.

[49]   J. Zhu, H. Fan, X. Periole, B. Honig, and A. E. Mark, "Refining homology models by combining replica-exchange molecular dynamics and statistical potentials," Proteins Struct. Funct. Genet., vol. 72, no. 4, pp. 1171–1188, Mar. 2008.

[50]   X.-Y. Meng, H.-X. Zhang, M. Mezei, and M. Cui, "Molecular Docking: A Powerful Approach for Structure-Based Drug Discovery," Curr. Comput. Aided-Drug Des., vol. 7, no. 2, pp. 146–157, Jun. 2011.

[51]   G. C. P. van Zundert et al., "The HADDOCK2.2 webserver: User-friendly integrative modeling of biomolecular complexes," J. Mol. Biol., vol. 428, no. 4, pp. 720–725, Feb. 2016.

[52]   A. Shkumatov, D. Svergun, and A. M. J. J. Bonvin, "Selection and Refinement of HADDOCK Solutions Using Experimental Small-Angle X-ray Scattering Data."

[53]   D. Provasi and M. Filizola, "Putative active states of a prototypic g-protein-coupled receptor from biased molecular dynamics.," Biophys. J., vol. 98, no. 10, pp. 2347–2355, May 2010.

[54]   D. A. Case et al., AMBER17. 2017.

[55]   B. R. Brooks, R. E. Bruccoleri, B. D. Olafson, D. J. States, S. Swaminathan, and M. Karplus, "CHARMM: A program for macromolecular energy, minimization, and dynamics calculations," J. Comput. Chem., vol. 4, no. 2, pp. 187–217, 1983.

[56]   B. Hess, C. Kutzner, D. Van Der Spoel, and E. Lindahl, "GRGMACS 4: Algorithms for highly efficient, load-balanced, and scalable molecular simulation," J. Chem. Theory Comput., vol. 4, no. 3, pp. 435–447, Mar. 2008.

[57]   L. Bu, M. Michino, R. M. Wolf, and C. L. Brooks, "Improved model building and assessment of the Calcium-sensing receptor transmembrane domain.," Proteins, vol. 71, no. 1, pp. 215–226, Apr. 2008.

[58]   X.-Y. Meng, M. Mezei, and M. Cui, "Computational approaches for modeling GPCR dimerization.," Curr. Pharm. Biotechnol., vol. 15, no. 10, pp. 996–1006, Nov. 2014.

[59]   B. Webb and A. Sali, "Comparative protein structure modeling using MODELLER," Curr. Protoc. Bioinforma., vol. 2016, no. 1, p. 5.6.1-5.6.37, Jun. 2016.

[60]   E. Y. T. Chien et al., "Structure of the Human Dopamine D3 Receptor in Complex with a D2/D3 Selective Antagonist," Science (80-.)., vol. 330, no. 6007, pp. 1091–1095, 2010.

[61]   S. Wang et al., "D4dopamine receptor high-resolution structures enable the discovery of selective agonists," Science (80-.)., vol. 358, no. 6361, pp. 381–386, 2017.

[62]   S. Altschul, "Basic Local Alignment Search Tool," J. Mol. Biol., vol. 215, no. 3, pp. 403–410, 1990.

[63]   M. Shen and A. Sali, "Statistical potential for assessment and prediction of protein structures," Protein Sci., vol. 15, no. 11, pp. 2507–2524, Jan. 2006.

[64]   M. Wiederstein and M. J. Sippl, "ProSA-web: interactive web service for the recognition of erros in three-dimensional structures of proteins," Nucleic Acids Res., vol. 35, no. suppl_2, pp. W407–W410, Jul. 2007.

[65]   B. Wallner and A. Elofsson, "Identification of correct regions in protein models using structural, alignment, and consensus information.," Protein Sci., vol. 15, no. 4, pp. 900–913, Jan. 2006.

[66] S. Cristobal, A. Zemla, D. Fischer, L. Rychlewski, and A. Elofsson, "A study of quality measures for protein threading models," BMC Bioinformatics, vol. 2, p. 5, 2001.

[67] N. Siew, A. Elofsson, L. Rychlewski, and D. Fischer, "MaxSub: An automated measure for the assessment of protein structure prediction quality," Bioinformatics, vol. 16, no. 9, pp. 776–785, 2000.

[68] L. J. McGuffin, K. Bryson, and D. T. Jones, "The PSIPRED protein structure prediction server," Bioinformatics, vol. 16, no. 4, pp. 404–405, 2000.

[69] J. A. Ballesteros and H. Weinstein, "Integrated methods for the construction of three-dimensional models and computational probing of structure-function relations in G protein-coupled receptors," Methods Neurosci., vol. 25, no. C, pp. 366–428, 1995.

[70] C. Z. Floresca and J. A. Schetz, "Dopamine Receptor Microdomains Involved in Molecular Recognition and the Regulation of Drug Affinity and Function," J. Recept. Signal Transduct., vol. 24, no. 3, pp. 207–239, Jan. 2004.

[71] B. Bueschbell, A. J. Preto, C. A. V. Barreto, A. C. Schiedel, and I. S. Moreira, "Creating a valid in silico Dopamine D2-receptor model for small molecular docking studies," in MOL2NET, International Conference Series on Multidisciplinary Sciences, 2017, vol. 3, pp. 1–6.

[72] M. A. Lomize, I. D. Pogozheva, H. Joo, H. I. Mosberg, and A. L. Lomize, "OPM database and PPM web server: Resources for positioning of proteins in membranes," Nucleic Acids Res., vol. 40, no. D1, pp. D370–D376, Jan. 2012.

[73] M. H. M. Olsson, C. R. SØndergaard, M. Rostkowski, and J. H. Jensen, "PROPKA3: Consistent treatment of internal and surface residues in empirical p Kapredictions," J. Chem. Theory Comput., vol. 7, no. 2, pp. 525–537, Feb. 2011.

[74] M. G. Wolf, M. Hoefling, C. Aponte-SantamaríA, H. Grubmüller, and G. Groenhof, "G-membed: Efficient insertion of a membrane protein into an equilibrated lipid bilayer with minimal perturbation," J. Comput. Chem., vol. 31, no. 11, pp. 2169–2174, Mar. 2010.

[75] D. Van Der Spoel, E. Lindahl, B. Hess, G. Groenhof, A. E. Mark, and H. J. C. Berendsen, "GROMACS: Fast, flexible, and free," J. Comput. Chem., vol. 26, no. 16, pp. 1701–1718, Oct. 2005.

[76] S. Pronk et al., "GROMACS 4.5: A high-throughput and highly parallel open source molecular simulation toolkit," Bioinformatics, vol. 29, no. 7, pp. 845–854, Apr. 2013.

[77] J. Huang and A. D. Mackerell, "CHARMM36 all-atom additive protein force field:

Validation based on comparison to NMR data," J. Comput. Chem., vol. 34, no. 25, pp. 2135–2145, Jul. 2013.

[78]   J. Lee et al., "CHARMM-GUI Input Generator for NAMD, GROMACS, AMBER, OpenMM, and CHARMM/OpenMM Simulations Using the CHARMM36 Additive Force Field," J. Chem. Theory Comput., vol. 12, no. 1, pp. 405–413, Jan. 2016.

[79]   E. L. Wu et al., "CHARMM-GUI membrane builder toward realistic biological membrane simulations," J. Comput. Chem., vol. 35, no. 27, pp. 1997–2004, Aug. 2014.

[80]   M. J. Abraham et al., "Gromacs: High performance molecular simulations through multi-level parallelism from laptops to supercomputers," SoftwareX, vol. 1–2, pp. 19–25, Sep. 2015.

[81]   N. M. O'Boyle, M. Banck, C. A. James, C. Morley, T. Vandermeersch, and G. R. Hutchison, "Open Babel: An Open chemical toolbox," J. Cheminform., vol. 3, no. 10, pp. 1–14, 2011.

[82]   C. P. Lawler et al., "Interactions of the novel antipsychotic aripiprazole (OPC-14597) with dopamine and serotonin receptor subtypes," Neuropsychopharmacology, vol. 20, no. 6, pp. 612–627, 1999.

[83]   P. Seeman and H. H. Van Tol, "Dopamine receptor pharmacology," Trends Pharmacol.Sci., vol. 15, no. 7, pp. 264–270, 1994.

[84]   R. E. Salmas, M. Yurtsever, M. Stein, and S. Durdagi, "Modeling and protein engineering studies of active and inactive states of human dopamine D2 receptor (D2R) and investigation of drug/receptor interactions," Mol. Divers., vol. 19, no. 2, pp. 321–332, 2015.

[85]   A. Abhijnhan, C. E. Adams, A. David, and M. Ozbilen, "Depot fluspirilene for schizophrenia," Cochrane Database Syst. Rev., no. 1, 2007.

[86]   C. W. Lindsley and C. R. Hopkins, "Return of D $_4$ Dopamine Receptor Antagonists in Drug Discovery," J. Med. Chem., vol. 60, no. 17, pp. 7233–7243, 2017.

[87]   C. L. Newton, M. D. Wood, and P. G. Strange, "Examining the effects of sodium ions on the binding of antagonists to dopamine D2 and D3 receptors," PLoS One, vol. 11, no. 7, pp. 1–11, 2016.

[88]   E. Y. T. Chien et al., "Structure of the human dopamine D3 receptor in complex with a D2/D3 selective antagonist," Science (80-.)., vol. 330, no. 6007, pp. 1091–1095, 2011.

[89]   F. López-Muñoz and C. Alamo, "The consolidation of neuroleptic therapy: Janssen, the discovery of haloperidol and its introduction into clinical practice," Brain Res. Bull., vol. 79, no. 2, pp. 130–141, 2009.

[90]   N. Tschammer, M. Dörfler, H. Hübner, and P. Gmeiner, "Engineering a GPCR-ligand pair that simulates the activation of D 2L by dopamine," ACS Chem. Neurosci., vol. 1, no. 1, pp. 25–35, 2010.

[91]   S. Wang, T. Che, A. Levit, B. K. Shoichet, D. Wacker, and B. L. Roth, "Structure of the D2 dopamine receptor bound to the atypical antipsychotic drug risperidone," Nat. 2018, pp. 1–24, 2018.

[92]   B. Zhang, X. Yang, and M. Tiberi, "Functional importance of two conserved residues in intracellular loop 1 and transmembrane region 2 of Family A GPCRs: Insights from ligand binding and signal transduction responses of D1 and D5 dopaminergic receptor mutants," Cell. Signal., vol. 27, no. 10, pp. 2014–2025, 2015.

[93]   G. Andringa, B. Drukarch, J. E. Leysen, A. R. Cools, and J. C. Stoof, "The alleged dopamine D1 receptor agonist SKF 83959 is a dopamine D1 receptor antagonist in primate cells and interacts with other receptors," Eur. J. Pharmacol., vol. 364, no. 1, pp. 33–41, 1999.

[94]   J. A. Ballesteros and H. Weinstein, "Integrated methods for the construction of three dimensional models and computational probing of structure-function relations in G-protein coupled receptors," Methods Neurosci., vol. 25, pp. 366–428, 1995.

[95]   B. Männel et al., "Structure-guided screening for functionally selective D2 dopamine receptor ligands from a virtual chemical library.," ACS Chem. Biol., p. acschembio.7b00493, 2017.

[96]   M. Y. S. Kalani et al., "The predicted 3D structure of the human D2 dopamine receptor and the binding site and binding affinities for agonists and antagonists.," Proc. Natl. Acad. Sci., vol. 101, no. 11, pp. 3815–3820, 2004.

[97]   C. B. M. Platania, S. Salomone, G. M. Leggio, F. Drago, and C. Bucolo, "Homology Modeling of Dopamine D 2 and D 3 Receptors : Molecular Dynamics Refinement and Docking Evaluation," vol. 7, no. 9, 2012.

[98]   P. Egloff et al., "Structure of signaling-competent neurotensin receptor 1 obtained by directed evolution in Escherichia coli," Proc. Natl. Acad. Sci., vol. 111, no. 6, pp. E655–E662, Feb. 2014.

[99]   B. E. Krumm, J. F. White, P. Shah, and R. Grisshammer, "Structural prerequisites for G-protein activation by the neurotensin receptor," Nat. Commun., vol. 6, p. 7895, Jul. 2015.

[100]   S. G. F. Rasmussen et al., "Crystal structure of the β 2 adrenergic receptor-Gs protein complex," Nature, vol. 477, no. 7366, pp. 549–557, Jul. 2011.

[101] Y. Kang et al., "Crystal structure of rhodopsin bound to arrestin determined by femtosecond X-ray laser," Nature, vol. 523, p. 561, Jul. 2015.

[102] J. Hou, C. L. Charron, M. M. Fowkes, and L. G. Luyt, "Bridging computational modeling with amino acid replacements to investigate GHS-R1a-peptidomimetic recognition," Eur. J. Med. Chem., vol. 123, pp. 822–833, 2016.

[103] N. Siew, A. Elofsson, L. Rychlewski, and D. Fischer, "MaxSub: An automated measure for the assessment of protein structure prediction quality," Bioinformatics, vol. 16, no. 9, pp. 776–785, 2000.

[104] J. Mokrosin, T. M. Frimurer, B. Sivertsen, T. W. Schwartz, and B. Holsts, "Modulation of constitutive activity and signaling bias of the ghrelin receptor by conformational constraint in the second extracellular loop," J. Biol. Chem., vol. 287, no. 40, pp. 33488–33502, Sep. 2012.

[105] L. Schrödinger, "The {PyMOL} Molecular Graphics Development Component, Version~1.3," Nov. 2010.

[106] B. Webb, A. Sali, and S. Francisco, "Comparative Protein Structure Modeling Using MODELLER," Curr Protoc Bioinforma., vol. 54, no. ii, pp. 1–55, 2017.

[107] P. Werner, N. Hussy, G. Buell, K. a Jones, and R. a North, "D2, D3, and D4 dopamine receptors couple to G protein- regulated potassium channels in Xenopus oocytes," Mol.Pharmacol., vol. 49, pp. 656–661, 1996.

[108] S. Durdagi, R. E. Salmas, M. Stein, M. Yurtsever, and P. Seeman, "Binding Interactions of Dopamine and Apomorphine in D2High and D2Low States of Human Dopamine D2 Receptor Using Computational and Experimental Techniques," ACS Chem. Neurosci., vol. 7, no. 2, pp. 185–195, 2016.

[109] K. N. Boyd and R. B. Mailman, "Dopamine receptor signaling and cirrent and future antipyschotic drugs," Handb Exp Pharmacol, vol. 212, no. 212, pp. 53–86, 2012.

[110] J. Bergman, B. K. Madras, and R. D. Spealman, "Behavioral effects of D1 and D2 dopamine receptor antagonists in squirrel monkeys," J.Pharmacol.Exp.Ther., vol. 258, no. d, pp. 910–917, 1991.

[111] T. Chen et al., "Dopamine signaling regulates the projection patterns in the mouse chiasm," Brain Res., vol. 1625, pp. 324–336, 2015.

[112] K. Hidaka, M. Matsumoto, S. Tada, Y. Tasaki, and T. Yamaguchi, "Differential effects of [3H]nemonapride and [3H]spiperone binding on human dopamine D4 receptors," Neurosci. Lett., vol. 186, pp. 145–148, 1995.

[113] D. E. V. Pires and D. B. Ascher, "CSM-lig: a web server for assessing and comparing protein-small molecule affinities," Nucleic Acids Res., vol. 44, no. W1,

pp. W557–W561, 2016.

[114] Z. Liu et al., "PDB-wide collection of binding data: Current status of the PDBbind database," Bioinformatics, vol. 31, no. 3, pp. 405–412, 2015.

[115] A. C. Pan, D. W. Borhani, R. O. Dror, and D. E. Shaw, "Molecular determinants of drug-receptor binding kinetics," Drug Discov. Today, vol. 18, no. 13–14, pp. 667–673, 2013.

[116] R. K. Sunahara et al., "Cloning of the gene for a human dopamine D5 receptor with higher affinity for dopamine than D1," Nature, vol. 350, no. 6319, pp. 614–619, 1991.

[117] M. Tiberi and M. G. Caron, "High agonist-independent activity is a distinguishing feature of the dopamine D1B receptor subtype," J. Biol. Chem., vol. 269, no. 45, pp. 27925–27931, 1994.

[118] J. a Schetz, P. S. Benjamin, and D. R. Sibley, "Nonconserved residues in the second transmembrane-spanning domain of the D(4) dopamine receptor are molecular determinants of D(4)-selective pharmacology.," Mol. Pharmacol., vol. 57, no. 1, pp. 144–52, 2000.

[119] P. Sokoloff, B. Giros, M. P. Martres, M. L. Bouthenet, and J. C. Schwartz, "Molecular cloning and characterization of a novel dopamine receptor (D3) as a target for neuroleptics," Nature, vol. 347, no. 6289, pp. 146–151, 1990.

[120] K. D. Burris, M. A. Pacheco, T. M. Filtz, M.-P. Kung, H. F. Kung, and P. B. Molinoff, "Lack of Discrimination by Agonists for D2 and D3 Dopamine Receptors," Neuropsychopharmacology, vol. 12, pp. 335–345, 1995.

[121] S. B. Freedman et al., "Expression and pharmacological characterization of the human D3 dopamine receptor.," J. Pharmacol. Exp. Ther., vol. 268, no. 1, pp. 417–426, 1994.

[122] F. Sautel, N. Griffon, D. Lévesque, C. Pilon, J. C. Schwartz, and P. Sokoloff, "A functional test identifies dopamine agonists selective for D3 versus D2 receptors," Neuroreport, vol. 6, no. 2. pp. 329–332, 1995.

[123] H. H. M. Van Tol et al., "Cloning of the gene for a human dopamine D4 receptor with high affinity for the antipsychotic clozapine," Nature, vol. 350, p. 610, Apr. 1991.

[124] R. G. MacKenzie et al., "Characterization of the human dopamine D3 receptor expressed in transfected cell lines.," Eur. J. Pharmacol., vol. 266, no. 1, pp. 79–85, 1994.

[125] S. Chumpradit, M. P. Kung, J. Vessotskie, C. Foulon, M. Mu, and H. F. Kung, "Iodinated 2-aminotetralins and 3-amino-1-benzopyrans: ligands for dopamine D2

and D3 receptors," J. Med. Chem., vol. 37, no. 24, pp. 4245–4250, Nov. 1994.

[126] a Ricci, F. Veglio, and F. Amenta, "Radioligand binding characterization of putative dopamine D3 receptor in human peripheral blood lymphocytes with [3H]7-OH-DPAT.," J. Neuroimmunol., vol. 58, pp. 139–144, 1995.

[127] M. J. Millan, L. Maiofiss, D. Cussac, V. Audinot, J.-A. Boutin, and A. Newman-Tancredi, "Differential Actions of Antiparkinson Agents at Multiple Classes of Monoaminergic Receptor. I. A Multivariate Analysis of the Binding Profiles of 14 Drugs at 21 Native and Cloned Human Receptor Subtypes," J. Pharmacol. Exp. Ther., vol. 303, no. 2, pp. 791–804, 2002.

[128] P. Sokoloff et al., "Pharmacology of human dopamine D3 receptor expressed in a mammalian cell line: comparison with D2 receptor," Eur. J. Pharmacol. Mol. Pharmacol., vol. 225, no. 4, pp. 331–337, 1992.

[129] M. Shahid, G. B. Walker, S. H. Zorn, and E. H. F. Wong, "Asenapine: A novel psychopharmacologic agent with a unique human receptor signature," J. Psychopharmacol., vol. 23, no. 1, pp. 65–73, 2009.

[130] L. Tang, R. D. Todd, A. Heller, and K. L. O'Malley, "Pharmacological and functional characterization of D2, D3 and D4 dopamine receptors in fibroblasts and dopaminergic cell lines," J. Pharmacol. Exp. Ther., vol. 268, pp. 495–502, 1994.

[131] R. Lathi, D. Evans, N. Stratman, and L. Figur, "Dopamine D4 versus D2 receptor selectivity of dopamine receptor antagonists: possible therapeutic implications," Eur. J. Pharmacol., vol. 236, pp. 483–486, 1993.

[132] R. Maggio, M. Scarselli, F. Novi, M. J. Millan, and G. U. Corsini, "Potent activation of dopamine D3/D2 heterodimers by the antiparkinsonian agents, S32504, pramipexole and ropinirole," J. Neurochem., vol. 87, no. 3, pp. 631–641, 2003.

[133] P. Seeman, H. C. Guan, H. H. Van Tol, and H. B. Niznik, "Low density of dopamine D4 receptors in Parkinson's,schizofeenia,and control brain striata.," Synapse, vol. 14, pp. 247–253, 1993.

[134] S. Patel et al., "Identification and pharmacological characterization of [125I]L-750,667, a novel radioligand for the dopamine D4 receptor.," Mol. Pharmacol., vol. 50, no. 6, pp. 1658–64, 1996.

[135] Q. Y. Zhou et al., "Cloning and expression of human and rat D1 dopamine receptors.," Nature, vol. 347, no. 6288. pp. 76–80, 1990.

[136] M. J. Durcan, G. C. Rigdon, M. H. Norman, and P. F. Morgan, "Is clozapine selective for the dopamine D4 receptor?," Life Sci., vol. 57, no. 18, pp. 275–283, 1995.

[137] J. Arnt and T. Skarsfeldt, "Do novel antipsychotics have similar pharmacologial characteristics? A review of the evidence," Neuropsychopharmacology, vol. 18, no. 2. pp. 63–101, 1998.

[138] M. J. Millan et al., "Functional Correlates of Dopamine D3 Receptor Activation in the Rat In Vivo and Their Modulation by the Selective Antagonist, (+)-S 14297: I. Activation of Postsynaptic D3 Receptors Mediates Hypothermia, Whereas Blockade of D2 Receptors Elicits Prolactin ," J. Pharmacol. Exp. Ther., vol. 275, pp. 885–898, 1995.

[139] P. Zajdel et al., "Antidepressant and antipsychotic activity of new quinoline- and isoquinoline-sulfonamide analogs of aripiprazole targeting serotonin 5-HT 1A/5-HT2A/5-HT7 and dopamine D 2/D3 receptors," Eur. J. Med. Chem., vol. 60, pp. 42–50, 2013.

[140] J. A. Allen et al., "Discovery of -Arrestin-Biased Dopamine D2 Ligands for Probing Signal Transduction Pathways Essential for Antipsychotic Efficacy," Proc. Natl. Acad. Sci., vol. 108, no. 45, pp. 18488–18493, 2011.

[141] J. Mierau, F. J. Schneider, H. A. Ensinger, C. L. Chio, M. E. Lajiness, and R. M. Huff, "Pramipexole binding and activation of cloned and expressed dopamine D2, D3and D4receptors," Eur. J. Pharmacol. Mol. Pharmacol., vol. 290, no. 1, pp. 29–36, 1995.

[142] M. A. B. Tice, T. Hashemi, L. A. Taylor, R. A. Duffy, and R. D. McQuade, "Characterization of the binding of SCH 39166 to the five cloned dopamine receptor subtypes," Pharmacol. Biochem. Behav., vol. 49, no. 3, pp. 567–571, 1994.

[143] J. R. Bunzow et al., "Cloning and expression of a rat D2 dopamine receptor cDNA," Nature, vol. 336, pp. 783–787, Dec. 1988.

[144] S. R. J. Hoare, M. C. Coldwell, D. Armstrong, and P. G. Strange, "Regulation of human D1, D(2(long)), D(2(short)), D3and D4dopamine receptors by amiloride and amiloride analogues," Br. J. Pharmacol., vol. 130, no. 5, pp. 1045–1059, 2000.

[145] J. Zhen, T. Antonio, A. K. Dutta, and M. E. A. Reith, "Concentration of receptor and ligand revisited in a modified receptor binding protocol for high-affinity radioligands: [3H]Spiperone binding to D2 and D3 dopamine receptors," J. Neurosci. Methods, vol. 188, no. 1, pp. 32–38, 2010.

[146] M. Olivella, G. Caltabiano, and A. Cordomí, "The role of Cysteine 6.47 in class A GPCRs," BMC Struct. Biol., vol. 13, no. 1, p. 3, 2013.

8 SCIENTIFIC PUBLICATIONS RESULTING FROM THIS WORK

8.1 Review Article

Prediction and Targeting of Interaction Interfaces in G-Protein Coupled Receptor Oligomers

Anke C. Schiedel[1,#], Meryem Köse[1#], Carlos Barreto[2], Beatriz Bueschbell[1], Giulia Morra[3,4], Ozge Sensoy[5,*] and Irina S. Moreira[2,6,*]

[1]*Pharmaceutical Chemistry I, PharmaCenter Bonn, University of Bonn, 53121 Bonn, Germany;* [2]*Data-driven Molecular Design, CNC - Center for Neuroscience and Cell Biology, University of Coimbra;* [3]*Weill-Cornell Medical College, Department of Physiology and Biophysics, 1300 York Ave, New York, NY 10065, USA;* [4]*ICRM-CNR Istituto di Chimica del Riconoscimento Molecolare, Consiglio Nazionale delle Ricerche, Via Mario Bianco 9, 20131 Milano, Italia;* [5]*Istanbul Medipol University, The School of Engineering and Natural Sciences, 34810, Istanbul, Turkey;* [6]*Bijvoet Center for Biomolecular Research, Faculty of Science - Chemistry, Utrecht University, Utrecht, 3584CH, The Netherlands*

Abstract: *Background:* Communication within a protein complex is mediated by physical interactions made among the protomers. Evidence for both the allosteric regulation present among the protomers of the protein oligomer and of the direct effect of membrane composition on this regulation has made it essential to investigate the underlying molecular mechanism that drives oligomerization, the type of interactions present within the complex, and to determine the identity of the interaction interface. This knowledge allows a holistic understanding of dynamics and also modulation of the function of the resulting oligomers/signalling complexes. G-protein-coupled receptors (GPCRs), which are targeted by 40% of currently prescribed drugs in the market, are widely involved in the formation of such physiological oligomers/signalling complexes.

Scope of the Review: This review highlights the importance of studying protein-protein interactions (PPI) by using a combination of data obtained from cutting-edge experimental and computational methods that were developed for this purpose. In particular, we focused on interaction interfaces found at GPCR oligomers as well as signalling complexes, since any problem associated with these interactions causes the onset of various crucial diseases.

Major Conclusions: In order to have a holistic mechanistic understanding of allosteric PPIs that drive the formation of GPCR oligomers and also to determine the composition of interaction interfaces with respect to different membrane compositions, it is essential to combine both relevant experimental and computational data. In this way, efficient and specific targeting of these interaction interfaces in oligomers/complexes can be achieved. Thus, effective therapeutic molecules with fewer side effects can be designed to modulate the function of these physiologically important receptor family.

Keywords: GPCRs, dimerization, PPI, oligomers, ghrelin, molecular dynamics, umbrella sampling, hot spot.

8.2 Conference Proceedings

Bueschbell, B.; Preto, A.; Barreto, C.; Schiedel, A.; Moreira, I. Creating a valid in silico Dopamine D2-receptor model for small molecular docking studies. In Proceedings of the MOL2NET 2017, International Conference on Multidisciplinary Sciences, 3rd edition, 15 February–20 December 2017; Sciforum Electronic Conference Series, Vol. 3, 2017 ; doi:10.3390/mol2net-03-05088

Barreto C, Machuqueiro M, Bonvin AMJJ, Moreira IS, Structural and dynamic understanding of the ghrelin receptor high constitutive activity. In Proceedings of the MOL2NET 2017, International Conference on Multidisciplinary Sciences, 3rd edition, doi:10.3390/mol2net-03-05089.

8.3 Posters

Barreto C, Machuqueiro M, Bonvin AMJJ, Moreira IS, Structural and dynamic understanding of the ghrelin receptor high constitutive activity. In Encontro Jovens Investigadores de Biologia Computacional e Estrutural, 2017 edition